U.S. DEPARTMENT OF COMMERCE
National Technical Information Service

PB-292 703

Predictions of Highway Emissions by a Second Order Closure Model

Aeronautical Research Associates of Princeton, Inc, NJ

Prepared for

Environmental Sciences Research Lab, Research Triangle Park, NC

Feb 79

United States
Environmental Protection
Agency

Environmental Sciences Research
Laboratory
Research Triangle Park NC 27711

EPA-600/4-79-013
February 1979

Research and Development

PB 292703

EPA

Predictions of Highway Emissions by a Second Order Closure Model

REPRODUCED BY
NATIONAL TECHNICAL
INFORMATION SERVICE
U. S. DEPARTMENT OF COMMERCE
SPRINGFIELD, VA. 22161

RESEARCH REPORTING SERIES

Research reports of the Office of Research and Development, U.S. Environmental Protection Agency, have been grouped into nine series. These nine broad categories were established to facilitate further development and application of environmental technology. Elimination of traditional grouping was consciously planned to foster technology transfer and a maximum interface in related fields. The nine series are:

1. Environmental Health Effects Research
2. Environmental Protection Technology
3. Ecological Research
4. Environmental Monitoring
5. Socioeconomic Environmental Studies
6. Scientific and Technical Assessment Reports (STAR)
7. Interagency Energy-Environment Research and Development
8. "Special" Reports
9. Miscellaneous Reports

This report has been assigned to the ENVIRONMENTAL MONITORING series. This series describes research conducted to develop new or improved methods and instrumentation for the identification and quantification of environmental pollutants at the lowest conceivably significant concentrations. It also includes studies to determine the ambient concentrations of pollutants in the environment and/or the variance of pollutants as a function of time or meteorological factors.

This document is available to the public through the National Technical Information Service, Springfield, Virginia 22161.

TECHNICAL REPORT DATA
(Please read Instructions on the reverse before completing)

1. REPORT NO. EPA-600/4-79-013	2.
3. RECIPIENT'S ACCESSION NO. PB292703	
4. TITLE AND SUBTITLE PREDICTIONS OF HIGHWAY EMISSIONS BY A SECOND ORDER CLOSURE MODEL	5. REPORT DATE February 1979 6. PERFORMING ORGANIZATION CODE
7. AUTHOR(S) M.E. TESKE and W.S. LEWELLEN	8. PERFORMING ORGANIZATION REPORT NO.
9. PERFORMING ORGANIZATION NAME AND ADDRESS Aeronautical Research Associates of Princeton 50 Washington Rd. Princeton, N. J. 08540	10. PROGRAM ELEMENT NO. 1AA601B CA-31 (FY-78) 11. CONTRACT/GRANT NO. 68-02-2285
12. SPONSORING AGENCY NAME AND ADDRESS Environmental Sciences Research Laboratory - RTP,NC Office of Research and Development U.S. Environmental Protection Agency Research Triangle Park, NC 27711	13. TYPE OF REPORT AND PERIOD COVERED Final 3/77-3/78 14. SPONSORING AGENCY CODE EPA/600/09
15. SUPPLEMENTARY NOTES	

16. ABSTRACT

The dispersion of sulfur hexafloride tracer and sulfate from automobile emissions in the immediate vicinity of a highway were estimated for conditions similar to those existing during the General Motors sulfate dispersion experiment conducted at a GM test track. A second-order closure model of turbulent transport in the planetary boundary layer was used to predict the steady-state dispersion under two conditions: with the mean wind and velocity component variances specified by the data or predicted with the aid of an automobile wake model. The GM measured wind data apparently suffered from low vertical velocity variance readings at the 1.5 meter height, and led to an overprediction of the SF_6 levels by an average factor of 1.77 for the 18 tower collection points during the 15 test days. The correlation fell to 0.96 of the measured levels when the model also predicted the wind fields. The results indicate that close to the highway, buoyancy effects were small even in the critical case when the wind is light and aligned with the roadway.

17. KEY WORDS AND DOCUMENT ANALYSIS

a. DESCRIPTORS	b. IDENTIFIERS/OPEN ENDED TERMS	c. COSATI Field/Group
*Air pollution *Turbulent flow Automobiles *Exhaust emissions *Sulfates *Predictions *Mathematical models *Boundary layer		13B 13F 21B 07B 12A 20D

18. DISTRIBUTION STATEMENT RELEASE TO PUBLIC	19. SECURITY CLASS *(This Report)* UNCLASSIFIED 20. SECURITY CLASS *(This page)* UNCLASSIFIED	21. NO. OF PAGES 95 22. PRICE PC A05 MF A01

EPA Form 2220-1 (9-73)

EPA-600/4-79-013
February 1979

PREDICTIONS OF HIGHWAY EMISSIONS BY A SECOND ORDER CLOSURE MODEL

by

M. E. Teske and W. S. Lewellen
Aeronautical Research Associates of Princeton, Inc.
50 Washington Road, P.O. Box 2229
Princeton, New Jersey 08540

Contract No. 68-02-2285

Project Officer

Francis S. Binkowski
Meteorology and Assessment Division
Environmental Sciences Research Laboratory
Research Triangle Park, North Carolina 27711

ENVIRONMENTAL SCIENCES RESEARCH LABORATORY
OFFICE OF RESEARCH AND DEVELOPMENT
U.S. ENVIRONMENTAL PROTECTION AGENCY
RESEARCH TRIANGLE PARK, NORTH CAROLINA 27711

DISCLAIMER

This report has been reviewed by the Environmental Sciences Research Laboratory, U.S. Environmental Protection Agency, and approved for publication. Approval does not signify that the contents necessarily reflect the views and policies of the U.S. Environmental Protection Agency, nor does mention of trade names or commercial products constitute endorsement or recommendation for use.

ABSTRACT

The dispersion of sulfur hexafloride tracer and sulfate from automobile emissions in the immediate vicinity of a highway were estimated for conditions similar to those existing during the General Motors sulfate dispersion experiment conducted at a GM test track. A second-order closure model of turbulent transport in the planetary boundary layer was used to predict the steady-state dispersion under two conditions: with the mean wind and velocity component variances specified by the data or predicted with the aid of an automobile wake model. The GM measured wind data apparently suffered from low vertical velocity variance readings at the 1.5 meter height, and led to an overprediction of the SF_6 levels by an average factor of 1.77 for the 18 tower collection points during the 15 test days. The correlation fell to 0.96 of the measured levels when the model also predicted the wind fields. The results indicate that close to the highway, buoyancy effects were small even in the critical case when the wind is light and aligned with the roadway.

CONTENTS

Abstract iii
Figures vi
Symbols ix

1. Introduction 1
2. Conclusions and Recommendations 3
3. General Motors Experiment 4
4. Numerical Simulation 6
5. Automobile Wake Model 9
6. Model Results 13

References 31

Appendices

A. The programmed second-order closure equations for two-dimensional, unsteady flows 33

B. Model dispersion predictions of SF_6 and sulfate for 13 typical test periods in the GM experiment 35

C. Model comparisons of the velocity and variance fields predicted by the closure model and measured by GM for the two critical test days 293 and 296 62

Preceding page blank

FIGURES

Number		Page
1	A sketch of the General Motors proving grounds test site, showing the relative positions of the data towers, instruments, and traffic pattern.....	5
2	Contours of predicted ΔSO_4 levels (above background) using the measured GM mean wind fields and turbulence data for the second test period of day 293. In this case the ambient winds were nearly cross-wind to the traffic, and S = 28.9 mg/mile/vehicle. When the background SO_4 level is included, S = 16.2 mg/mile/vehicle, so that the ΔSO_4 levels shown here should be multiplied by a factor of 0.56	14
3	Contours of predicted ΔSO_4 levels (above background) using the measured GM mean wind fields and turbulence data for the second test period of day 296. In this case the ambient winds were nearly aligned with the traffic and S = 28.9 mg/mile/vehicle.....	15
4	A point-plot of the predicted vs measured levels of ΔSO_4 using the measured GM mean wind fields and turbulence data with an assumed emission level of S = 28.9 mg/mile/vehicle. Each second-period sample from the 15 simulated days contributes 18 points to this plot. The days are denoted as: 1 = day 275; 2 = day 276; 3 = day 279; 4 = day 281; 5 = day 285; 6 = day 286; 7 = day 290; 8 = day 293; 9 = day 294; A = day 295; B = day 296; C = day 297; D = day 300; E = day 302; and F = day 303.....	17
5	A point-plot of the predicted vs measured levels of total SO_4 using the measured GM mean wind fields and turbulence data with an assumed emission level of S = 16.2 mg/mile/vehicle based on the ΔSO_4 levels plus the mean ambient background. Each second-period sample for the 15 simulated days contributes 18 points to this plot, as denoted in Figure 4....	18

Number		Page
6	Contours of predicted SF_6 levels using the measured GM mean wind fields and turbulence data for the second test period of day 293.....	19
7	Contours of predicted SF_6 levels using the measured GM mean wind fields and turbulence data for the second test period of day 296.....	20
8	A point-plot of the predicted vs measured levels of SF_6 using the measured GM mean wind fields and turbulence data, showing a least-squares slope of 1.77 . Each second-period sample from the 15 simulated days contributes 18 points to the plot. The days are numbered in ascending order with the keys explained in Figure 4.....	21
9	Contours of predicted ΔSO_4 levels (above background) using the predicted mean wind fields and turbulence data for the second test period of day 293, with S = 51.7 mg/mile/vehicle. When the background SO_4 level is included, S = 17.3 mg/mile/vehicle, so that the ΔSO_4 levels shown here should be multiplied by a factor of 0.33.....	24
10	Contours of predicted ΔSO_4 levels (above background) using the predicted mean wind fields and turbulence data for the second test period of day 296, with S = 51.7 mg/mile/vehicle.....	25
11	A point-plot of the predicted vs measured levels of ΔSO_4 using the predicted mean wind fields and turbulence data with an assumed emission level of S = 51.7 mg/mile/vehicle. The notation is discussed in Figure 4..	26
12	A point-plot of the predicted vs measured levels of total SO_4 using the predicted mean wind fields and turbulence data with an assumed emission level of S = 17.3 mg/mile/vehicle based on the ΔSO_4 levels plus the mean ambient background. The notation is discussed in Figure 4.....	27
13	Contours of predicted SF_6 levels using the predicted mean wind fields and turbulence data for the second test period of day 293.....	28

Number		Page
14	Contours of predicted SF_6 levels using the predicted mean wind fields and turbulence data for the second test period of day 296.....	29
15	A point-plot of the predicted vs measured levels of SF_6 using the predicted mean wind fields and turbulence data, showing a least-squares slope of 0.96 . The notation is discussed in Figure 4.....	30

LIST OF SYMBOLS

SYMBOLS

c	-- concentration fluctuation
C	-- mean concentration
g	-- gravity
L_c	-- average distance between cars
L_t	-- average distance between trucks
p	-- pressure
q^2	-- turbulent kinetic energy
$\dot{Q}_{q^2}, \dot{Q}_{SF_6}, \dot{Q}_{SO_4}, \dot{Q}_U, \dot{Q}_\Theta$	-- automobile source functions for turbulence, SF_6, SO_4, velocity and temperature
S	-- SO_4 emission level
t	-- time
u^*	-- surface shear stress velocity
u_i	-- velocity fluctuations (u,v,w)
U	-- mean horizontal windspeed aligned with the roadway
U_i	-- mean velocity
V	-- mean horizontal windspeed normal to the roadway
V_a	-- effective mean windspeed
W	-- mean vertical windspeed
x_i	-- Cartesian directions (x,y,z)
z_o	-- hydrodynamic roughness
η	-- vorticity $= \frac{\partial V}{\partial z} - \frac{\partial W}{\partial y}$
κ	-- vonKarman constant
θ	-- temperature fluctuation
Θ	-- mean potential temperature
Θ_o	-- reference temperature
Λ	-- turbulent macroscale

ν -- kinematic viscosity

σ_y, σ_z -- y,z Gaussian source spreads

ψ -- stream function

SECTION 1

INTRODUCTION

For the last several years, the Environmental Protection Agency (EPA) has supported the development by Aeronautical Research Associates of Princeton, Inc. (A.R.A.P.) of a second-order closure turbulence model. The first summarization of the model development is contained in Donaldson (Ref. 1), with a more recent recapitulation found in Lewellen and Teske (Ref. 2). The strength of the model rests upon the added physics of the Reynolds stress equations carried for the turbulence correlations $\overline{u_i u_j}$, $\overline{u_i \theta}$ and $\overline{\theta^2}$. In the incompressible case, five constants must be evaluated exclusive of the constants appearing in a companion equation for the turbulent scale length Λ. These constants are determined by fitting a wide variety of shear and wake flows (see Ref. 2 for details). Once determined, these constants are then unchanged when an application is made to other, more complicated flow problems. In the main, the model has performed admirably in several two-dimensional unsteady calculations (Refs. 3-5) and appears to give satisfactory flow results when applied to other simple laboratory flows not used to evaluate the modeling constants (Ref. 6).

Of particular interest to EPA is the prediction by the model of plume dispersal. To date, the work has centered around individual plume dynamics (Refs. 2, 6-9) and has not yet been concerned with multiple plume dynamics.

In September and October of 1975, General Motors conducted what they termed their "Great Sulfate Experiment" using a large fleet of test automobiles on their proving grounds in Milford, Michigan. Considerable data were taken of the ambient winds and turbulence, the temperature, SO_4, and an SF_6 tracer emitted from several trucks. The executive summary (Chock, Ref. 10) highlights the results of a more detailed volume (Cadle, et al., Ref. 11). Subsequent comparisons of the data with predictions by the standard Gaussian plume models used at EPA to estimate roadway sulfate concentrations were not very favorable (Ref. 12).

Eskridge and Demerjian (Ref. 13) assess this shortcoming of the EPA model and advance their own "finite difference" model. They use an eddy viscosity approach in which the effects of the automobile have been parameterized with coefficients

dependent only upon the vertical direction, with the assumption that the horizontal coefficient is five times larger than the vertical coefficient. They assume that the SF_6 release may be taken as a steady phenomenon, and use the case with the wind aligned with the traffic to determine the incremental eddy viscosity caused by the wake turbulence of the cars. With this incremental eddy viscosity function held fixed, they do a creditable job for the other simulation days.

In this report, our A.R.A.P. model will be run in two different modes. First, the predictions are made using the available wind and turbulence fields measured at the GM site to establish the background into which a steady tracer source is released. Second, the calculations are repeated with all the turbulent correlations predicted by our planetary boundary layer model with the addition of simulated car wakes.

SECTION 2

CONCLUSIONS AND RECOMMENDATIONS

By modeling the automobile wake, it is possible to calculate complete turbulence distributions in the immediate vicinity of a roadway. When these velocity variances are used in the prediction of tracer dispersion, good agreement is obtained with the measured distributions of SF_6. The predicted turbulence field indicates that the GM measurements of σ_w near the surface are as much as a factor of 2 low.

As a result of these numerical simulations, we estimate that the effective average emissions rate of SO_4 is 17.3 mg/mile/vehicle. A great deal of uncertainty, however, surrounds this number because of the assumptions made on the background SO_4 level.

We also conclude that buoyancy is relatively unimportant to dispersion in the immediate proximity of the roadway where the towers were located.

The computer time required for our program's prediction (of up to 1 hour of c.p.u. time on a PDP 11/70) is probably too long for it to be used as an integral part of a three-dimensional air quality model. However, we believe the code could be streamlined to produce a viable three-dimensional unsteady code using the A.R.A.P. second-order closure technique. One particularly attractive approach to trim the computational restrictions considerably is to integrate across the vertical direction (Ref. 6).

Although the code's present speed is not very good for regional modeling, it is still adequate for the solution of local two-dimensional unsteady phenomena where second-order closure yields the full modeled effect of turbulence.

SECTION 3

GENERAL MOTORS EXPERIMENT

A fleet of 352 late-model automobiles were driven on a north-south track (two lanes each, Figure 1) of 10 km length for 17 test days in 1975 (from Refs. 10 and 11). The cars were grouped into 32 packs of 11 cars each (16 packs per lane), with the lead car averaging 80 km/hr. Uniformly spaced throughout the automobiles were eight pick-up trucks releasing SF_6 tracer gas (one truck for every four packs). The vehicles also emitted from 2.6 to 52 mg/mile SO_4 sulfate into the air, to be added to the environmental sulfate present at the site. Tests were conducted in the early morning hours.

The traffic passed a tower grid at one pack per 29 seconds. The towers were positioned on an angle to compensate for local terrain, and were placed at distances from the center of the test track of -42.7 m, -14.6 m, 0 m, +16.5 m, +27.7 m and +42.7 m as shown. Two stands further to the east also recorded wind data, but those results are not amenable to a rectangular grid simulation. Each tower measured the wind fields with Gill model 27004 UVW anemometers at three heights: 1.5 m, 4.5 m and 10.5 m (the equipment on the +16.5 m tower was actually positioned back to +14.6 m). Temperatures were recorded on towers 1 and 6 only at the same heights. At different levels (0.5 m, 3.5 m and 9.5 m), collectors measured SF_6 and SO_4 levels.

The SF_6 and SO_4 data are assembled in 30-minute averages and presented in tables in Ref. 11. We decided to discard the first two recorded days (272 and 274) because of faulty SF_6 release data. Because of the complexity and computer time required to exercise our numerical code, we arbitrarily selected the second 30-minute average for the other 15 reported days. The average temperatures on towers 1 and 6 are also given for these periods in Ref. 11. In order to make accurate predictions, it was essential to gain access to the wind fields and turbulence fluctuations. These data were calculated at EPA and given to us. To be consistent with SF_6 and SO_4 data, we averaged the mean wind field turbulence data over the same second-sampling period. Thus, we have 15 cases to simulate, with wind fields and turbulence given, and the results for both SF_6 and SO_4 dispersion available.

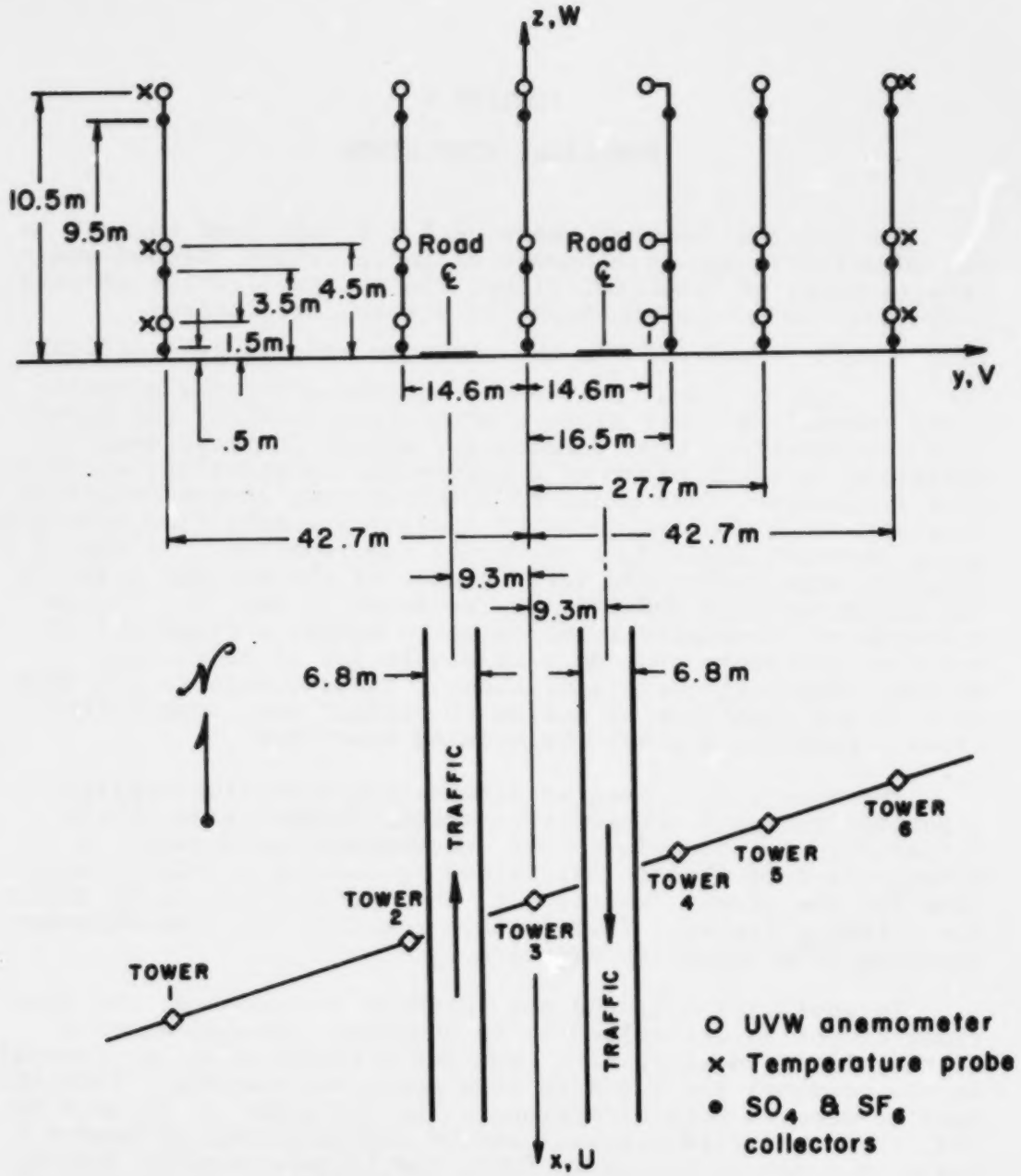

Figure 1. A sketch of the General Motors proving grounds test site, showing the relative positions of the data towers, instruments and traffic pattern.

SECTION 4

NUMERICAL SIMULATION

For the last several years, A.R.A.P. has been engaged in the formulation and development of an invariant, second-order closure model of turbulent flows. In the application of this technique, we retain the Reynolds stress correlations $\overline{u_i u_j}$, $\overline{u_i \theta}$, and $\overline{\theta^2}$ in the momentum and energy equations for U_i and Θ, and write exact equations for the correlations themselves. Our closure comes from modeling the higher-order correlations that necessarily appear in these exact equations in terms of known second-order correlations and mean flow gradients. Such a procedure introduces several modeling constants that are evaluated by examining simple flow configurations in which individual constants are important. A fairly complete examination and verification of the current state of our incompressible modeling may be found in Ref. 2. The assumption of invariance requires us to select a fixed set of modeling constants that do a reputable job of predicting several simple flow configurations. These constants are then used in the equations of motion to predict more complicated flows. Appendix A gives the modeled equations.

The code itself uses an alternating-direction-implicit algorithm to solve the centered-space, forward-time finite difference equations in a y-z rectangular grid mesh. A divergence-free flow is maintained by solving a Poisson equation for the stream function Ψ and differentiating to obtain the velocity fields. This feature requires the time-dependent solution of a vorticity equation.

In application to the near-highway environment, the equations of motion are solved in an unsteady, two-dimensional rectangular grid stretching from -60 m to +60 m in y (normal to the roadway) and 0.2 m to 20 m above the surface. Nonuniform mesh is used in both directions. The $\pm$60 m in y is used so that the boundaries are well beyond the positions of towers 1 and 6, but not so far as to force too large a minimum spacing in y (in this case Δy_{min} = 1 m). The lowest z location of 0.2 m is well above the assumed z_o = 3 cm (Ref. 10) and permits a sufficient number of grid points to establish the wall layer before the 0.5 m tower stations are reached. Likewise, the 20 m top permits several points above the last tower

height of 10.5 m.

Two types of calculations are performed. In the first, we take as given the basic velocity and turbulence fields (interpolated and extrapolated from the 18 measuring points to every one of the grid points in the 32 by 31 mesh). Since the temperature is known only at towers 1 and 6, we initially linearly interpolate its value across the mesh. We then hold the kinetic energy components and velocity field fixed throughout the calculation while the temperature adjusts inside the mesh to a wake source function $\dot{Q}_\theta$. The passive tracer $\dot{Q}_{SF_6}$ is run to establish a steady-state tracer level based on a steady-state wake source. The steady-state solution for SF_6 is appropriately renormalized to give the steady-state SO_4 dispersion predictions.

The second type of calculation involves solving for all the second-order turbulent correlations and mean flow variables with the wake source functions described in the next section. Thus, a consistent set of Reynolds stress correlations is obtained, along with compatible SF_6 and SO_4 levels.

It was necessary to make a correction to the mean wind field data before using them for the first calculation. Namely, the mean wind fields had to satisfy continuity. In order to effect this, we used the cross-wind velocity levels V to obtain the vorticity $\eta = \partial V/\partial z$ (the W contributions to η are negligible), solve the Poisson equation for the stream function, and differentiate to obtain divergence-free flow profiles for V and W . In all cases, the resulting V profiles are relatively unchanged from the measured levels, while the W profiles show some cross-sectional variation from the values measured. With the satisfaction of continuity, however, we can be sure that no extraneous sources or sinks are introduced into the simulation.

For boundary conditions we assumed that the neutral law-of-the-wall held along the lowest z row at 0.2 m, and that no heat or tracer mass was transferred to the surface ($\partial\theta/\partial z = 0$; $\partial C/\partial z = 0$). The inflow boundary (either at $\pm$60 m) was held at the conditions measured at the closest tower, while the outflow boundary and the top were permitted a zero slope condition. This assumption enabled the tracer to pass easily through the downstream boundary in any of the strong cross-wind cases studied. Since the critical fluxes $\overline{uw}$, $\overline{vw}$, $\overline{cw}$ and $\overline{w\theta}$ were not given, we also assumed that they exhibited a zero slope inflow condition. Such an assumption could prove ambiguous at an inflow boundary, but in this case, it does not seem to have bothered the results.

The initial values of the vorticity and stream function are obtained by differentiation and integration of the cross-

wind velocity V as mentioned above. The procedure is as follows.

We assume that

$$\eta = \frac{u^*}{\kappa z}$$
$$\Psi = -\frac{u^*}{\kappa[z\,\ell n(z/z_o) - z + z_o]} \qquad (1)$$

from the neutral wall conditions, where

$$\frac{u^*}{\kappa} = \frac{V}{\ell n(z/z_o)} \qquad (2)$$

and V is taken from the $z = 1.5$ m upstream tower. For $1.5\text{ m} < z < 4.5$ m, we assume that η is constant and equal to the difference in measured V values divided by the 3 m height difference. Between $4.5\text{ m} < z < 10.5$ m, η is likewise assumed constant, while above 10.5 m, we assume that η falls off inversely with z.

To obtain the stream function we integrate the known V velocity measurements by a trapezoidal rule, assuming that V grows logarithmically with z above 10.5 m. Along the top of the computational domain, we set $\partial\Psi/\partial z = -V$ while at $z = 0.2$ m we use the neutral law-of-the-wall condition

$$\frac{\partial\Psi}{\partial z} - \Psi\,\frac{\ell n(z/z_o)}{z\,\ell n(z/z_o) - z + z_o} = 0 \qquad (3)$$

To set the temperature levels, we assume that the upstream temperature reading at the lowest data height is the effective θ_o, and then compute the temperature as a variation from that value, i.e.,

$$\theta = (\text{measured temperature}) - \theta_o + \Gamma(z - 1.5) \qquad (4)$$

where Γ is the adiabatic lapse rate of $0.00976°C/m$.

A typical computation for the complete steady-state simulation may take up to 1 hour of c.p.u. time on our in-house PDP 11/70.

SECTION 5

AUTOMOBILE WAKE MODEL

It is beyond the scope of the present work to develop completely rigorous wake source functions for all the variables. Due to the mixture of cars used and the spacing chosen, considerable uncertainty exists in both the drag characteristics and the SO_4 emissions. This was a principal reason for choosing to take a first cut at simulation using the turbulence and winds measured by GM. For the first mode of calculation, then, only the models for heat release and SF_6 release had to be determined. Much of the desirability of this type of calculation is undermined by an apparent error in the data fields (particularly the $\overline{ww}$ correlation). An examination of the wind and turbulence left by the cars is then needed to make an estimate of the appropriate source terms for the second calculation where the full turbulence fields are predicted.

The effect of the automobile traffic on the equations of motion will center on several source terms added to the equations for the velocity U, temperature θ, passive tracer C, and energies q^2, $\overline{uu}$, $\overline{vv}$, and $\overline{ww}$. For simplicity, we choose to parameterize the wake of the automobiles in each pair of lanes as a single Gaussian source centered about the middle of each dual lane at ± 9.3 m as seen in Figure 1. Since the automobiles are close to the ground, we assume a ground release, so that only a half Gaussian actually exists.

It was assumed that the effective steady-state cross-section of the automobile wake is twice the roadway width, $\sigma_y = 6.8$ m. From a Masters' thesis by Brander (Ref. 14), wherein he concluded that a single body wake is half as tall as wide, we take $\sigma_z = 1.7$ m since we are dealing with two lanes of traffic. The total area under the Gaussian half source is then $\dot{Q}\pi\sigma_y\sigma_z/4$ with $\dot{Q}$ the maximum source strength. With the automobiles traveling in packs of 11 every 29 seconds, we can estimate <u>average</u> <u>steady</u> distance between cars to be

$$L_c = \left(\frac{80 \text{ km}}{\text{hr}}\right) \frac{(29 \text{ sec/pack})}{(11 \text{ cars/pack})} = 58.6 \text{ m/car} \qquad (5)$$

The effective rate of heat release is given as an average of 0.11 megajoules/sec/vehicle (Ref. 10). For a typical hydrocarbon C_8H_{18} (heat of formation = 11.4 Kcal/gm; density =

= 0.7 Kg/ℓ) this figure would correspond to 15.6 mpg. With the c_p of air factored in, this yields an incremental temperature release of 93 m^3°C/sec. Thus, the amplitude of the continuous source function for heat from two lanes of traffic when modeled as a Gaussian ground release is given by

$$L_c \dot{Q}_\Theta \frac{\pi \sigma_y \sigma_z}{2} = 2(93 \text{ m}^3\text{°C/sec}) \qquad (6)$$

or

$$\dot{Q}_\Theta = 0.175\text{°C/sec}$$

The velocity source term should come from the effective drag of the vehicles. Thus, we would expect

$$\frac{\dot{Q}_U \pi \sigma_y \sigma_z L_c}{4} = \tfrac{1}{2} C_D V_a^2 A \qquad (7)$$

where C_D is the automobile drag coefficient, V_a is the effective ambient wind and A is the automobile frontal area. An average drag coefficient from White (Ref. 15) is taken as $C_D = 0.45$ assuming that each car sees a mean wind of $V_a = 80$ km/hr. (Since the cars follow in packs, this assumption is not a particularly good one, because the interactive dynamics of 11 cars would tend to decrease either the effective C_D or wind V_a. The precise amount of this reduction is difficult to predict.) For purposes of the second set of calculations, we choose a maximum value for the axial momentum source strength for our assumed wake geometry of

$$\dot{Q}_U = 0.100 \text{ m/s}^2 \qquad (8)$$

This corresponds to a car frontal area $A = 1.5$ m^2 and the total effective drag reduced by 64 percent.

Since the energy lost to drag goes directly into turbulent kinetic energy, it is consistent to take

$$\dot{Q}_{q^2} = \frac{2 C_D V_a^3 A}{\pi \sigma_y \sigma_z L_c} = \dot{Q}_U V_a = 2.22 \text{ m}^2/\text{s}^3 \qquad (9)$$

The release of the SO_4 sulfate was determined in Ref. 11 to fall anywhere between 2.6 and 52 mg/mile per vehicle. This is quite a wide range. For our analysis we assume that the average release was S mg/mile, and determine S by matching our predictions of SO_4 with a least-squares fit of the measured values over the 15 test periods studied. If the GM experiment pinpointed the overall average release of the SO_4, that number could have been used and no parameterization would have been necessary. The S mg/mile figure translates to a release of 0.0138S mg/sec; to give

$$\dot{Q}_{SO_4} \frac{\pi \sigma_y \sigma_z L_c}{4} = 0.0138S \qquad (10)$$

or

$$\dot{Q}_{SO_4} = 0.026S \text{ microgms/m}^3\text{sec} \qquad (11)$$

The experiments attempted to maintain an SF_6 flow rate of 0.5 ℓ/min, although some departure from this rate did occur as shown in Table VII of Ref. 11, particularly when one of the trucks did not release the tracer. In these cases, the actual released average must be ratioed with a "perfect" average of 4 ℓ/min (eight trucks) to establish the release rate for each of the 15 cases to be simulated. Since the density of SF_6 is 6.6 gm/ℓ and its molecular weight is 146.05, the effective flow rate of the SF_6 gas is

$$\dot{c} = \frac{(0.5 \text{ ℓ/min})(6.6 \text{ gm/ℓ})}{6.18 \text{ kg/m}^3} = 9 \times 10^{-6} \text{ m}^3/\text{sec} \qquad (12)$$

Thus, for a steady-state emission of the SF_6 ,

$$\dot{Q}_{SF_6} \frac{\pi \sigma_y \sigma_z L_t}{4} = \dot{c} \qquad (13)$$

or

$$\dot{Q}_{SF_6} = 0.380 \text{ ppb/sec} \qquad (14)$$

where L_t is the average distance between trucks

$$L_t = L_c \frac{352 \text{ cars}}{8 \text{ trucks}} = 2580 \text{ m} \quad . \qquad (15)$$

A possible discrepancy in using $\dot{Q}_{SF_6}$ as a steady-state release might lie in the frequency at which the trucks pass the instruments. Since the trucks are also moving at 80 km/hr, we see that the time between truck passages is

$$\Delta t_t = \frac{L_t}{80 \text{ km/hr}} = 120 \text{ sec} \qquad (16)$$

Since the average winds recorded by the data are about 2 to 3 m/s, even a light cross-wind will convect the released SF_6 past the towers before the next truck passes the instruments. However, since the experiment involves integrating over the time dependence of the SF_6 release, and the diffusion equation is linear with respect to species concentration, a steady release is mathematically equivalent to a series of intensive puff releases.

The critical assumption is that the turbulent velocity fluctuations are stationary during the diffusion process. This may be questionable since the truck wake into which the SF_6 was released may be expected to be somewhat different from the ensemble mean car wake.

SECTION 5

MODEL RESULTS

We present the results of 30 different simulations. One averaging period for each of the 15 reported test days has been simulated using both calculation modes. In this section of the report, we present detailed results for two representative days (293 and 296) and summary comparisons between all the simulations and data. Appendix B contains the SF_6 and SO_4 contour predictions for the other 13 test days.

FIXED TURBULENCE PREDICTIONS

Because there exists a considerable amount of uncertainty in the wake source parameters (e.g., σ_y, σ_z, V_a, A and C_D), we first predicted the SF_6 and SO_4 fields by fixing the turbulence and mean wind (satisfying continuity) and solving for the dispersion of a steady source representing the sulfate and SF_6 tracer emissions. To this end, then, we selected the second averaging period for each of the reported test days after the first two, established the input conditions from the data supplied to us by EPA personnel or found in Ref. 11, and then ran the code to see the effects of our temperature and species source strengths. Figures 2 and 3 present the contour curves for the ΔSO_4 predictions for days 293 and 296. Here we have removed the background sulfate level to give the automobile emission effect.

In order to use our results to predict the SO_4 distributions, we needed to make several auxiliary assumptions. First, we have *a priori* assumed that no chemistry occurs. Therefore, our steady-state passive tracer levels may be conveniently scaled to give the SO_4 levels. To do this, we averaged the three upwind SO_4 levels recorded by Cadle, et al. (Ref. 11) and assumed that this value was the ambient value for the particular run in question. Subtracting this value everywhere gives us a ΔSO_4 level at each tower point for each of the 15 runs. A least-squares fit is then used to determine the effective SO_4 emission rate; in this case, S = 28.9 mg/mile for each vehicle. This level of emission then multiplies our steady-state prediction for each of the 15 test periods to obtain our ΔSO_4 predictions through all simulations. The rest of the contours are shown in Appendix B. A plot of the predicted levels at the 18 tower positions against the measured levels for all 15 test days

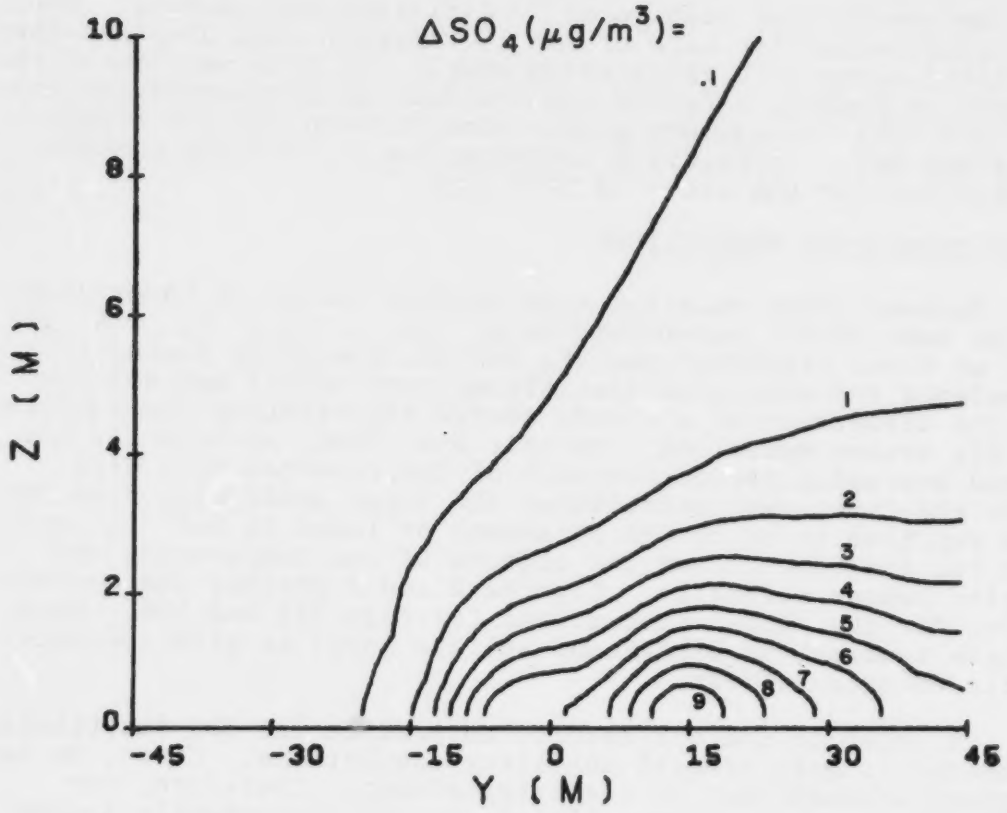

Figure 2. Contours of predicted ΔSO_4 levels (above background) using the measured GM mean wind fields and turbulence data for the second test period of day 293. In this case the ambient winds were nearly cross-wind to the traffic, and S = 28.9 mg/mile/vehicle. When the background SO_4 level is included, S = 16.2 mg/mile/vehicle, so that the ΔSO_4 levels shown here should be multiplied by a factor of 0.56 .

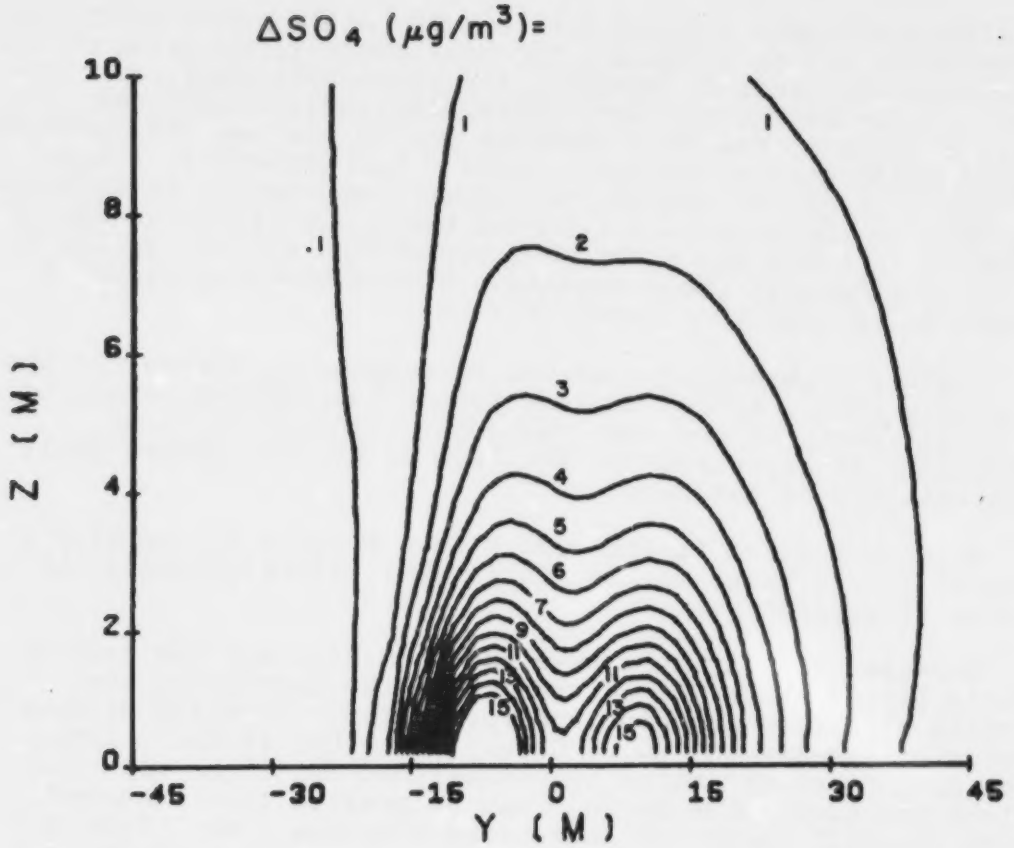

Figure 3. Contours of predicted ΔSO_4 levels (above background) using the measured GM mean wind fields and turbulence data for the second test period of day 296. In this case the ambient winds were nearly aligned with the traffic, and S = 28.9 mg/mile/vehicle.

is shown in Figure 4. Since the data were used to correlate with the predictions, the points on Figure 4 are forced to scatter about a 45° line. When the assumed average background levels of SO_4 are added to the ΔSO_4 levels, the considerably less-scatter point plot of Figure 5 results, where a match of the data with the predictions gives an emissions level of S = 16.2 mg/mile/vehicle. Clearly, our assumption on the background level is very important.

Although Figure 5 looks like a much better correlation, it is partially illusory because the relatively large value of the background SO_4 tends to dominate the automobile wake contribution. If the background level were completely determined, then Figure 4 would be the more accurate way to present the comparison between measurements and predictions. Unfortunately, a significant part of the scatter in Figure 4 appears to be directly traceable to the uncertainty in the background level caused by variation in the three upwind SO_4 measurements. We are led to the conclusion that the emissions estimate based on Figure 5 is more valid than that based on Figure 4.

Figures 6 through 8 show the corresponding curves for the SF_6 predictions. As can be seen from Figure 8 these predictions are consistently higher than the data. Since we have no flexibility in adjusting the SF_6 levels, we must either fault the prediction or the data.

A least-squares fit through Figure 8 gives a line with a slope of 1.77. Thus, we are, in general, overpredicting the data by 77 percent.

Because we apparently have too much SF_6 near the source and too little above it, we are led to the conclusion that vertical diffusion is being underpredicted. Vertical diffusion depends critically on $\overline{ww}$. Chock (Ref. 10), in fact, lays doubt upon these estimates by noting that for light wind conditions the true value of σ_w may be greater than measured due to the Gill model UVW anemometer response time. This apparent discrepancy in the data led us to consider solving for the complete wind fields; those results and a further examination of our automobile model are now presented.

FULL TURBULENCE PREDICTIONS

Since the $\overline{ww}$ levels at the 1.5 m height in the GM data are considered to be too low to give a good prediction of the SF_6 results, we proceeded to compute the full solution of the wind and turbulence field using second-order closure, enabling

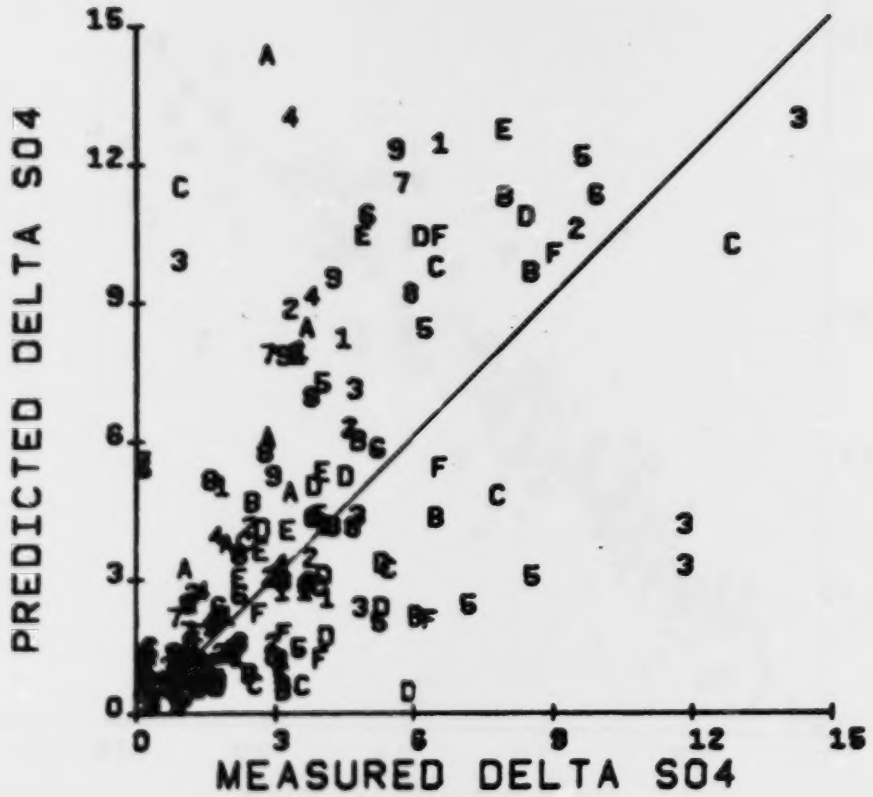

Figure 4. A point-plot of the predicted vs measured levels of ΔSO4 using the measure GH mean wind fields and turbulence data with an assumed emission level of S = 20.9 mg/mile/vehicle. Each second-period sample from the 15 simulated days contributes 18 points to this plot. The days are denoted as: 1 = day 275; 2 = day 276; 3 = day 279; 4 = day 281; 5 = day 283; 6 = day 286; 7 = day 290; 8 = day 293; 9 = day 294; A = day 295; B = day 296; C = day 297; D = day 300; E = day 302; and F = day 303.

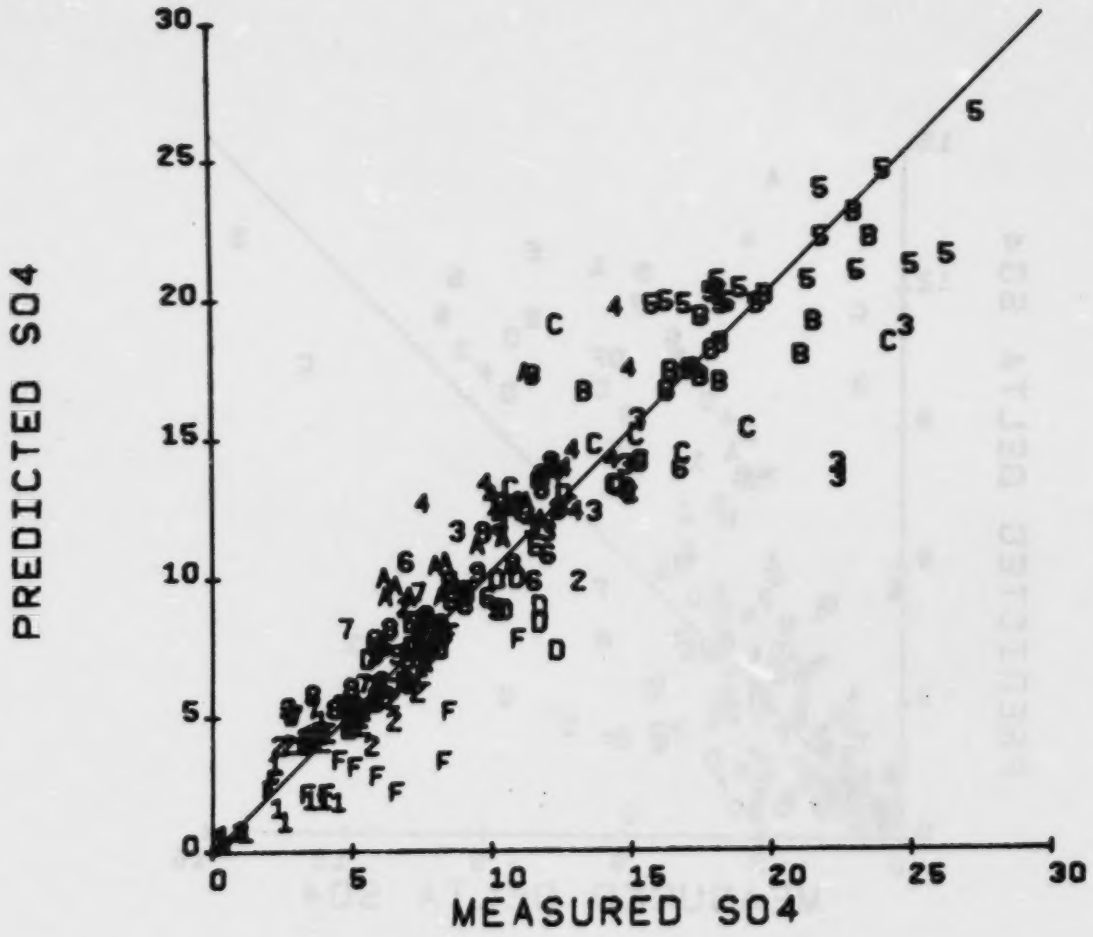

Figure 5. A point-plot of the predicted vs measured levels of total SO_4 using the measured GM mean wind fields and turbulence data with an assumed emission level of S = 16.2 mg/mile/vehicle based on the ΔSO_4 levels plus the mean ambient background. Each second-period sample for the 15 simulated days contributes 18 points to this plot, as denoted in Figure 4.

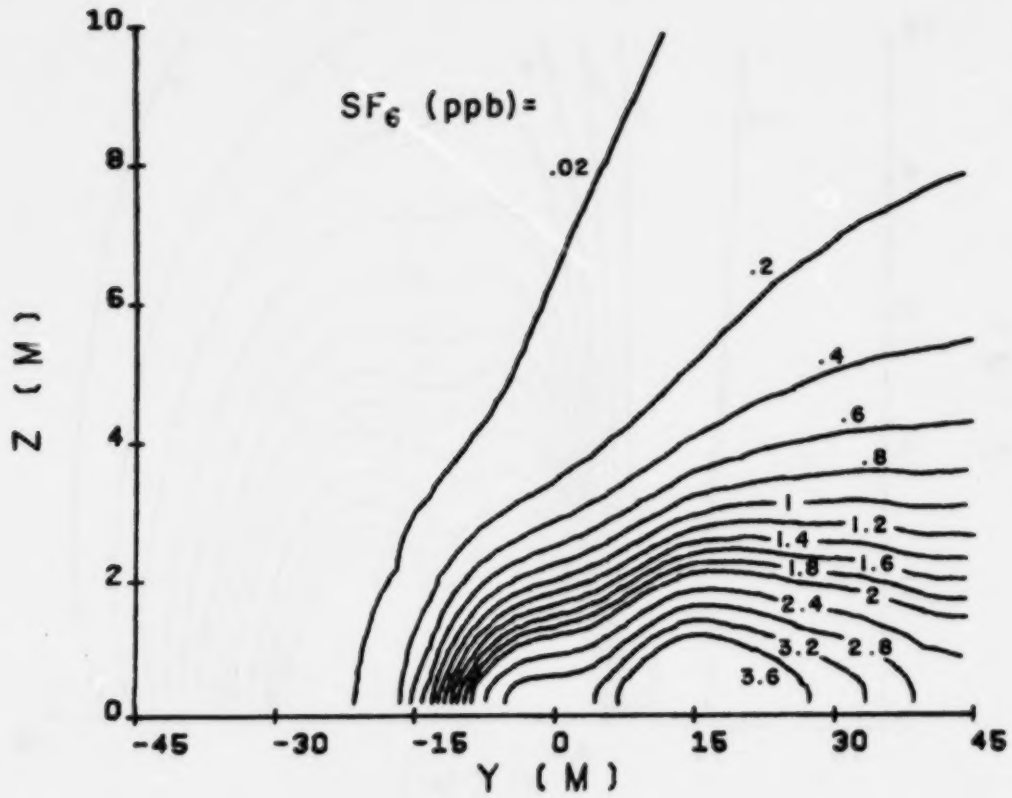

Figure 6. Contours of predicted SF_6 levels using the measured GM mean wind fields and turbulence data for the second test period of day 293.

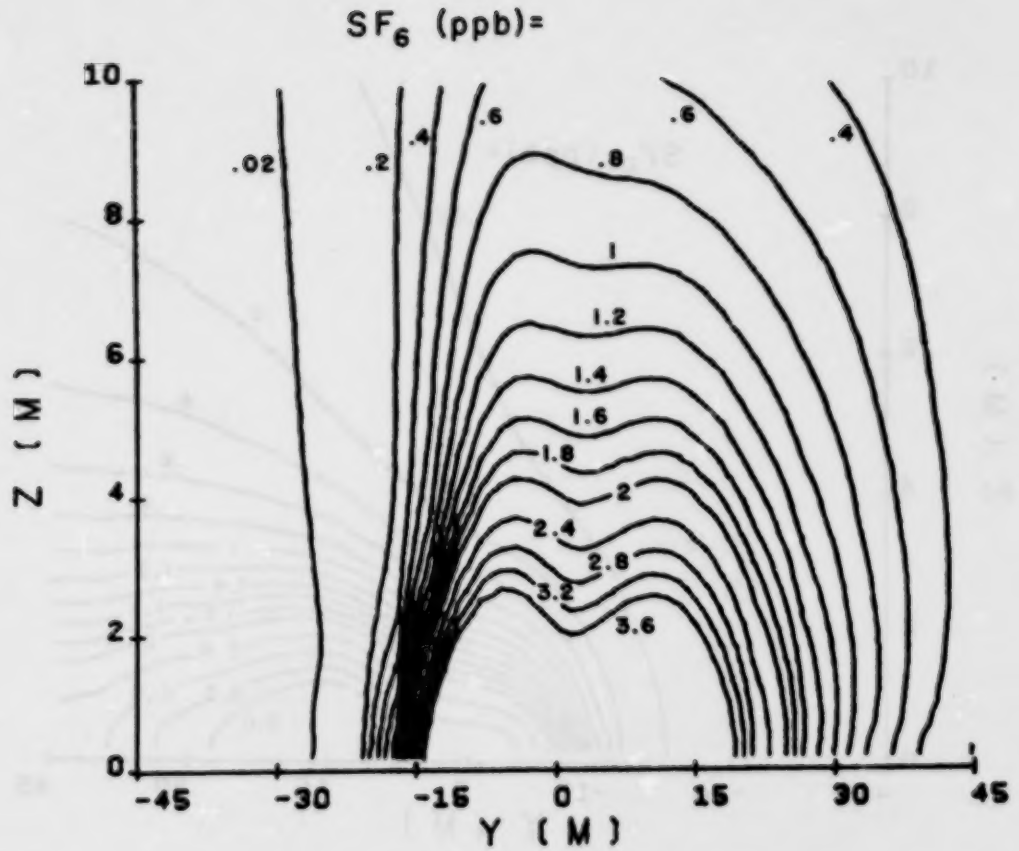

Figure 7. Contours of predicted SF_6 levels using the measured GM mean wind fields and turbulence data for the second test period of day 296.

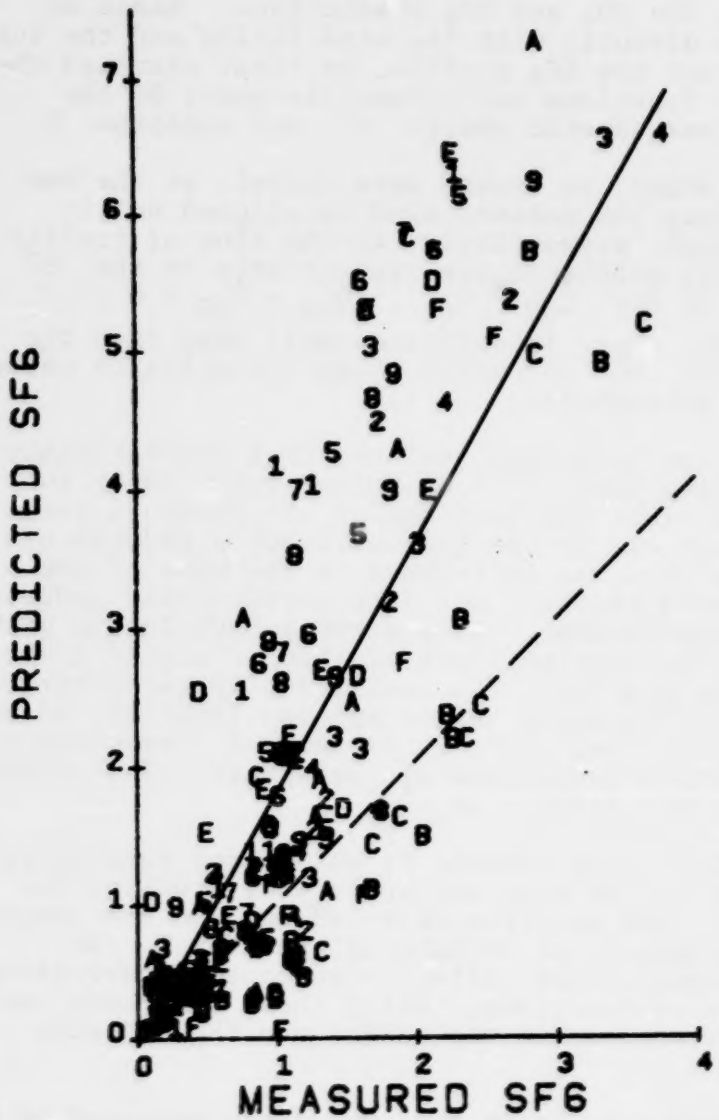

Figure 8. A point-plot of the predicted vs measured levels of SF_6 using the measured GM mean wind fields and turbulence data showing a least-square slope of 1.77. Each second-period sample from the 15 simulated days contributes 18 points to the plot. The days are numbered in ascending order with the keys explained in Figure 4.

us to provide at least a consistent $\overline{ww}$ prediction for the turbulent background of the SO4 and SF_6 predictions. Since we are now dealing more directly with the wind fields and the turbulence levels, and not the SF_6 profile, we first examined the effect of the source functions and automobile model on the generation of turbulent kinetic energy q^2 and momentum U .

To perform the study, we looked more closely at the two days 293 and 296, where the ambient wind is aligned nearly cross-wind and parallel, respectively, to the flow of traffic. Since the U velocity gradients are present only in the $\overline{uu}$ equation, we choose to set $Q_{\overline{uu}} = Q_{q^2}$, $Q_{\overline{vv}} = Q_{\overline{ww}} = 0$. Isotropy and turbulent shear interactions will feed into the equations for $\overline{vv}$ and $\overline{ww}$ to enable these variables to reflect the presence of the automobiles.

When the first car in a pack goes by, that car certainly encounters an effective wind V_a = 80 km/hr, since 25 or so seconds have elapsed since the last car of the previous pack went by. But the next car in the pack will see a reduced effective wind because this car is trapped in the wake of the first (drafting in auto racing), not also incidentally reducing its effective drag coefficient. Cars further back in the pack feel the effects of the cars in front of them to create a very difficult engineering problem. For comparison in the laboratory experiment of Chevray for wakes behind spheres (Ref. 2), we saw that the velocity defect was about 35 percent of freestream at a station five diameters downstream of the sphere. This number would give an effect of $(.65)^3$ in Q_{q^2} .

Taking this effect into account in our source functions, we obtain a consistent set of mean and turbulence profiles for all simulation days. The specific days 293 and 296 are compared with the smoothed interpolated GM data in Appendix C. We believe that these comparisons reflect a reasonable representation of the wake source functions. Using these functions, we now repeat the calculations for the $\Delta SO4$ and SF_6 emission levels.

The biggest difference is in the $\overline{ww}$ field measured by GM. Near the surface the predicted $\overline{ww}$ is approximately twice the reported data value. We believe this is a reflection of the relatively slow response time of the Gill anemometer. Even on the upwind towers, $\overline{ww}$ at the bottom measuring station (at 1.5 m) reports a value which is a factor of 2 lower than reported at 4.5 m. In the nearly neutral surface layer, $\overline{ww}$ should be constant with height. However, the characteristic time of the vertical fluctuations is a factor of 3 shorter at 1.5 m height than it is at the 4.5 m station.

The new predictions for SO_4 dispersion using the predicted turbulence and a steady pollutant source are given in Figures 9 and 10 for days 293 and 296 and may be compared with Figures 2 and 3. The new summary plots of predicted vs measured for all the cases predicted in this manner are given in Figures 11 and 12. The best estimate of the SO_4 emission rate based on ΔSO_4 levels is 51.7 mg/mile/vehicle, with a root-mean-square error from the linear curve fit of 0.574 . The SO_4 emission rate based on total SO_4 level is 17.3 mg/mile/vehicle, with a reduced root-mean-square error of 0.326 . As previously discussed, we believe the latter emissions estimate to be the more valid.

The difference in the SF_6 predictions is more striking since there is no uncertainty in the emissions rate in this case. Figures 13 and 14, which show the results of the simulation with the predicted turbulence, may be compared with Figures 6 and 7. By increasing $\overline{ww}$ near the surface, more of the SF_6 is moved away from the wake source to the top measuring stations. The comparison between predicted and measured values is now quite favorable (0.96) as seen in Figure 15. In this case, the root-mean-square error is 0.306.

The reason the difference between measurements and predictions shows a larger scatter for SO_4 (Figure 11), than for SF_6 (Figure 15) is most likely a reflection of the uncertainty in the background level. The upwind tower seldom showed the same SO_4 level at all three instruments. This indicates an ambient transfer of SO_4 between the surface and the atmosphere which would be disturbed by the automobile wake turbulence even without any SO_4 emissions. There is also the possibility of chemical transformations affecting the SO_4 dispersion.

The relative influence of buoyancy in the problem may be found by ratioing the integrated buoyancy term in the turbulent energy equation to the integrated dissipation rate. Thus, we write

$$B = \frac{8 \iint \frac{g}{\theta_o} \overline{w\theta} \, dA}{\iint \frac{q^3}{\Lambda} \, dA} \qquad (17)$$

Evaluating B for the predicted turbulence fields gives a value of B no larger than 0.109 for the aligned cases and 0.065 for the cross-wind cases. The effects of buoyancy in setting the turbulence field are thus quite small. A fundamental reason why the Gaussian plume model does not predict the GM data well is then the lack of any substantial influence of the wake turbulence fields, not the fact that buoyancy is not included.

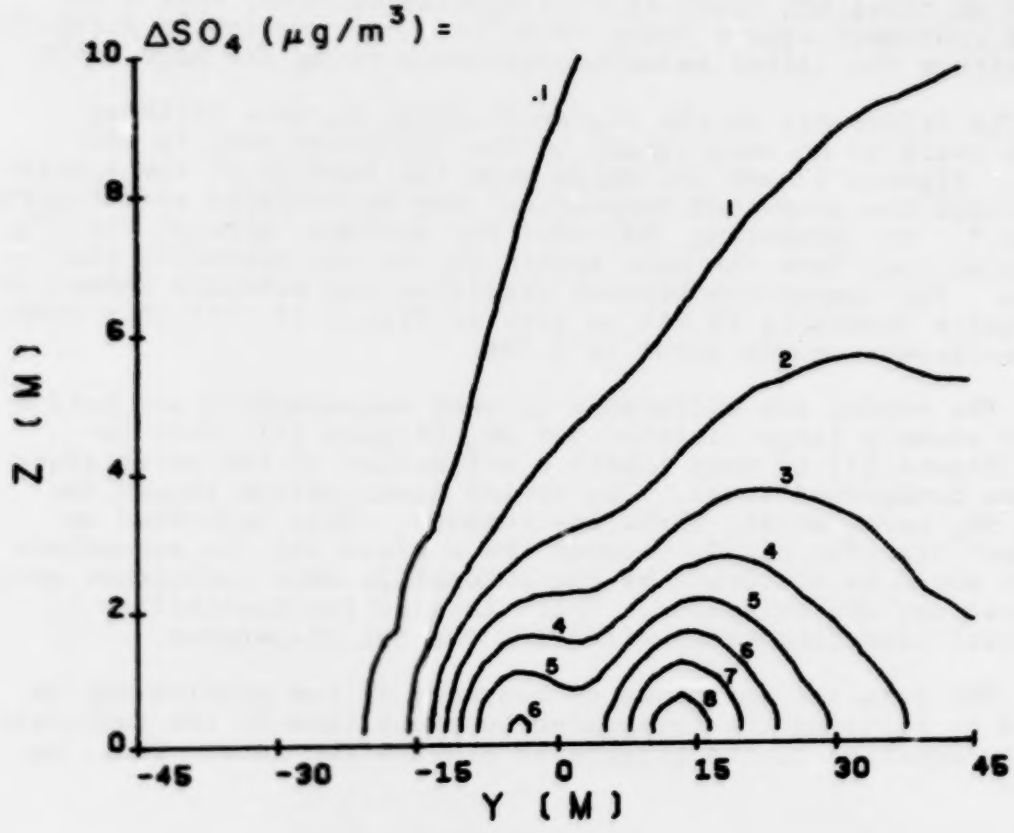

Figure 9. Contours of predicted ΔSO_4 levels (above background) using the predicted mean wind fields and turbulence data for the second test period of day 293, with S = 51.7 mg/mile/vehicle. When the background SO_4 level is included, S = 17.3 mg/mile/vehicle, so that the ΔSO_4 levels shown here should be multiplied by a factor of 0.33 .

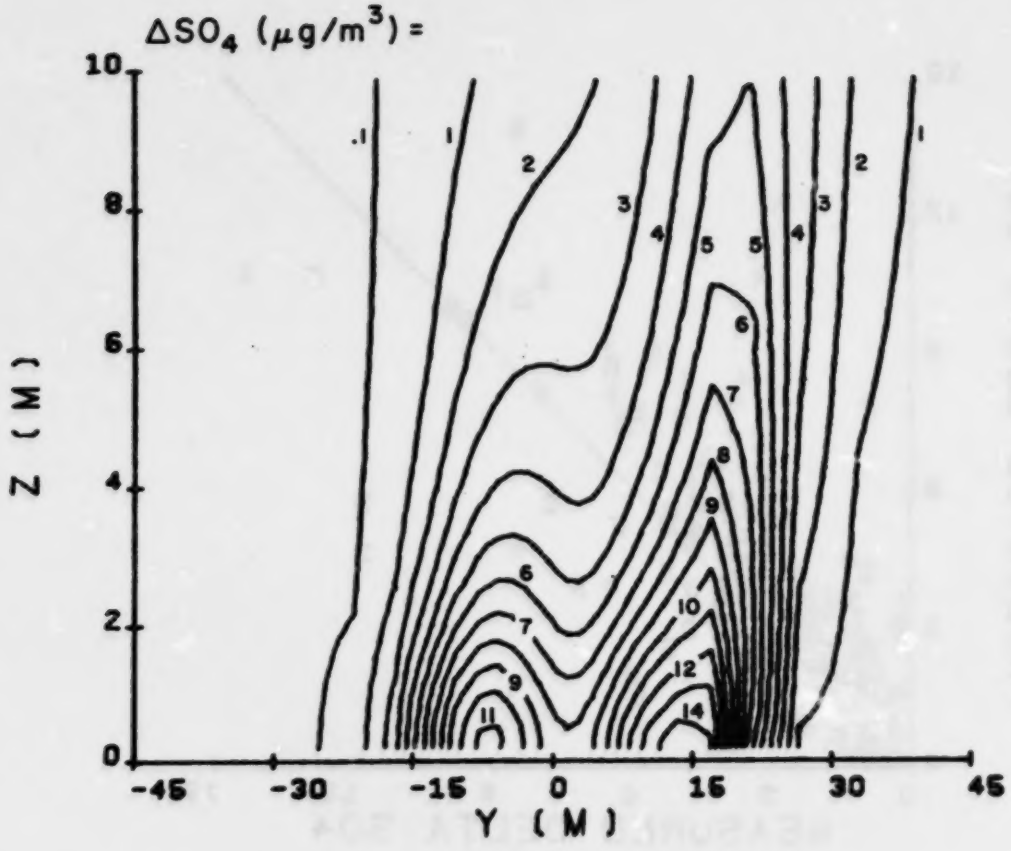

Figure 10. Contours of predicted ΔSO_4 levels (above background) using the predicted mean wind fields and turbulence data for the second test period of day 296, with S = 51.7 mg/mile/vehicle.

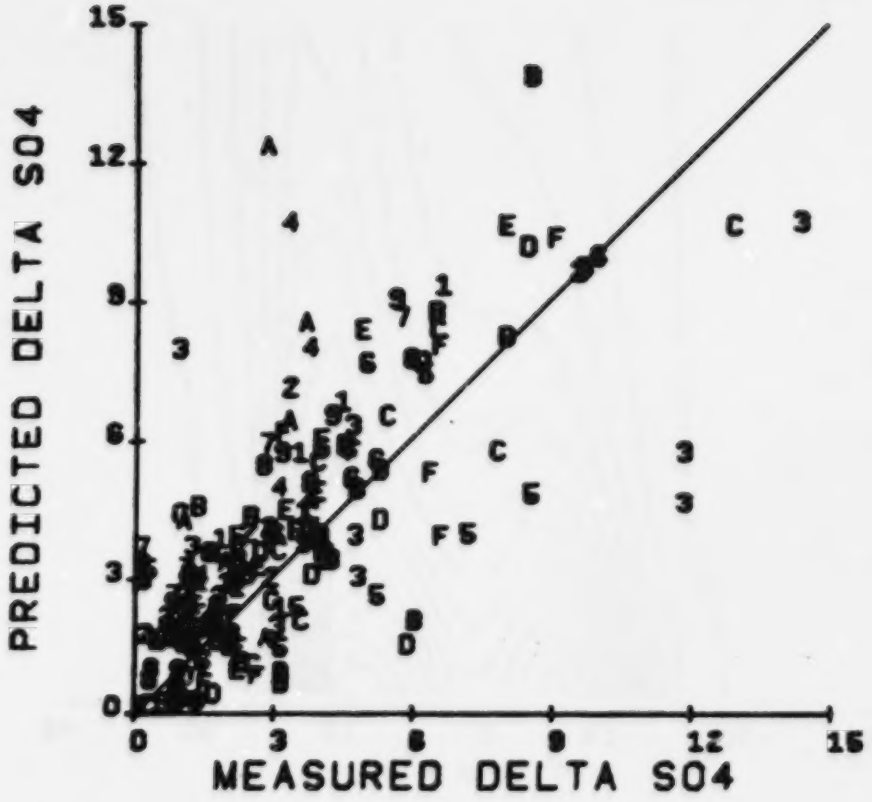

Figure 11. A point-plot of the predicted vs measured levels of ΔSO_4 using the predicted mean wind fields and turbulence data with an assumed emission level of S = 51.7 mg/mile/vehicle. The notation is discussed in Figure 4.

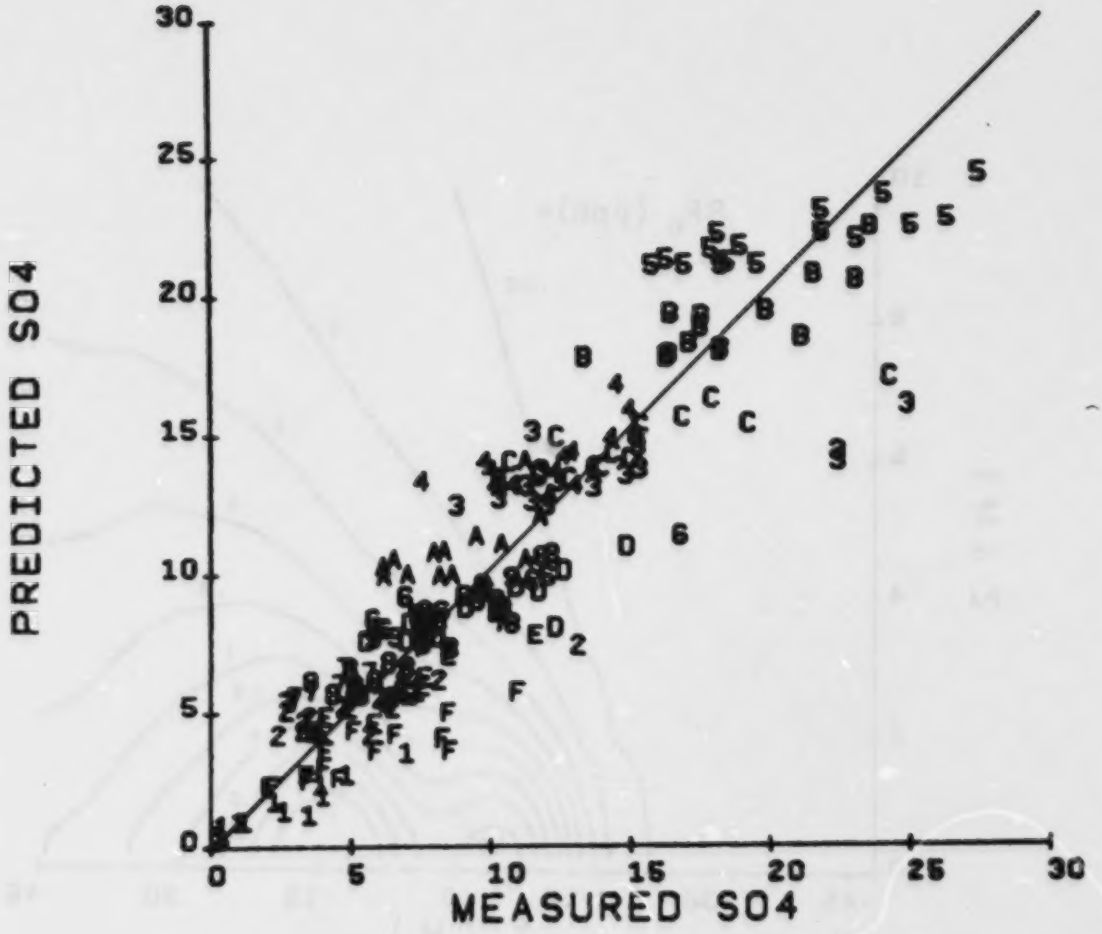

Figure 12. A point-plot of the predicted vs measured levels of total SO_4 using the predicted mean wind fields and turbulence data with an assumed emission level of S = 17.3 mg/mile/vehicle based on the ΔSO_4 levels plus the mean ambient background. The notation is discussed in Figure 4.

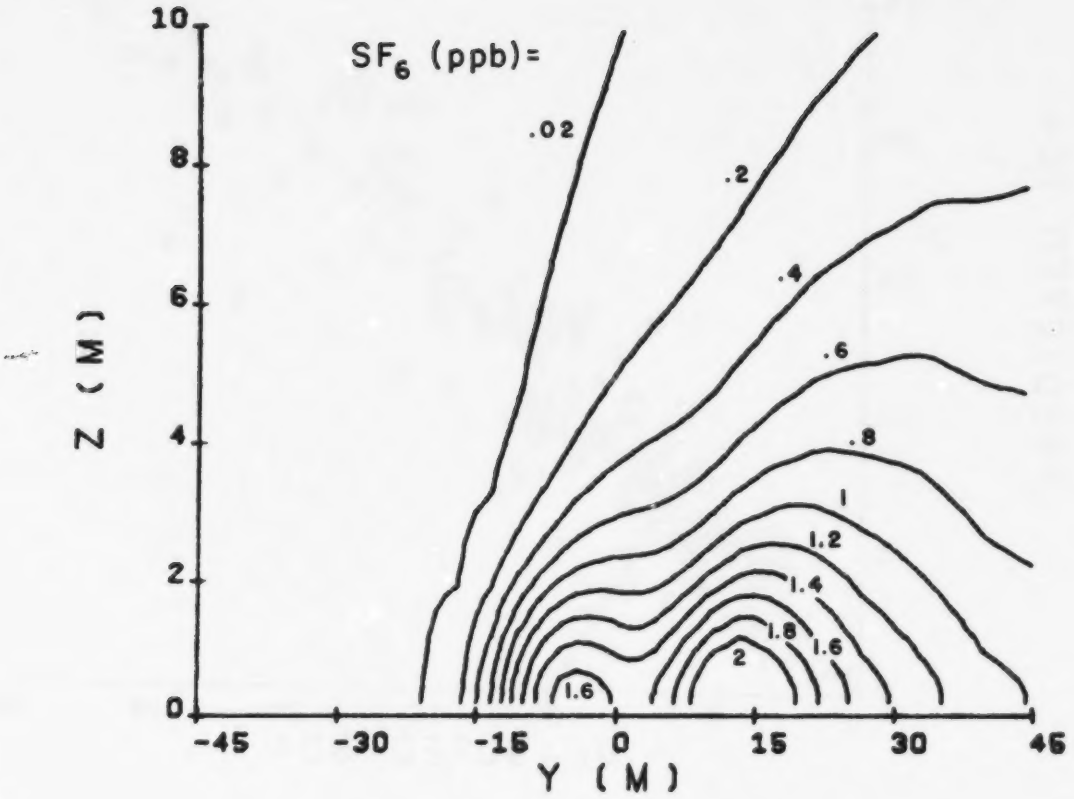

Figure 13. Contours of predicted SF_6 levels using the predicted mean wind fields and turbulence data for the second test period of day 293.

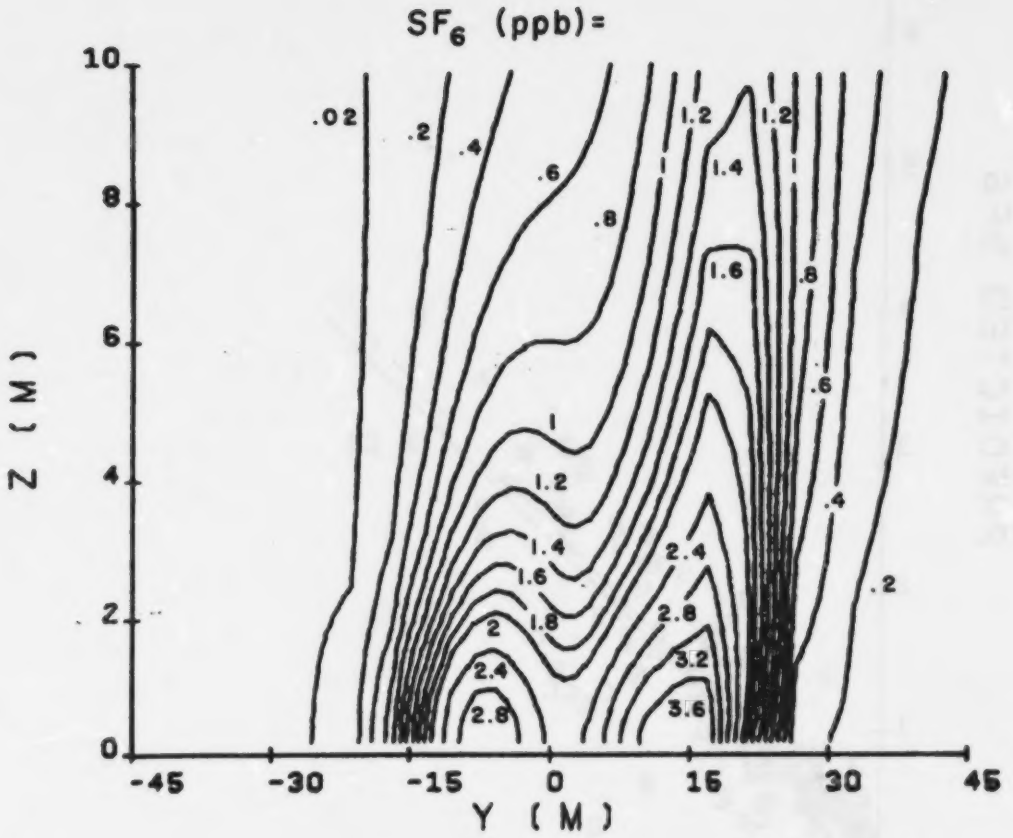

Figure 14. Contours of predicted SF_6 levels using the predicted mean wind fields and turbulence data for the second test period of day 296.

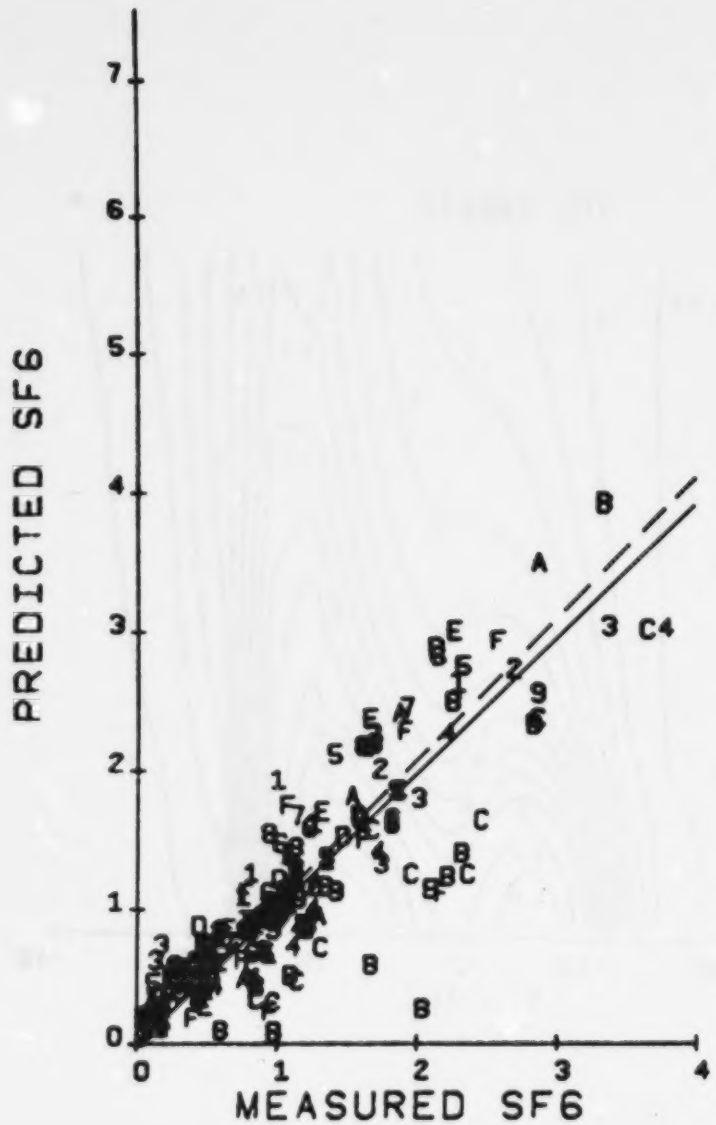

Figure 15. A point-plot of the predicted vs.measured levels of SF_6 using the predicted mean wind fields and turbulence data, showing a least-square slope of 0.96. The notation is discussed in Figure 4.

REFERENCES

1. Donaldson, C.duP. Atmospheric Turbulence and the Dispersal of Atmospheric Pollutants. In: Proceedings of the Workshop on Micrometeorology (D.A. Haugen, ed.), American Meteorological Society, 1973. pp. 313-390.

2. Lewellen, W.S., and M.E. Teske. Turbulence Modeling and Its Application to Atmospheric Diffusion. EPA-600/4-75-016, U.S. Environmental Protection Agency, Research Triangle Park, NC, 1975.

3. Teske, M.E., and W.S. Lewellen. Turbulence Transport Model of a Thunderstorm Gust Front. In: Proceedings of 10th Conference on Severe Local Storms, American Meteorological Society, Omaha, NE, 1977. pp. 143-150.

4. Lewellen, W.S., and M.E. Teske. Turbulent Transport Model of Low-Level Winds in a Tornado. In: Proceedings of 10th Conference on Severe Local Storms, American Meteorological Society, Omaha, NE, 1977. pp. 291-298.

5. Bilanin, A.J., M.E. Teske, and J.E. Hirsh. The Role of Atmospheric Shear, Turbulence and a Ground Plane on the Dissipation of Aircraft Vortex Wakes. AIAA 16th Aerospace Sciences Meeting, Paper 78-110, 1978.

6. Teske, M.E., W.S. Lewellen, and H. Segur. Turbulence Modeling Applied to Buoyant Plumes. U.S. Environmental Protection Agency, Research Triangle Park, NC, 1977.

7. Lewellen, W.S., M.E. Teske, R. Contiliano, G. Hilst, C.duP. Donaldson. Invariant Modeling of Turbulence and Diffusion in the Planetary Boundary Layer. EPA-650/4-74-035, U.S. Environmental Protection Agency, Research Triangle Park, NC, 1974.

8. Teske, M.E., and W.S. Lewellen. Example Calculations of Atmospheric Dispersion Using Second-Order Closure Modeling. In: Proceedings 3rd Symposium on Atmospheric Turbulence, Diffusion and Air Quality, American Meteorological Society, Raleigh, NC, 1976. pp. 149-154.

9. Teske, M.E., W.S. Lewellen, and H. Segur. Example Calculations of Buoyant Plume Dispersal Into Stable Atmospheres. In: Proceedings of Joint Conference on Applications of Air

Pollution Meteorology, American Meteorological Society, 1977. pp. 283-290.

10. Chock, D.P. General Motors Sulfate Dispersion Experiment: An Overview of the Wind, Temperature and Concentration Fields. GMR-2231.

11. Cadle, S.H., D.P. Chock, J.M. Heuss, P.R. Monson. Results of the General Motors Sulfate Dispersion Experiment. GMR-2107.

12. Maugh, T.H. II. Sulfuric Acid From Cars: A Problem That Never Materialized. Science, 198:280-284, 1976.

13. Eskridge, R.E., and K.L. Demerjian. A Highway Model for the Advection, Diffusion and Chemical Reaction of Pollutants Released by Automobiles: Part I - Advection and Diffusion of SF_6 Tracer Gas. In: Proceedings of Joint Conference on Applications of Air Pollution Meteorology, American Meteorological Society, 1977. pp. 337-342.

14. Brander, J.A. Dispersion of Pollutants in the Wakes of Blunt Objects. M.S. Thesis, Massachusetts Institute of Technology, 1974.

15. White, R.G.S. A Method of Estimating Automobile Drag Coefficients. SAE Transactions, 78:829-835, 1969.

APPENDIX A

THE PROGRAMMED SECOND-ORDER CLOSURE EQUATIONS FOR TWO-DIMENSIONAL, UNSTEADY FLOWS

The ensemble-averaged equations of motion, including the invariantly modeled terms, may be summarized in tensor form as

$$\frac{DU_i}{Dt} = \nu \frac{\partial^2 U_i}{\partial x_j^2} - \frac{\partial \overline{u_i u_j}}{\partial x_j} - \frac{\partial p}{\partial x_i} + \dot{Q}_U \tag{A1}$$

$$\frac{D\Theta}{Dt} = \nu \frac{\partial^2 \Theta}{\partial x_j^2} - \frac{\partial \overline{u_j \theta}}{\partial x_j} + \dot{Q}_\Theta \tag{A2}$$

$$\begin{aligned}\frac{D\overline{u_i u_j}}{Dt} = &-\overline{u_i u_k}\frac{\partial U_j}{\partial x_k} - \overline{u_k u_j}\frac{\partial U_i}{\partial x_k} + \frac{g_i}{\Theta_o}\overline{u_j \theta} + \frac{g_j}{\Theta_o}\overline{u_j \theta} \\ &+ \frac{\partial}{\partial x_k}\left[(\nu + 0.3q\Lambda)\frac{\partial \overline{u_i u_j}}{\partial x_k}\right] \\ &- \frac{q}{\Lambda}\left(\overline{u_i u_j} - \frac{1}{3}\delta_{ij}q^2\right) - \frac{q^3}{12\Lambda}\delta_{ij} + \delta_{i3}\delta_{j3}\dot{Q}_{q^2}\end{aligned} \tag{A3}$$

$$\begin{aligned}\frac{D\overline{u_i \theta}}{Dt} = &-\overline{u_i u_k}\frac{\partial \Theta}{\partial x_k} - \overline{u_k \theta}\frac{\partial U_i}{\partial x_k} + \frac{g_i}{\Theta_o}\overline{\theta^2} \\ &+ \frac{\partial}{\partial x_k}\left[(\nu + 0.3q\Lambda)\frac{\partial \overline{u_i \theta}}{\partial x_k}\right] - \frac{0.75q}{\Lambda}\overline{u_i \theta}\end{aligned} \tag{A4}$$

$$\frac{D\overline{\theta^2}}{Dt} = -2\overline{u_k \theta}\frac{\partial \Theta}{\partial x_k} + \frac{\partial}{\partial x_k}\left[(\nu + 0.3q\Lambda)\frac{\partial \overline{\theta^2}}{\partial x_k}\right] - \frac{0.45q\overline{\theta^2}}{\Lambda} \tag{A5}$$

with

$$q^2 = \overline{u_i u_i} \tag{A6}$$

$$\frac{D\Lambda}{Dt} = \frac{0.35\Lambda}{q^2}\overline{u_i u_j}\frac{\partial U_i}{\partial x_j} + 0.075q + 0.3\frac{\partial}{\partial x_i}\left(q\Lambda\frac{\partial \Lambda}{\partial x_i}\right)$$

$$- \frac{0.375}{q}\left(\frac{\partial}{\partial x_i} q\Lambda\right)^2 + \frac{0.8\Lambda}{q^2}\frac{g_i}{\Theta_o}\overline{u_i\theta} \qquad \text{(A7)}$$

$$g_i = (0,0,g)$$

The equations for C and its correlations may be found from equations similar to those for Θ and its correlations:

$$\frac{DC}{Dt} = \nu\frac{\partial^2 C}{\partial x_j^2} - \frac{\partial \overline{u_j c}}{\partial x_j} + \dot{Q}_c \qquad \text{(A8)}$$

$$\frac{D\overline{u_i c}}{Dt} = -\overline{u_i u_k}\frac{\partial C}{\partial x_k} - \overline{u_k c}\frac{\partial U_i}{\partial x_k} + \frac{g_i}{\Theta_o}\overline{c\theta}$$

$$+ \frac{\partial}{\partial x_k}\left[(\nu + 0.3q\Lambda)\frac{\partial \overline{u_i c}}{\partial x_k}\right] - \frac{0.75q}{\Lambda}\overline{u_i c} \qquad \text{(A9)}$$

$$\frac{D\overline{c\theta}}{Dt} = -\overline{u_k c}\frac{\partial \Theta}{\partial x_k} - \overline{u_k \theta}\frac{\partial C}{\partial x_k} + \frac{\partial}{\partial x_k}\left[(\nu + 0.3q\Lambda)\frac{\partial \overline{c\theta}}{\partial x_k}\right]$$

$$- \frac{0.45q}{\Lambda}\overline{c\theta} \qquad \text{(A10)}$$

$$\frac{D\overline{c^2}}{Dt} = -2\overline{u_k c}\frac{\partial C}{\partial x_k} + \frac{\partial}{\partial x_k}\left[(\nu + 0.3q\Lambda)\frac{\partial \overline{c^2}}{\partial x_k}\right] - \frac{0.45q}{\Lambda}\overline{c^2} \qquad \text{(A11)}$$

The cross-wind velocities are actually determined by cross-differentiating Eq. (A1) to obtain an equation for

$$\eta = \frac{\partial V}{\partial z} - \frac{\partial W}{\partial y} \qquad \text{(A12)}$$

from which we may solve for the stream function:

$$\frac{\partial^2 \Psi}{\partial y^2} + \frac{\partial^2 \Psi}{\partial z^2} = -\eta \qquad \text{(A13)}$$

where

$$V = -\frac{\partial \Psi}{\partial y}$$

$$W = +\frac{\partial \Psi}{\partial z} \qquad \text{(A14)}$$

APPENDIX B

MODEL DISPERSION PREDICTIONS OF SF_6 AND SULFATE FOR 13 TYPICAL TEST PERIODS IN THE GM EXPERIMENT

Figures B-1 through B-13 present the predicted ΔSO_4 levels (above background) using the predicted mean wind fields and turbulence data for the second test period in each day. These figures are drawn with the assumption that S = 51.7 mg/mile/vehicle. When the ambient background is included in the SO_4 levels, the value of S decreases to S = 17.3 mg/mile/vehicle, and all of the contours in Figures B-1 through B-13 should be multiplied by a factor of 0.33 .

Figures B-14 through B-26 present the predicted SF_6 levels under the same conditions for the same days. Here the emissions level is fixed by the data. The figure title contains the specific day simulated.

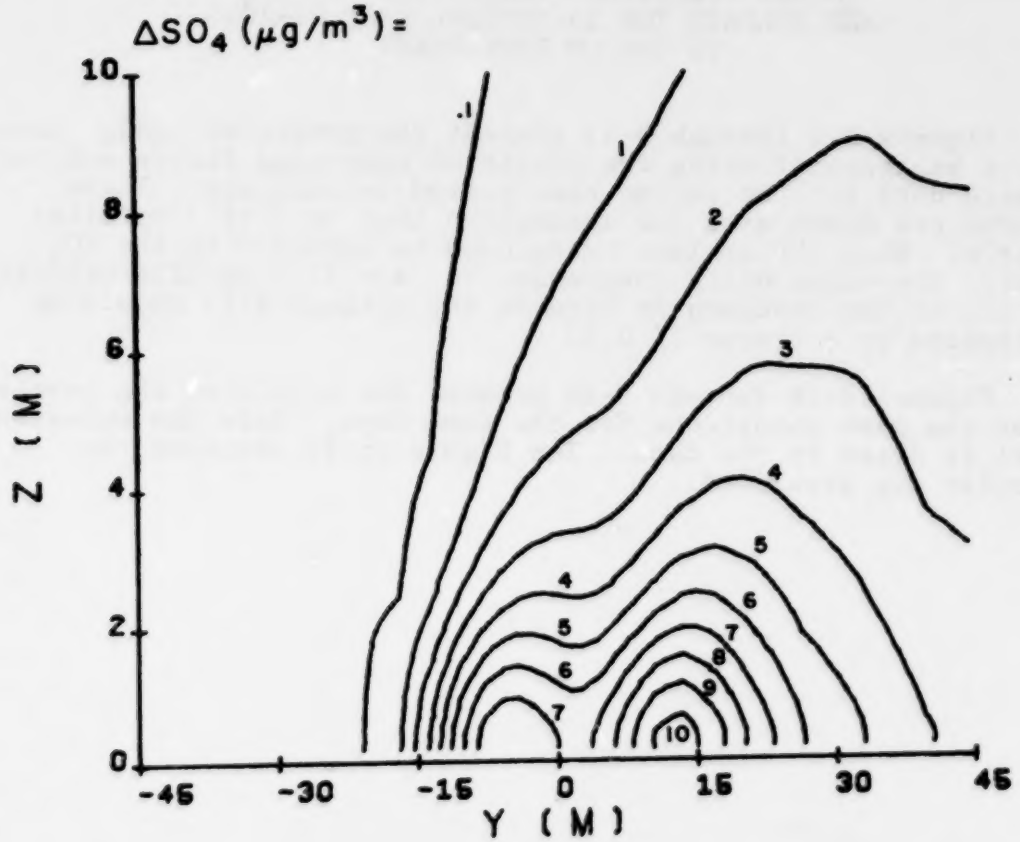

Figure B-1. Predicted ΔSO_4 levels for the second test period of day 275.

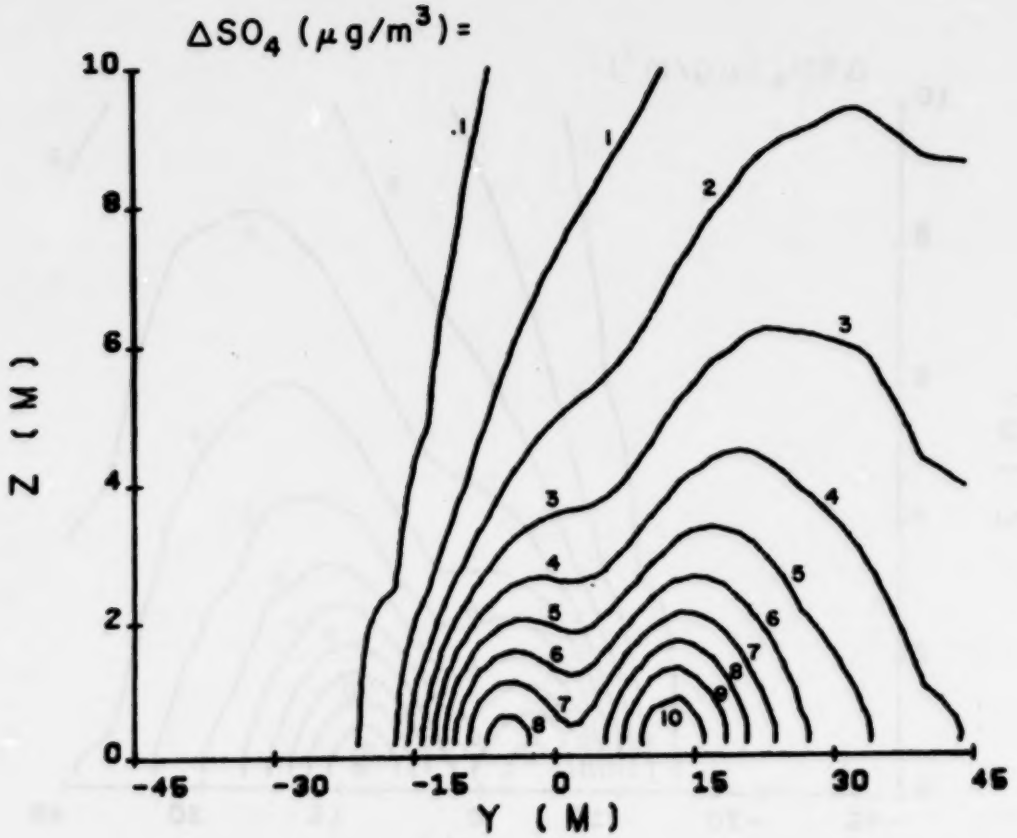

Figure B-2. Predicted ΔSO_4 levels for the second test period of day 276.

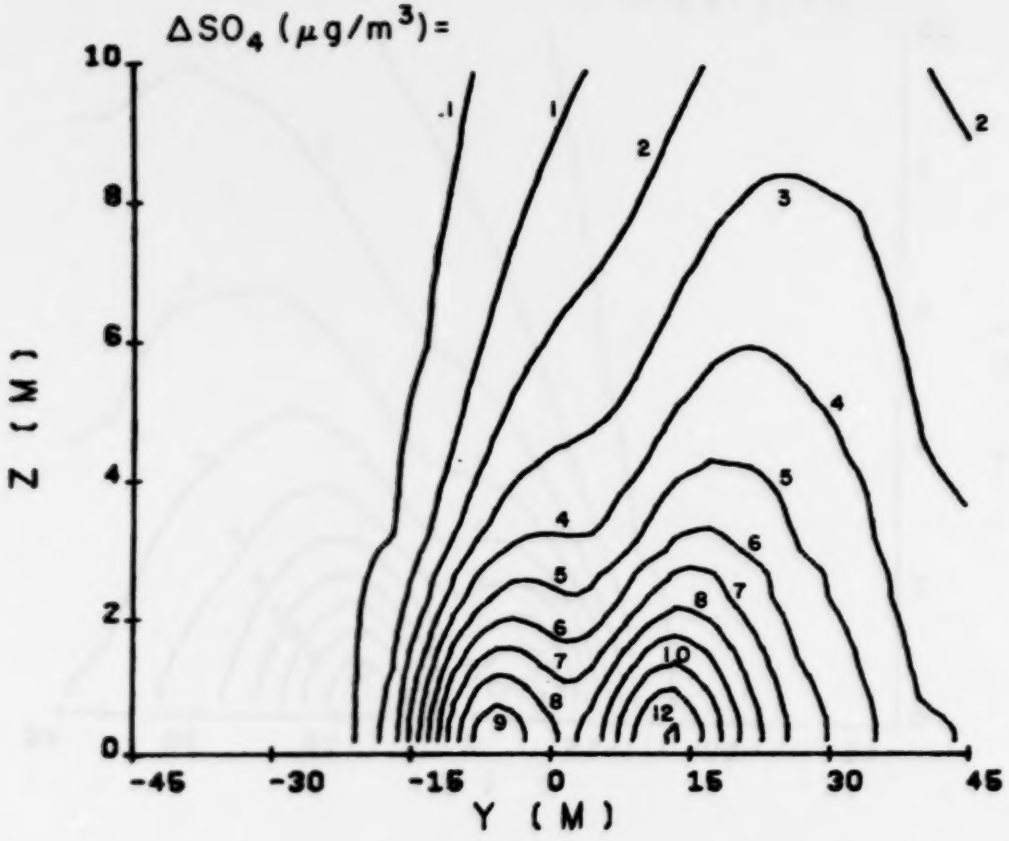

Figure B-3. Predicted ΔSO_4 levels for the second test period of day 279.

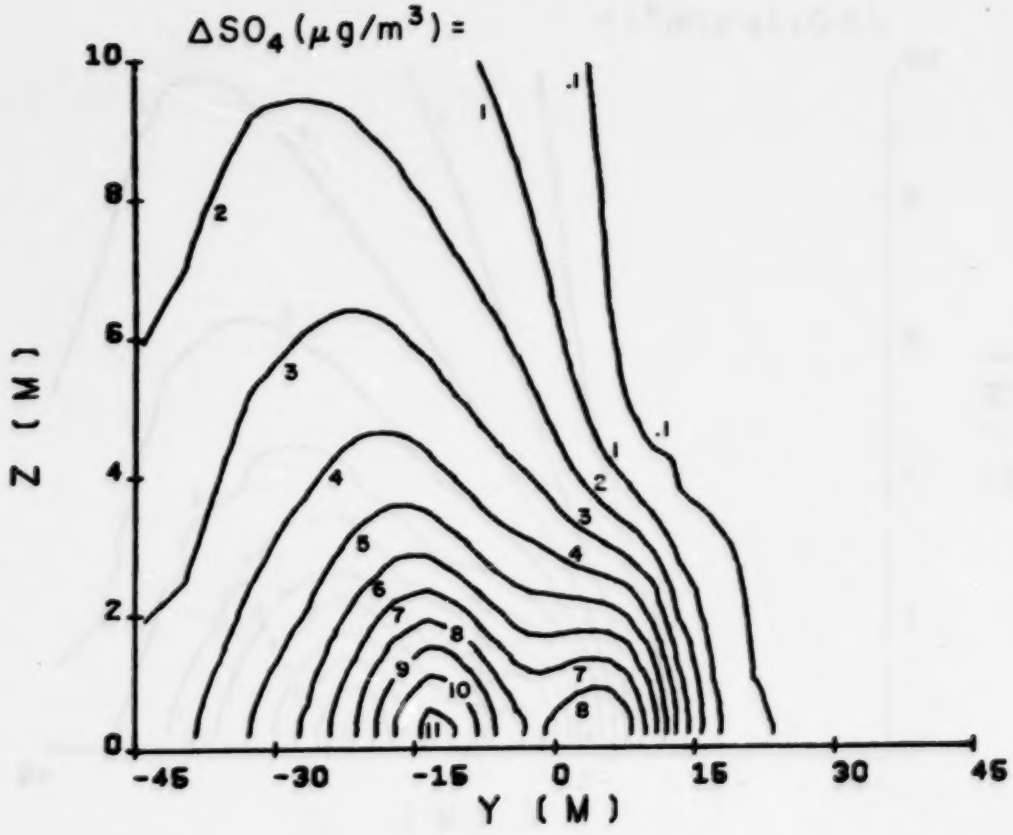

Figure B-4. Predicted ΔSO_4 levels for the second test period of day 281.

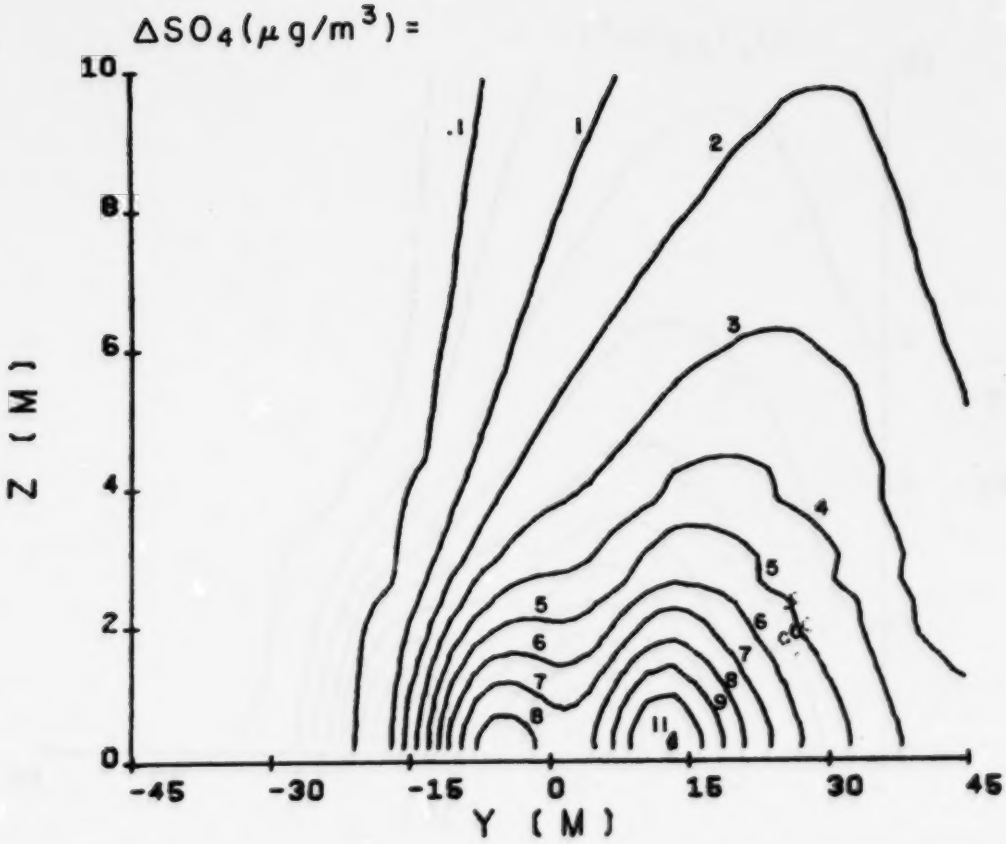

Figure B-5. Predicted ΔSO_4 levels for the second test period of day 283.

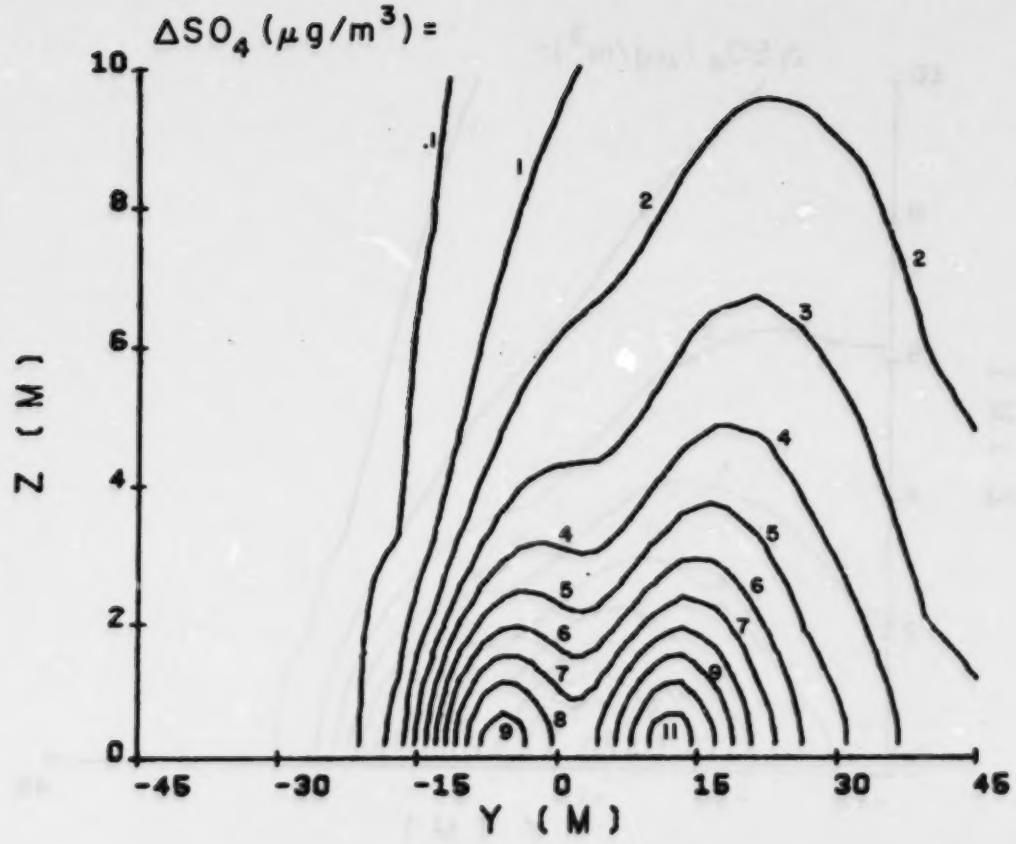

Figure B-6. Predicted ΔSO_4 levels for the second test period of day 286.

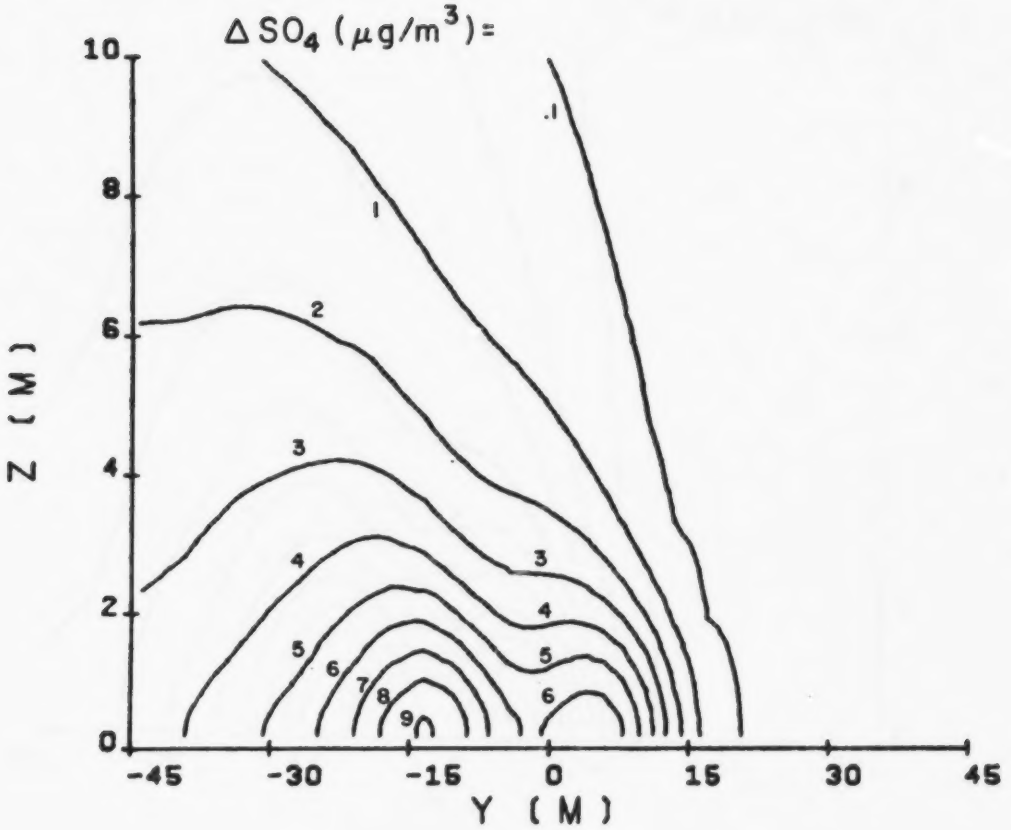

Figure B-7. Predicted ΔSO_4 levels for the second test period of day 290.

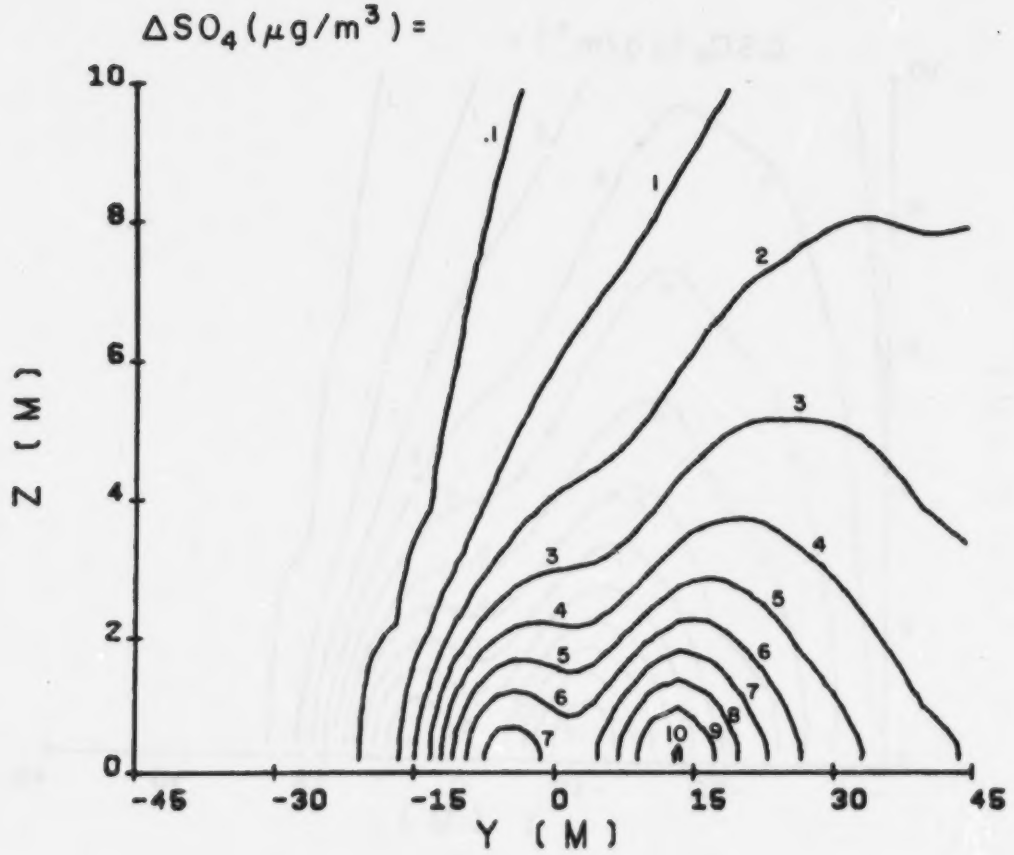

Figure B-8. Predicted ΔSO_4 levels for the second test period of day 294.

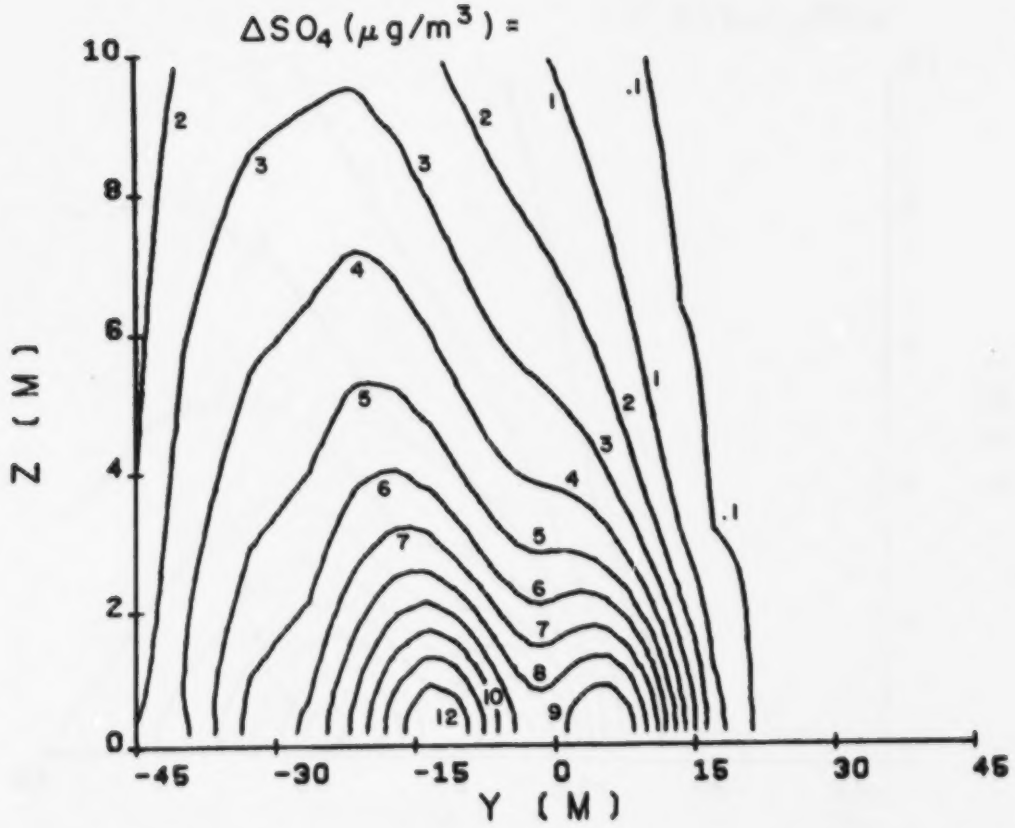

Figure B-9. Predicted ΔSO_4 levels for the second test period of day 295.

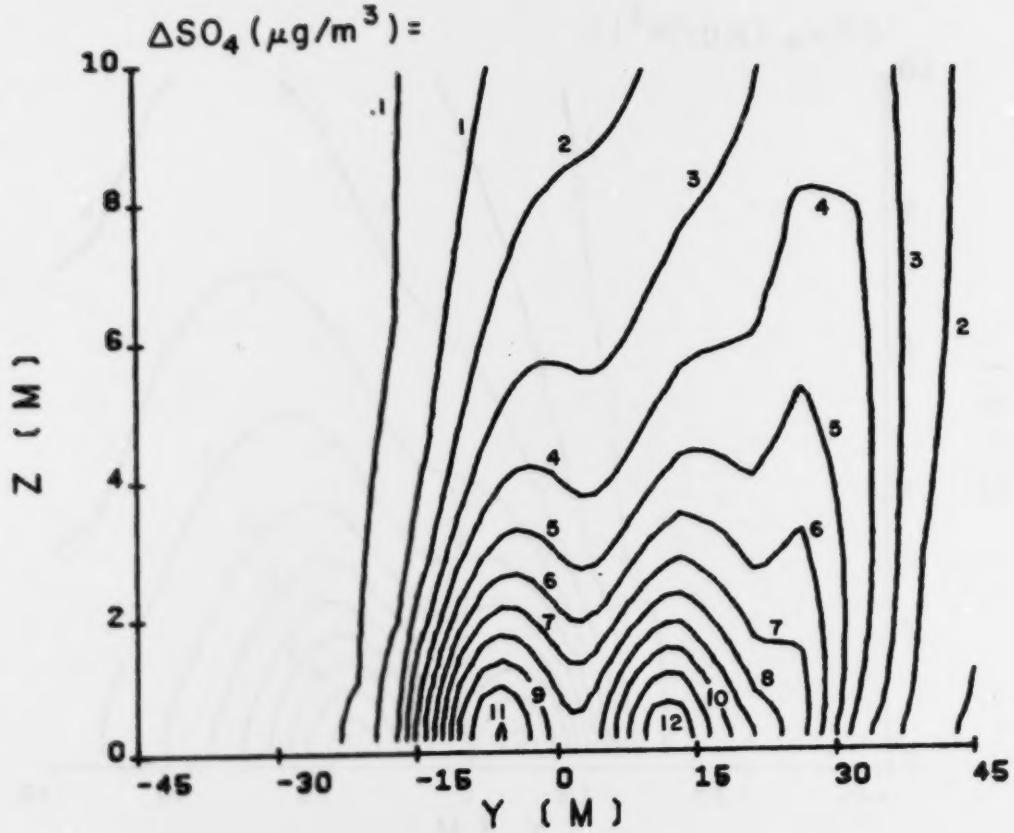

Figure B-10. Predicted ΔSO_4 levels for the second test period of day 297.

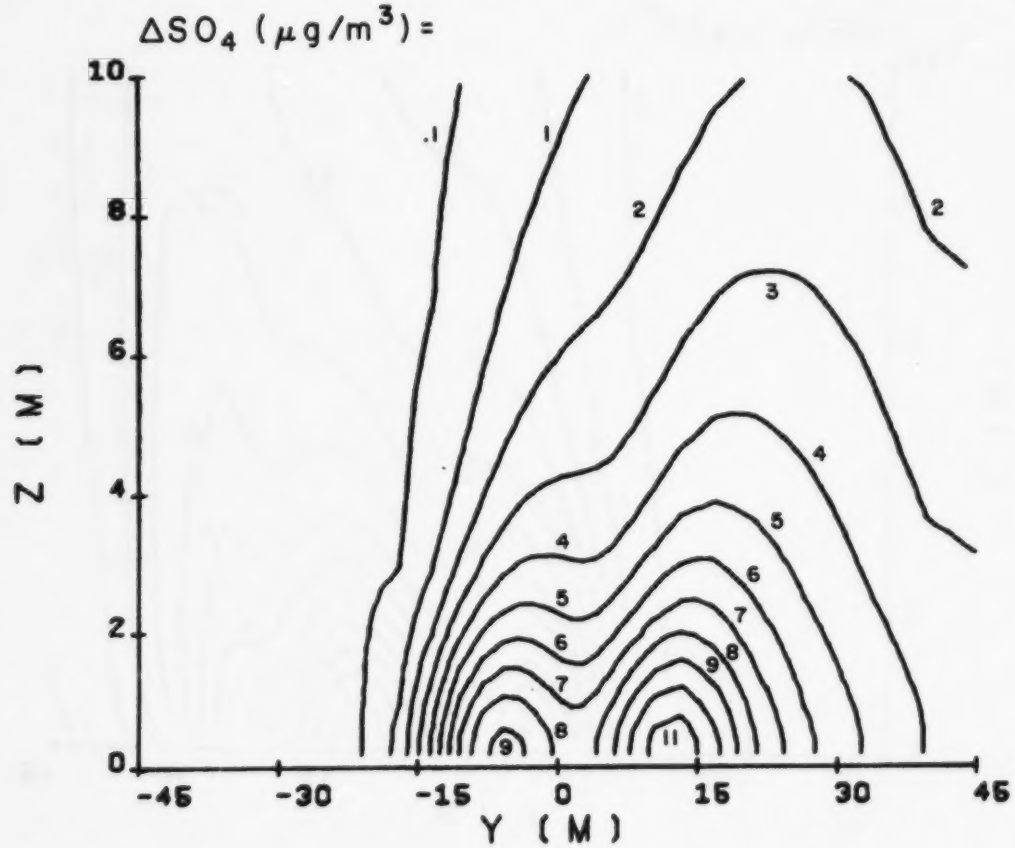

Figure B-11. Predicted ΔSO_4 levels for the second test period of day 300.

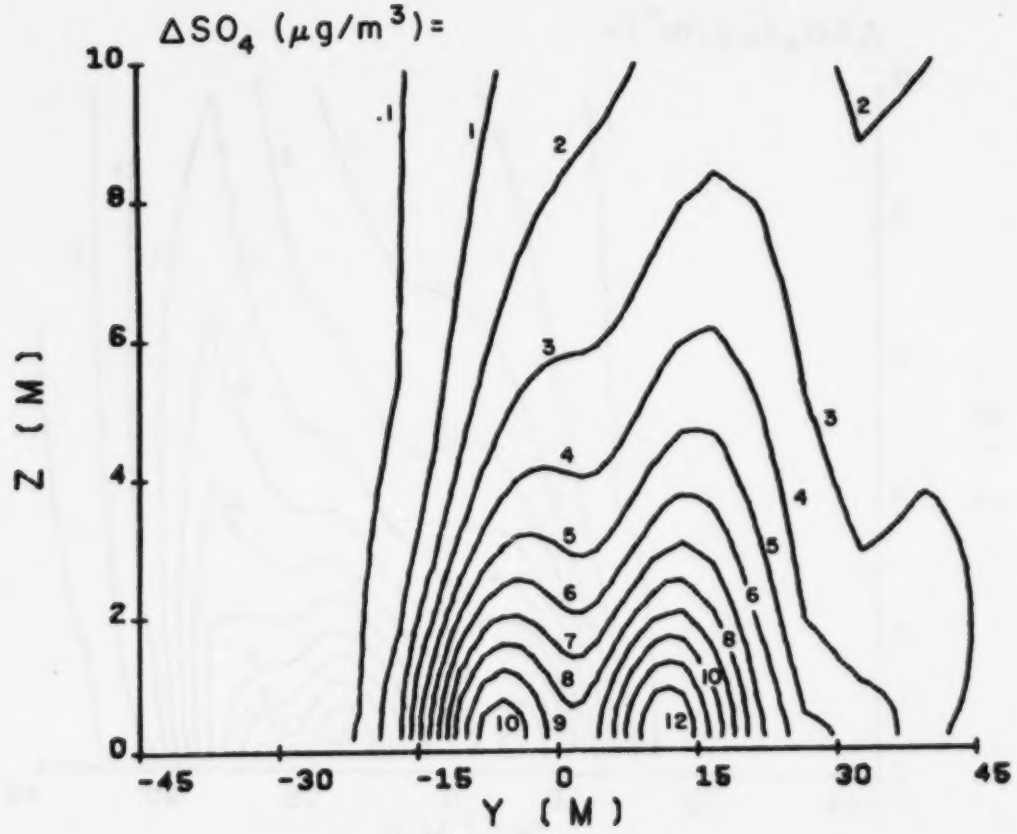

Figure B-12. Predicted ΔSO_4 levels for the second test period of day 302.

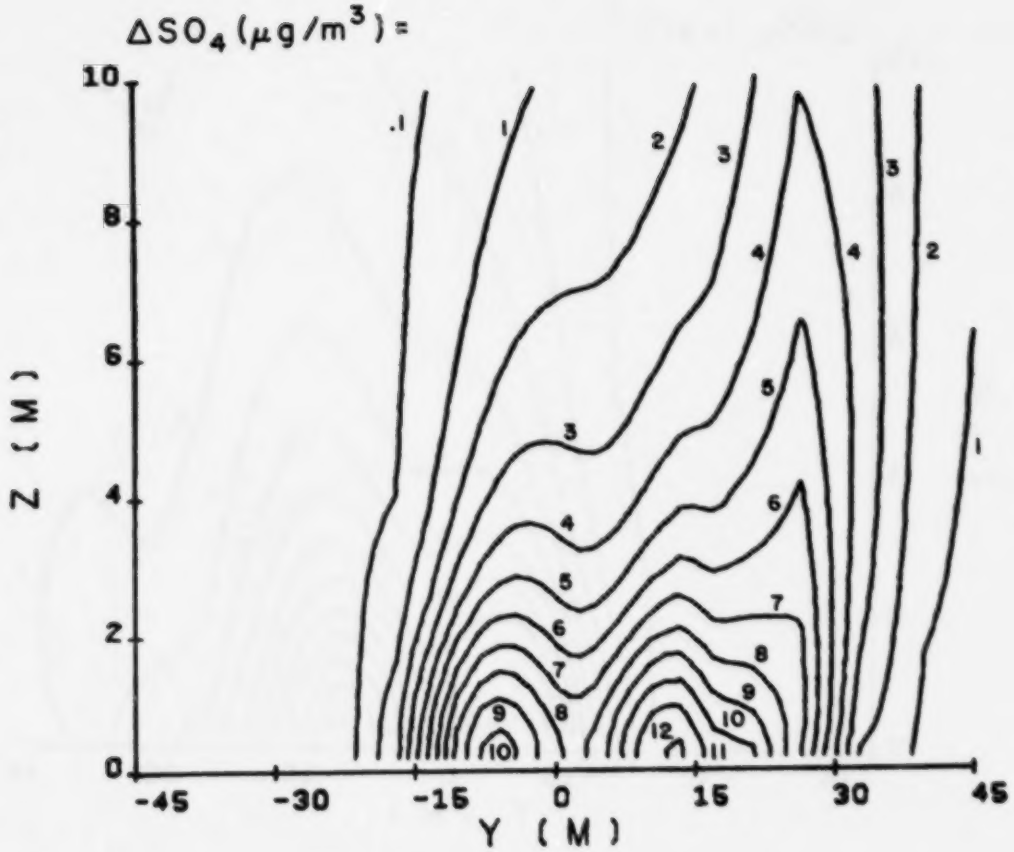

Figure B-13. Predicted ΔSO_4 levels for the second test period of day 303.

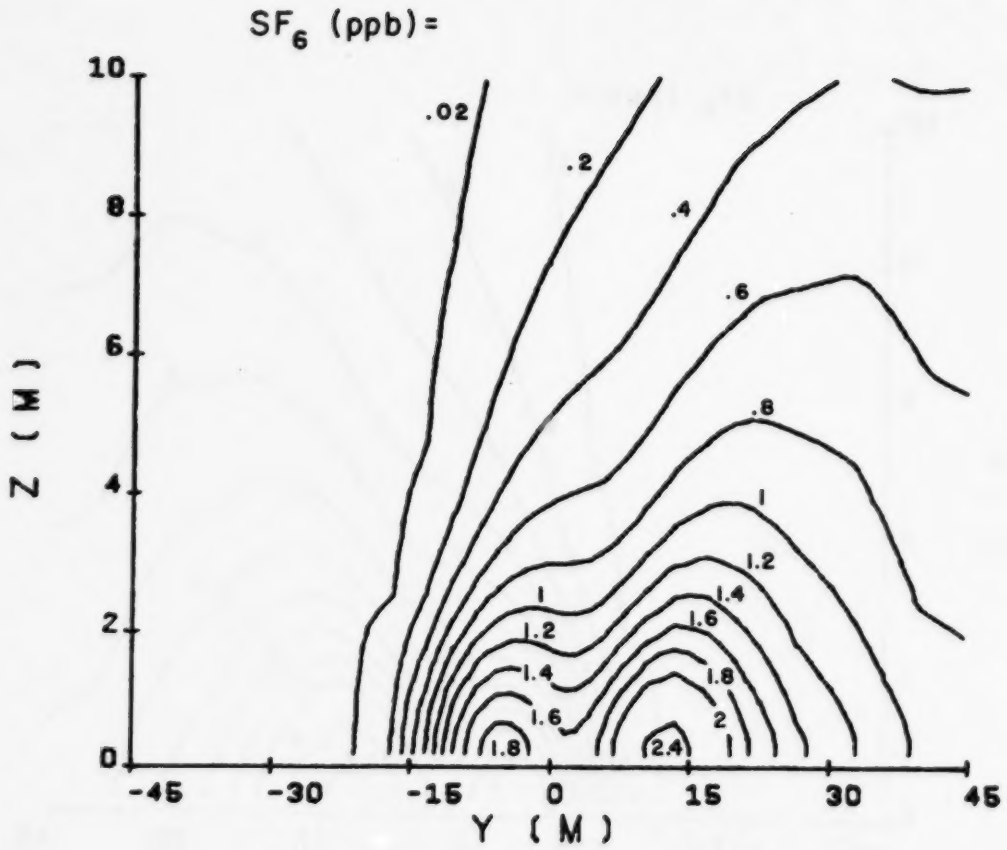

Figure B-14. Predicted SF_6 levels for the second test period of day 275.

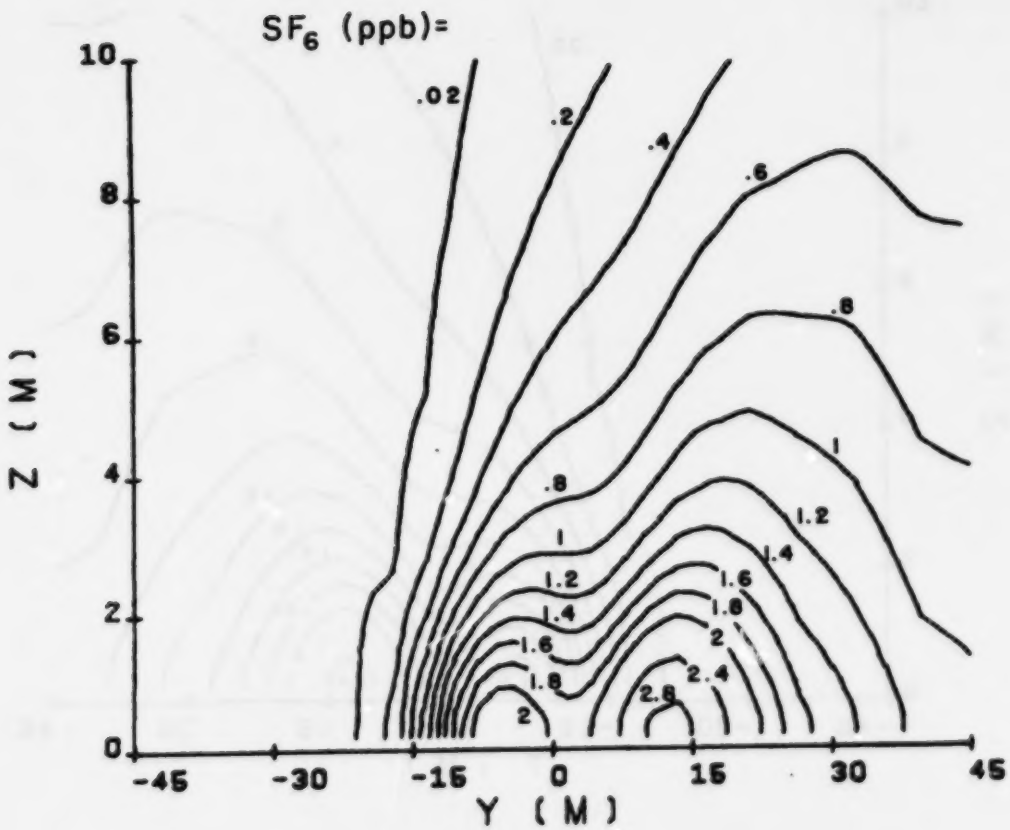

Figure B-15. Predicted SF_6 levels for the second test period of day 276.

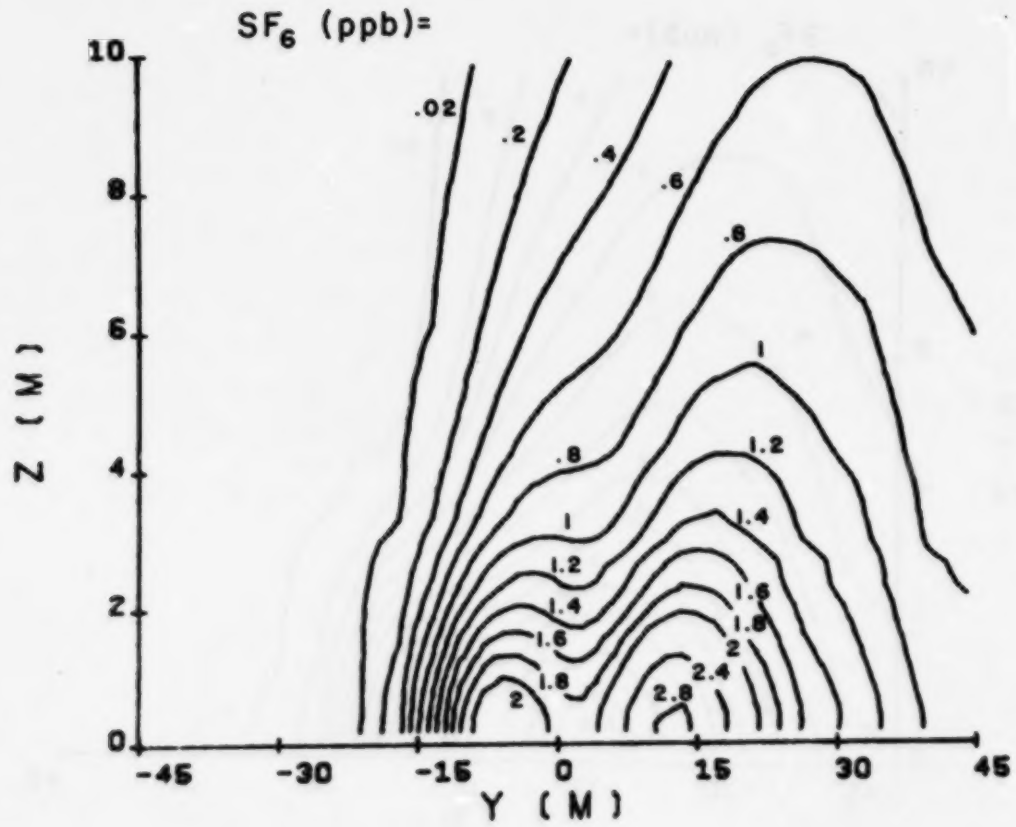

Figure B-16. Predicted SF_6 levels for the second test period of day 279.

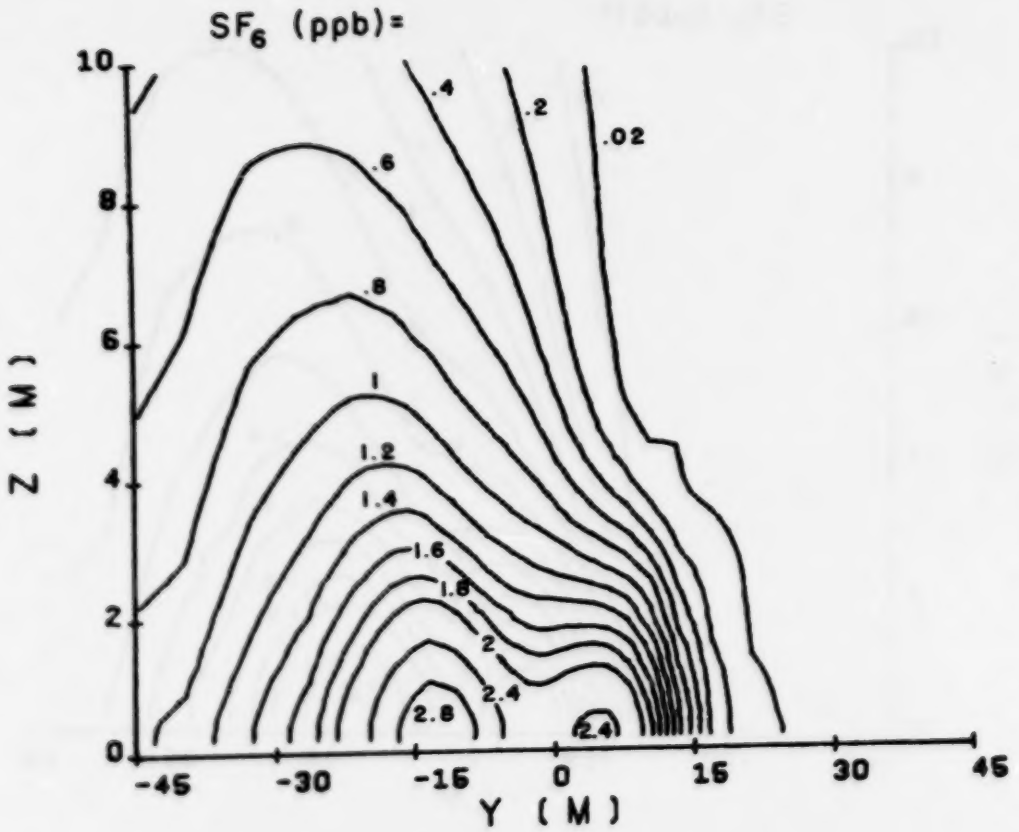

Figure B-17. Predicted SF_6 levels for the second test period of day 281.

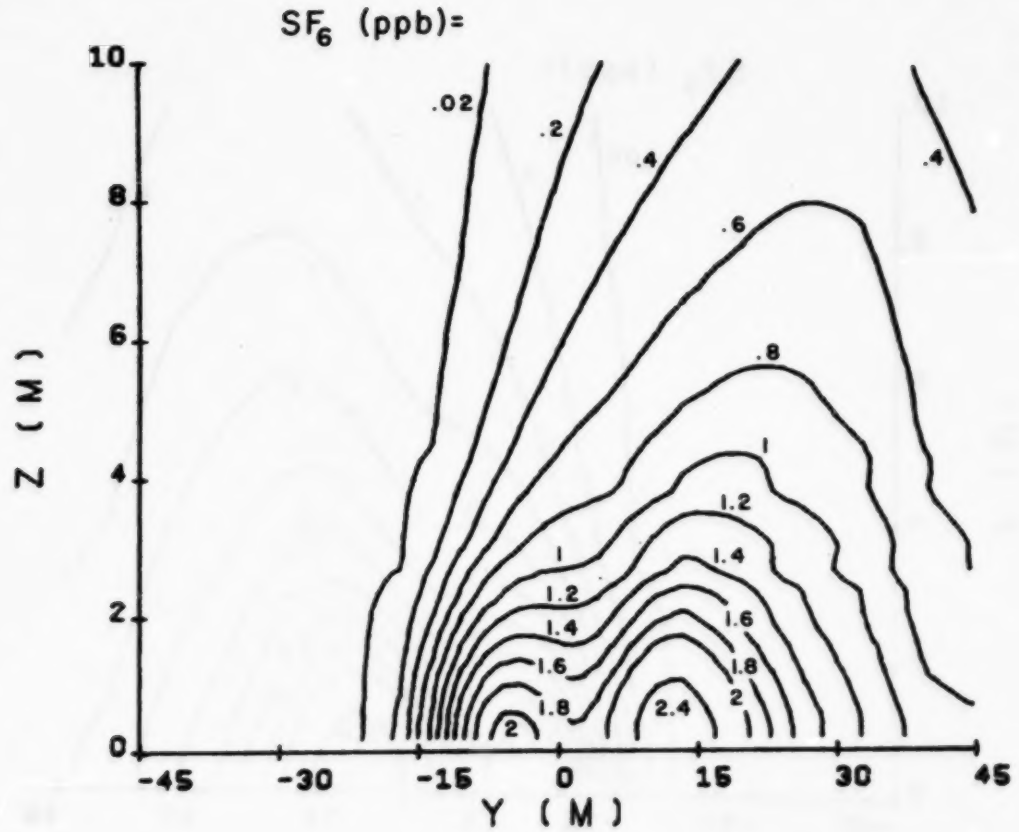

Figure B-18. Predicted SF_6 levels for the second test period of day 283.

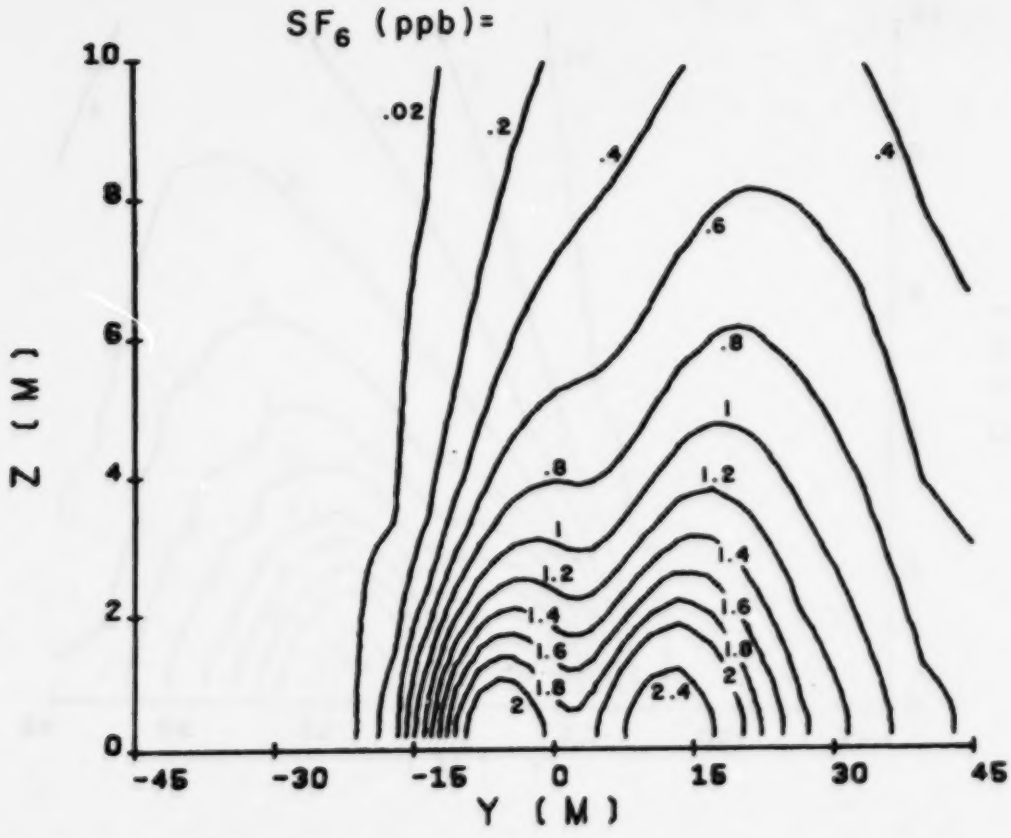

Figure B-19. Predicted SF_6 levels for the second test period of day 286.

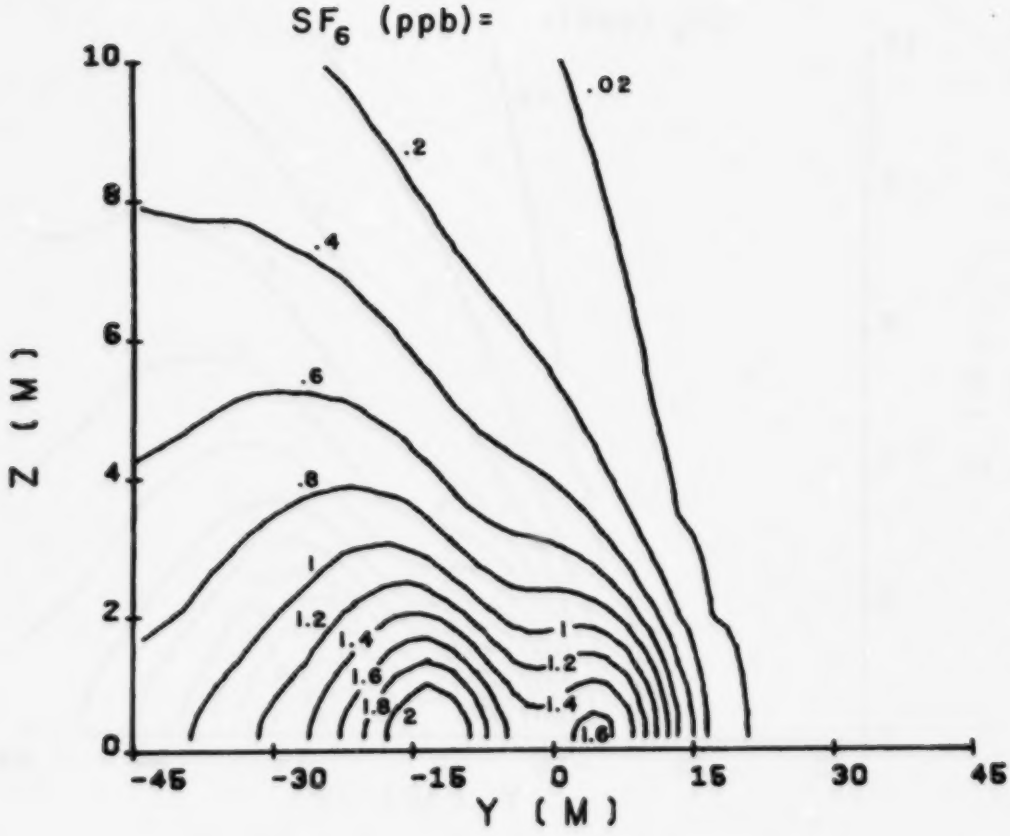

Figure B-20. Predicted SF_6 levels for the second test period of day 290.

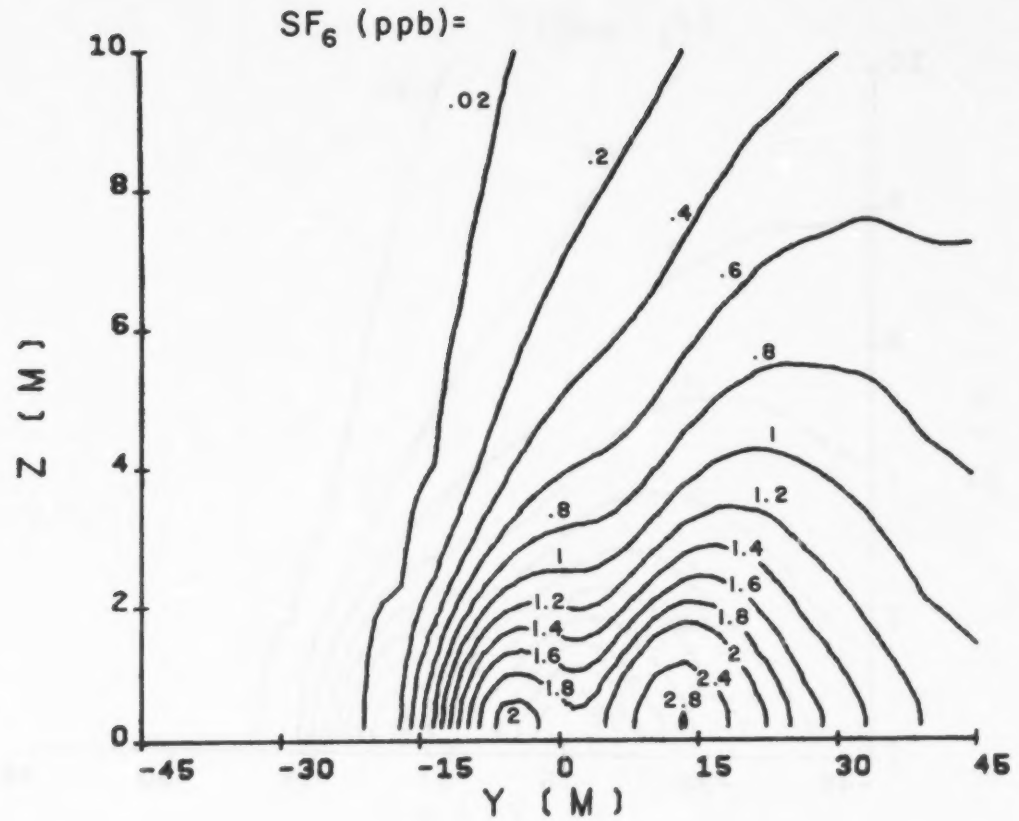

Figure B-21. Predicted SF_6 levels for the second test period of day 294.

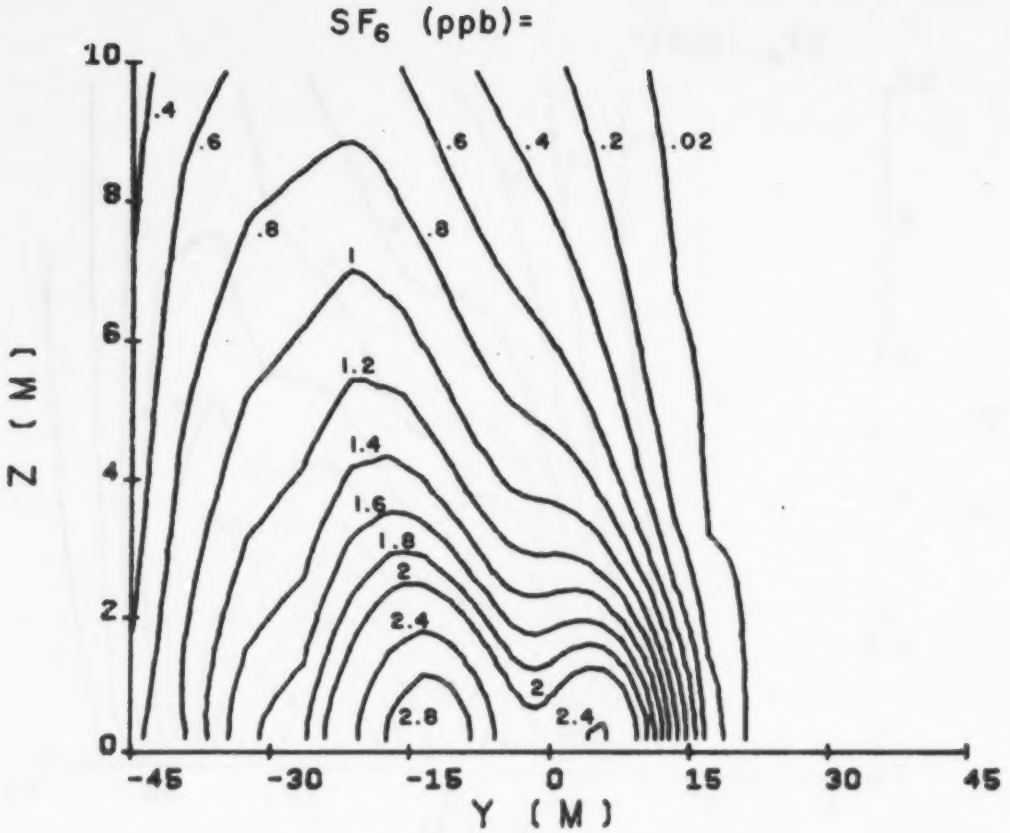

Figure B-22. Predicted SF_6 levels for the second test period of day 295.

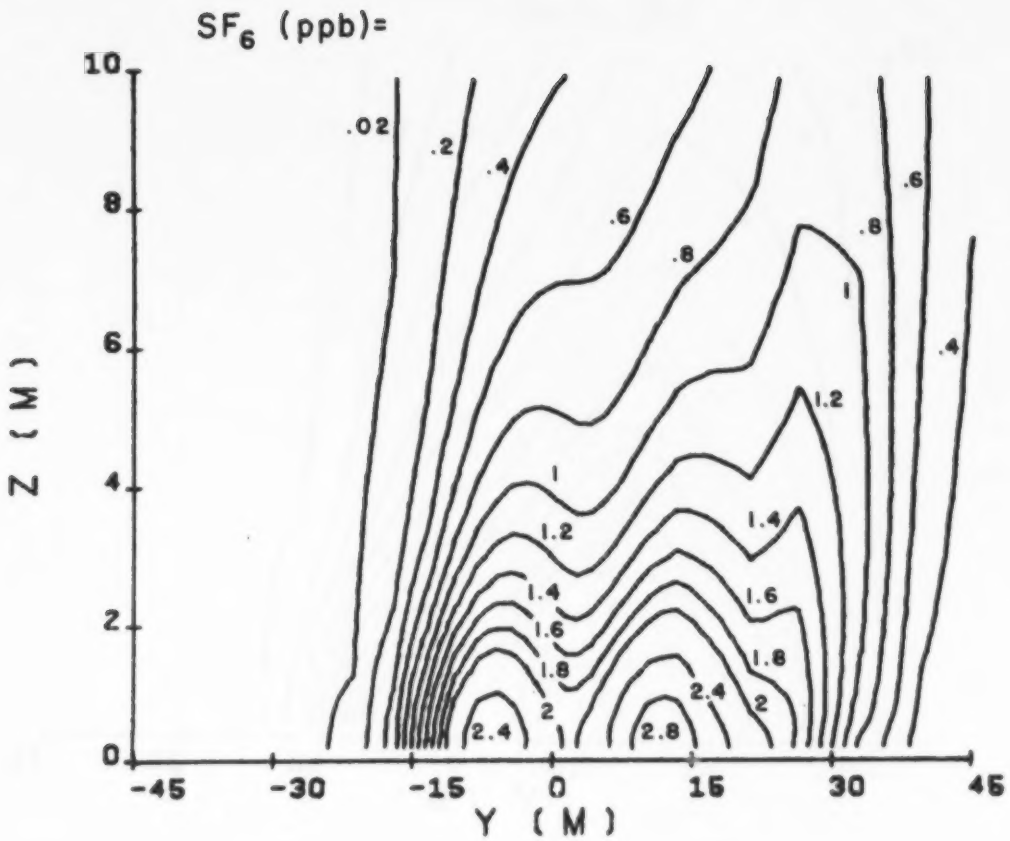

Figure B-23. Predicted SF_6 levels for the second test period of day 297.

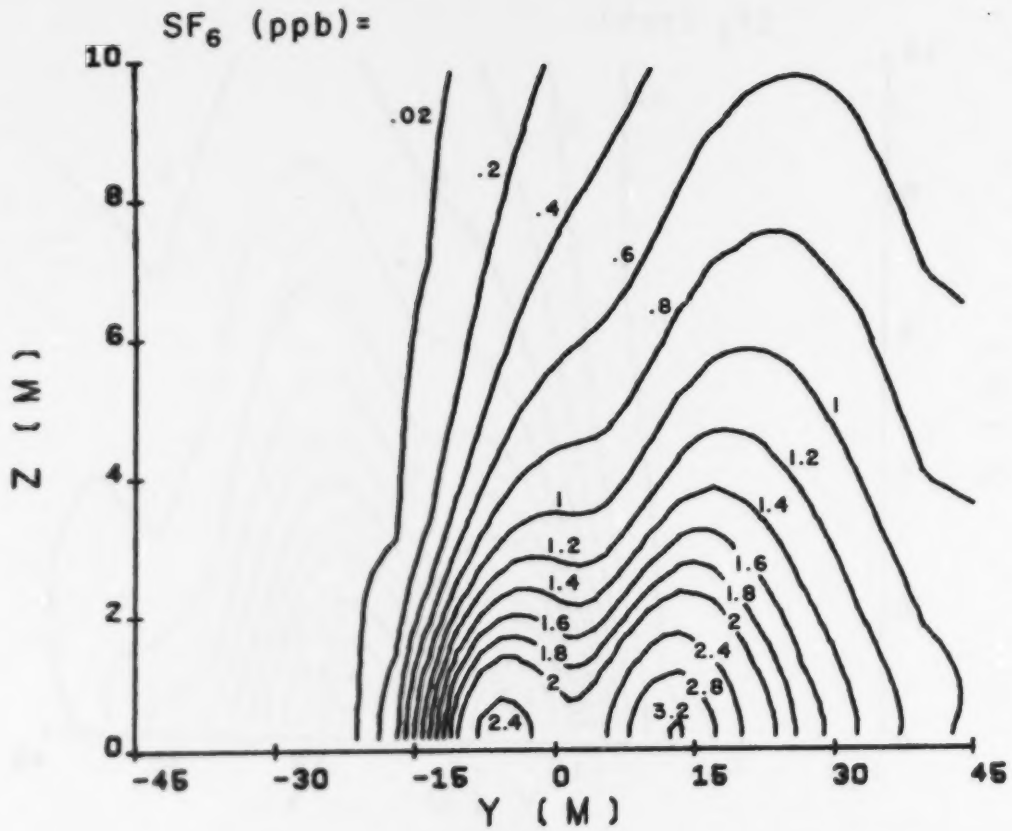

Figure B-24. Predicted SF_6 levels for the second test period of day 300.

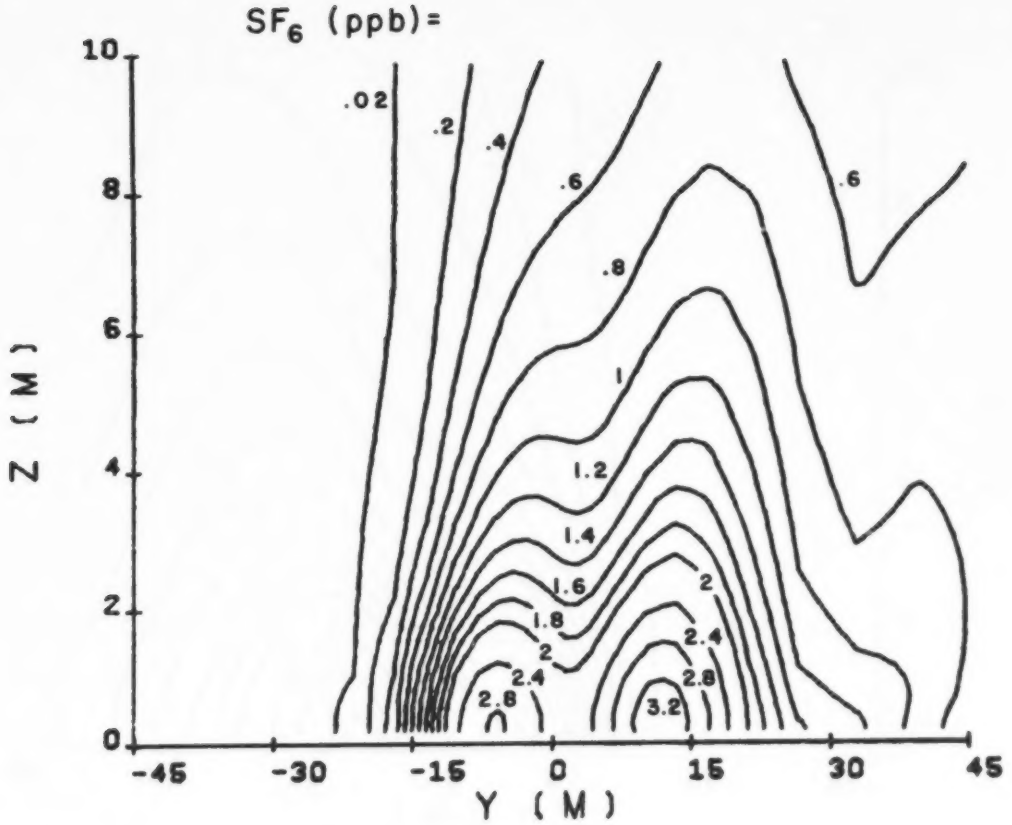

Figure B-25. Predicted SF_6 levels for the second test period of day 302.

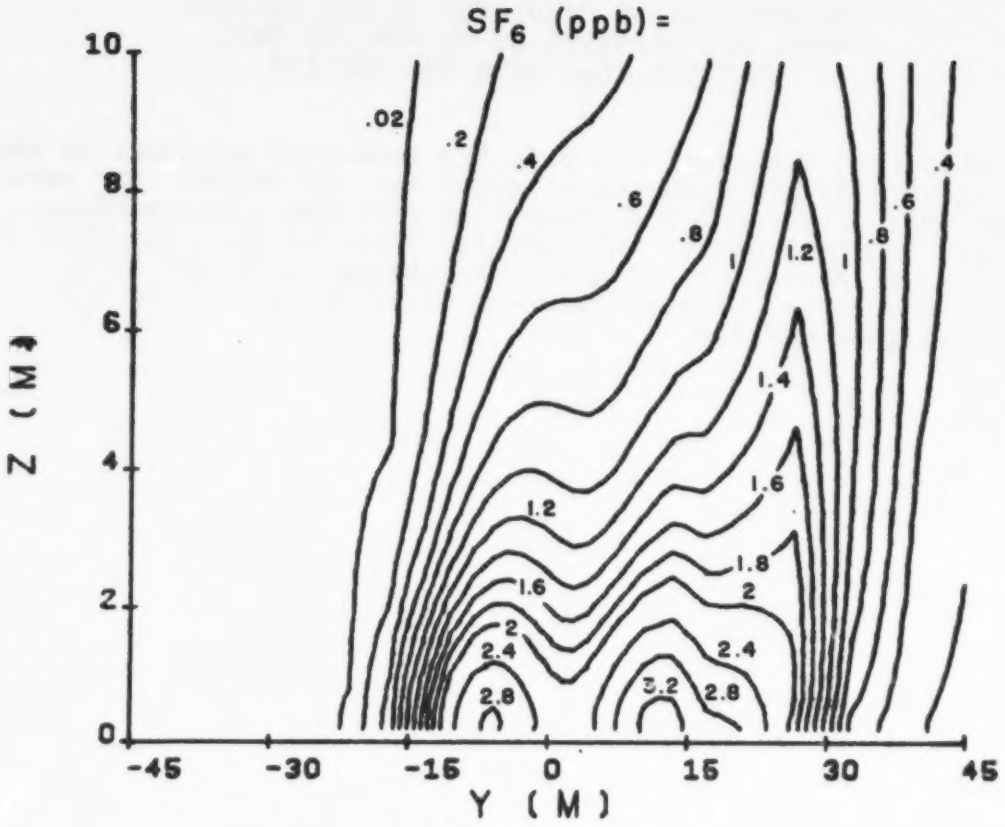

Figure B-26. Predicted SF_6 levels for the second test period of day 303.

APPENDIX C

MODEL COMPARISONS OF THE VELOCITY AND VARIANCE FIELDS PREDICTED BY THE CLOSURE MODEL AND MEASURED BY GM FOR THE TWO CRITICAL TEST DAYS 293 AND 296

Figures C-1 through C-5 give the predicted contours of the mean flowfields and turbulence levels for the second test period of day 293. Figures C-6 through C-10 give the corresponding measured levels linearly interpolated from the data recorded at the 18 tower positions. Figures C-11 through C-15 and C-16 through C-20 give the predicted and measured levels for the nearly-aligned day 296.

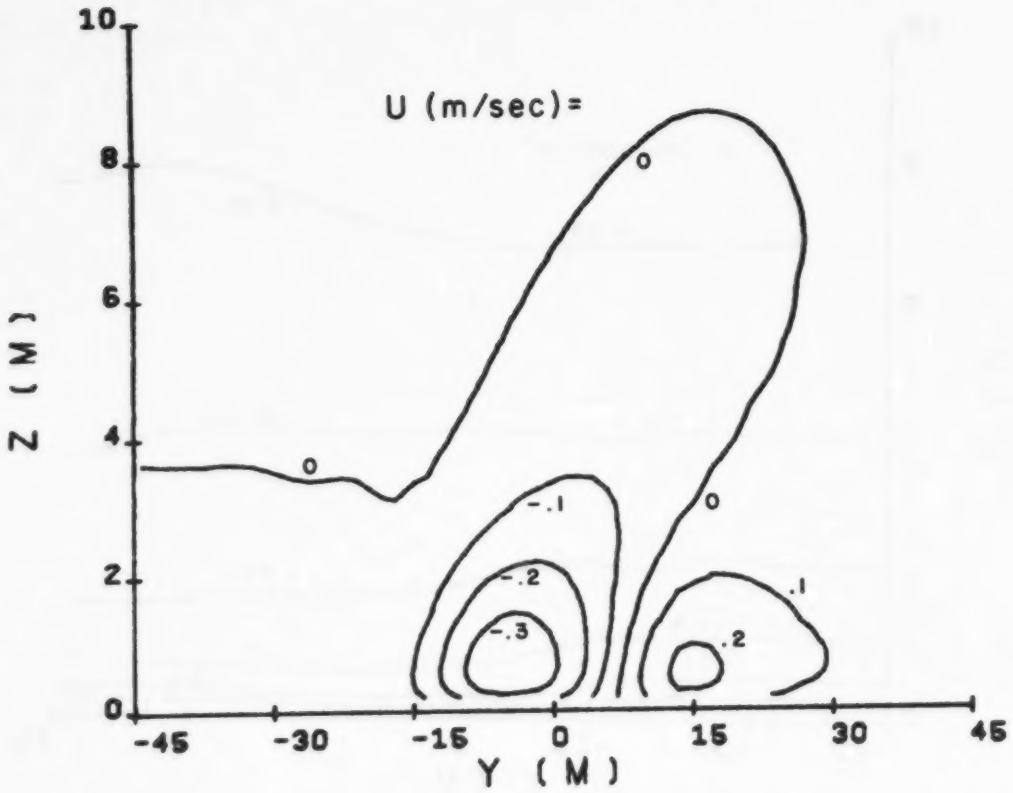

Figure C-1. Predicted contour levels of the U velocity for the second test period of day 293.

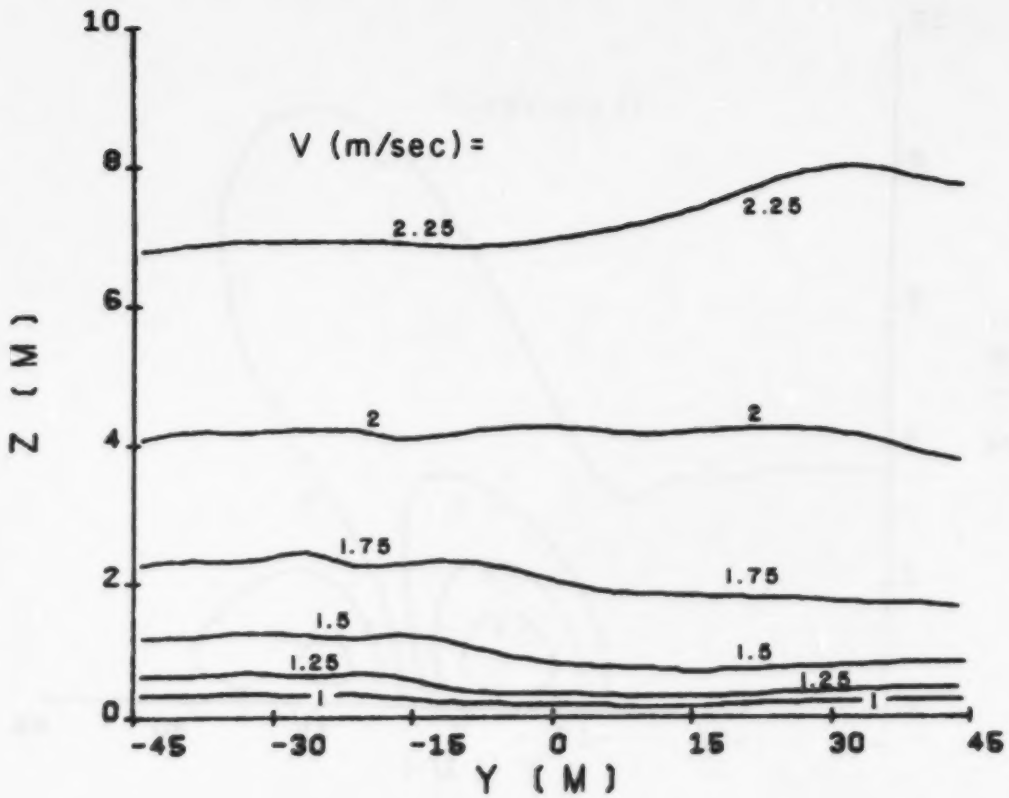

Figure C-2. Predicted contour levels of the V velocity for the second test period of day 293.

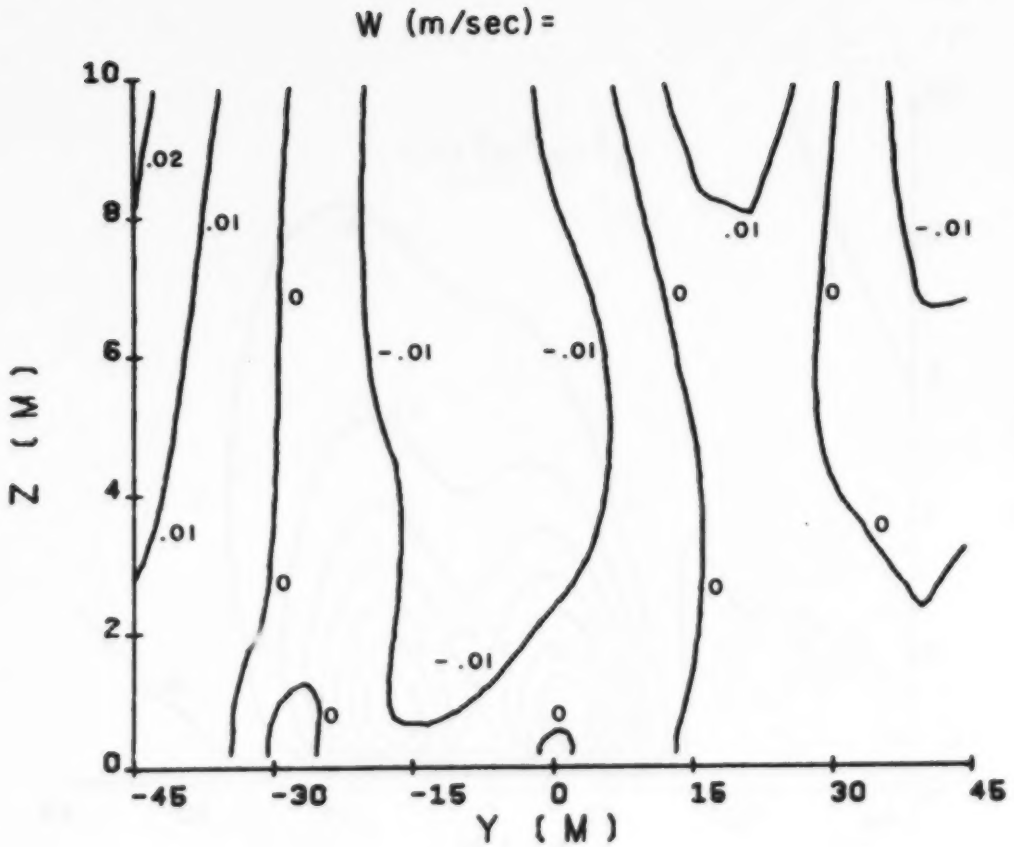

Figure C-3. Predicted contour levels of the W velocity for the second test period of day 293.

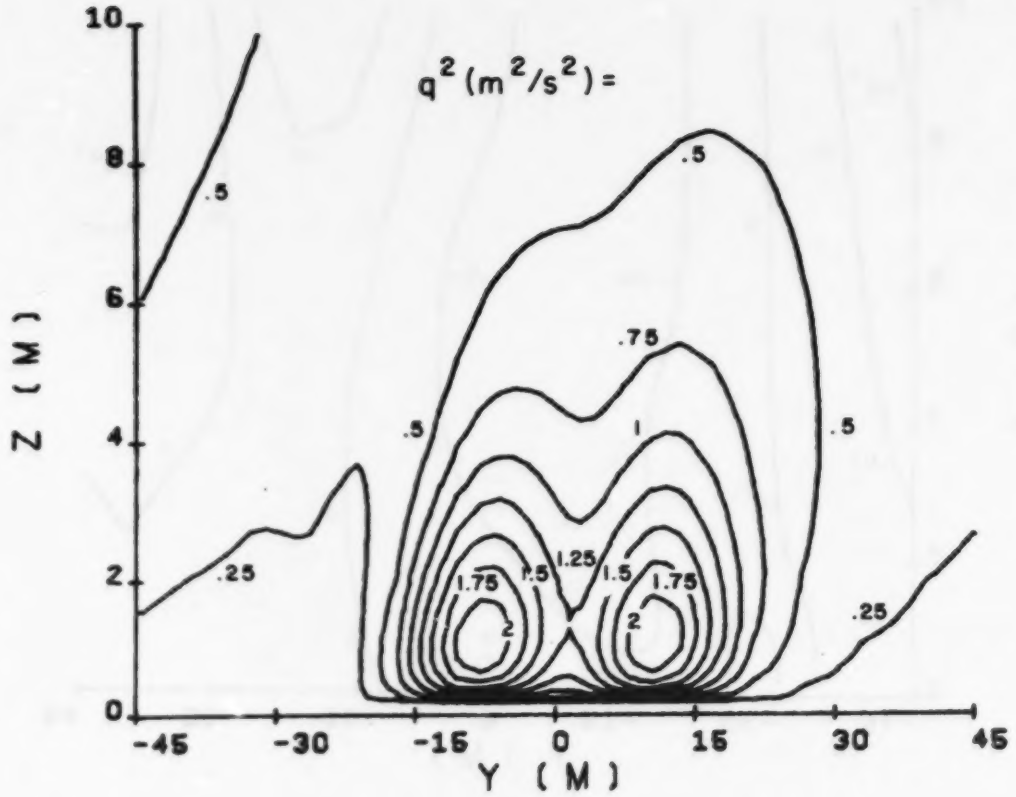

Figure C-4. Predicted contour levels of the q^2 velocity for the second test period of day 293.

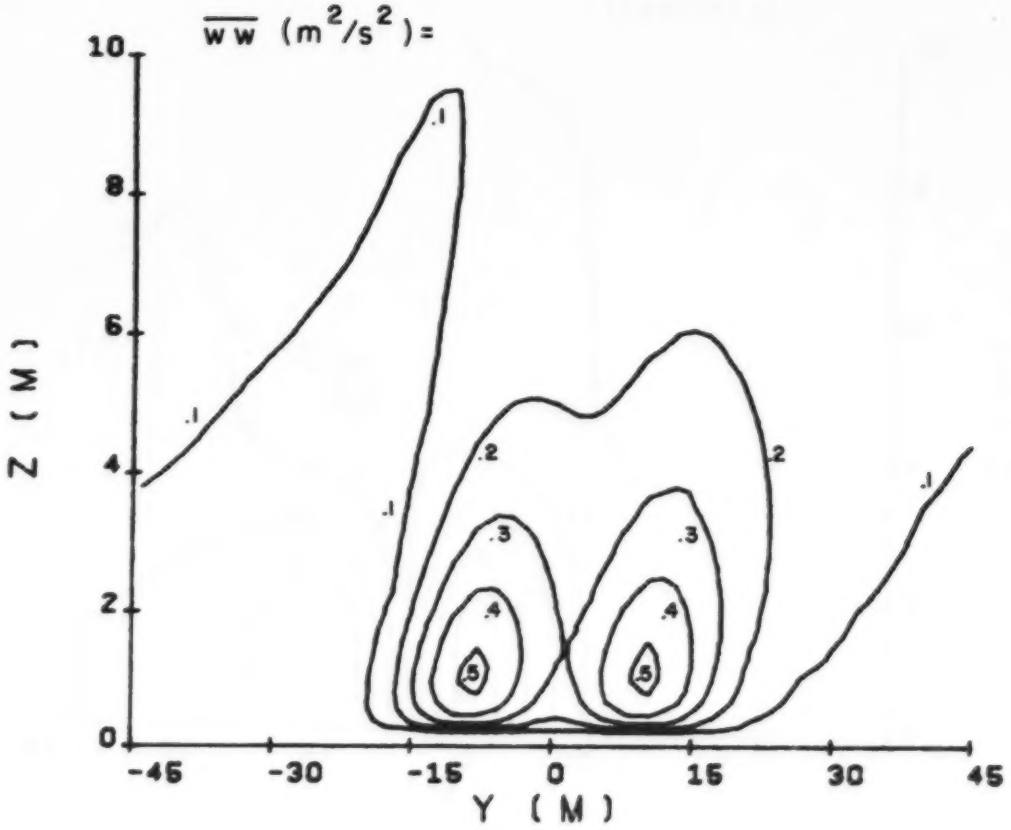

Figure C-5. Predicted contour levels of the $\overline{ww}$ velocity for the second test period of day 293.

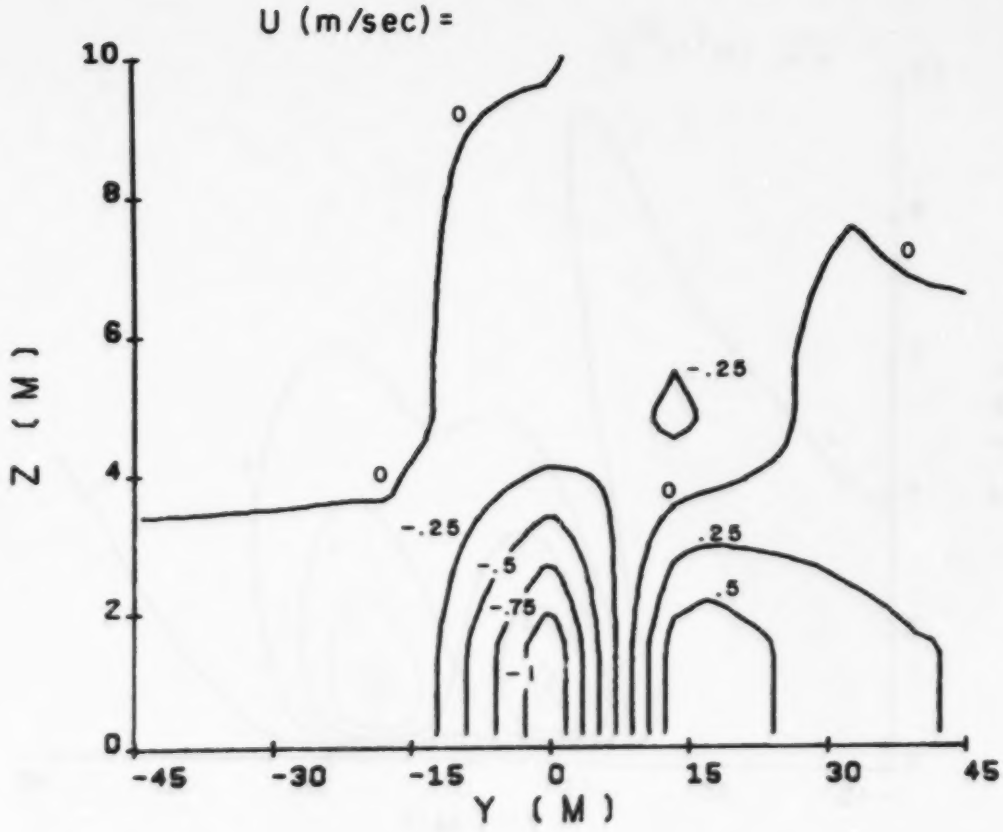

Figure C-6. The measured contours of the U velocity for day 293.

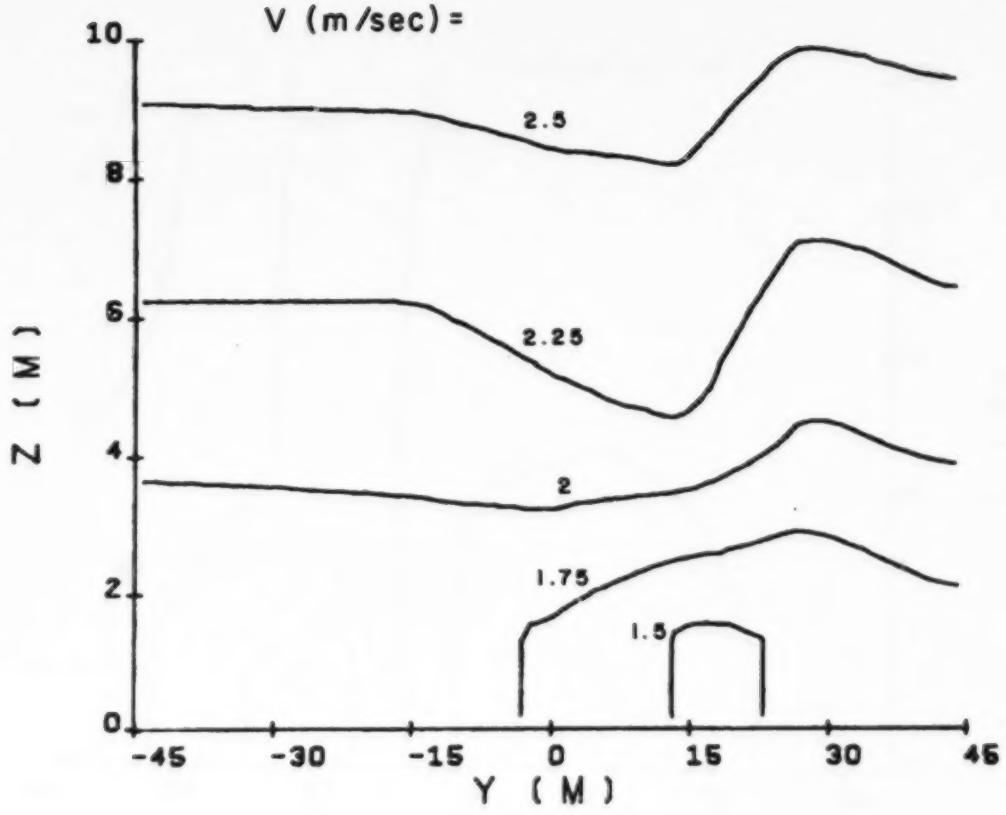

Figure C-7. The measured contours of the V velocity for day 293.

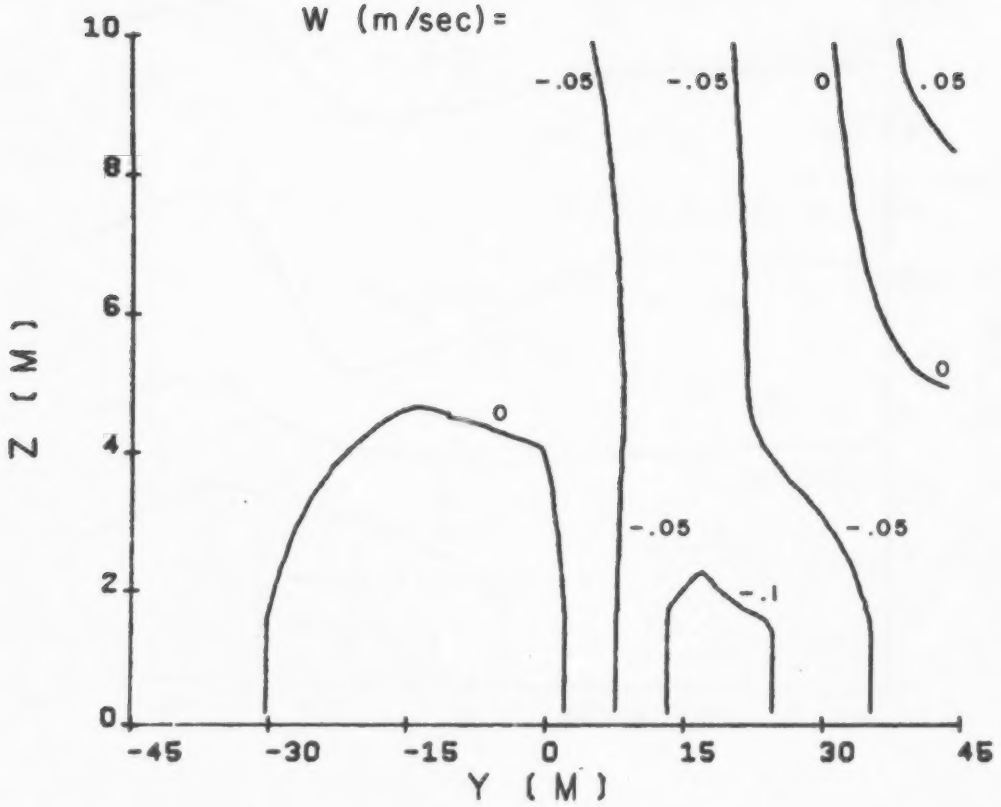

Figure C-8. The measured contours of the W velocity for day 293.

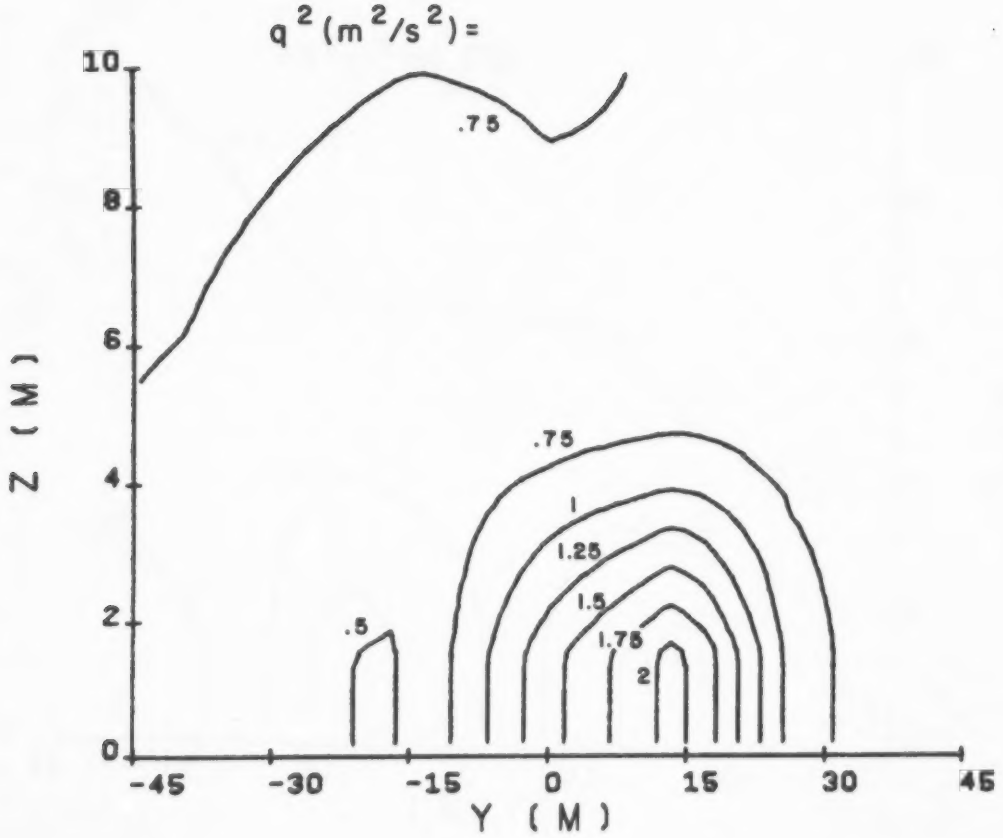

Figure C-9. The measured contours of the q^2 correlation for day 293.

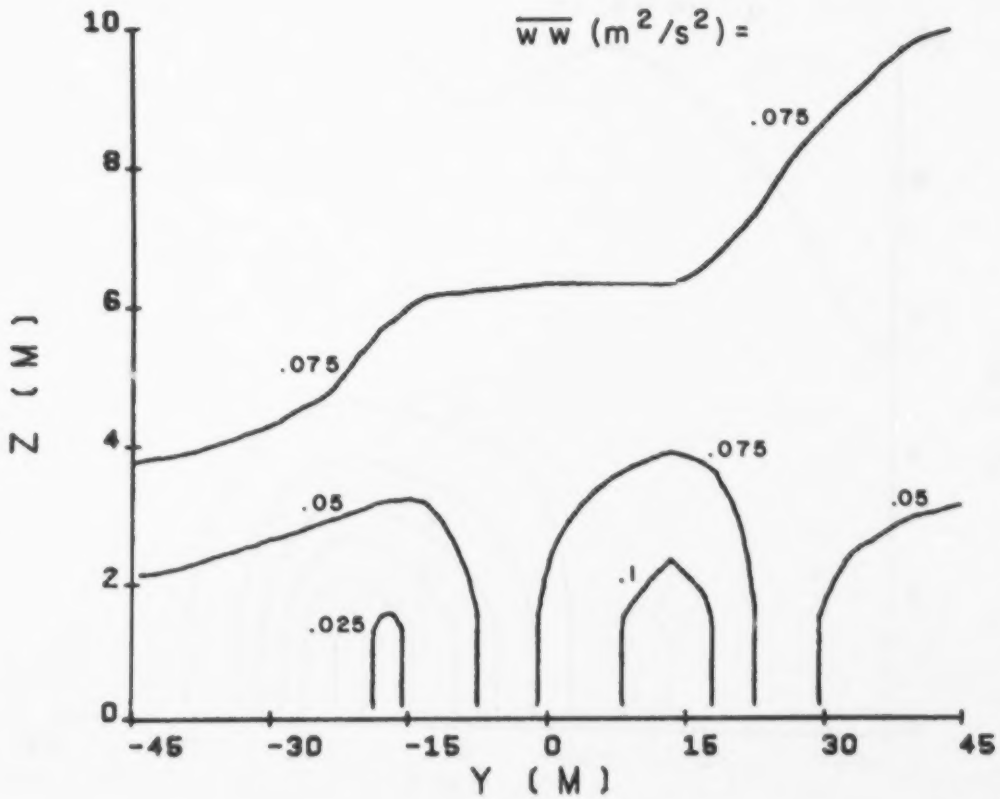

Figure C-10. The measured contours of the $\overline{ww}$ correlation for day 293.

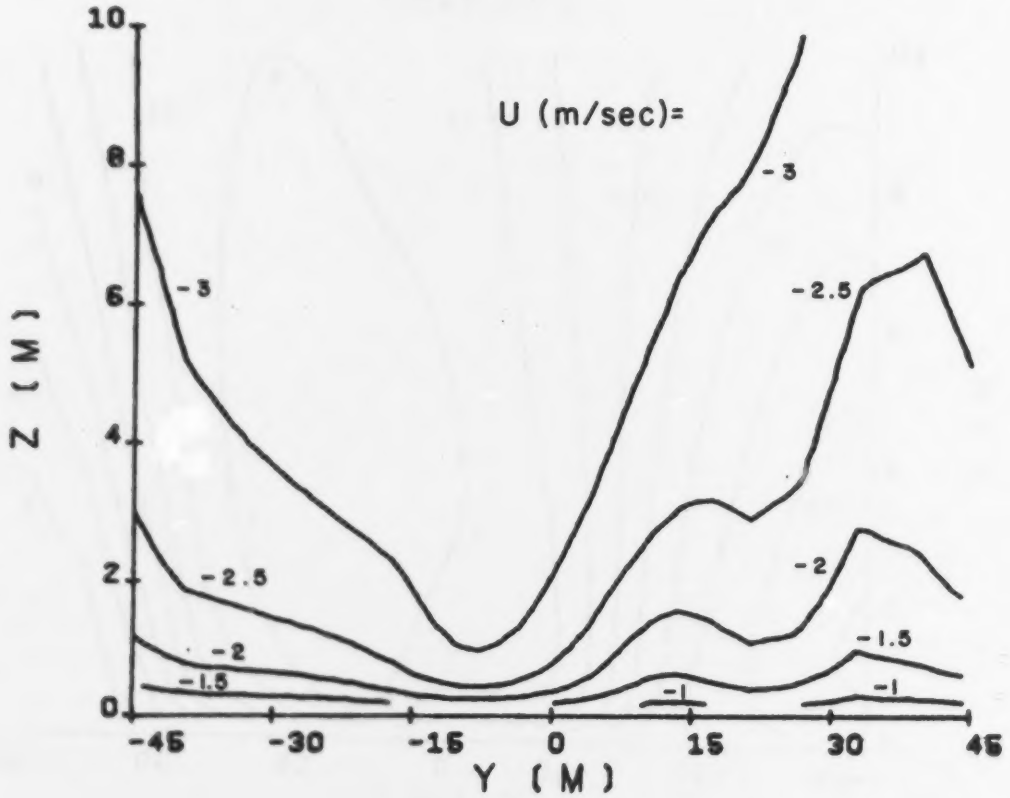

Figure C-11. The predicted contours of the U velocity for day 296.

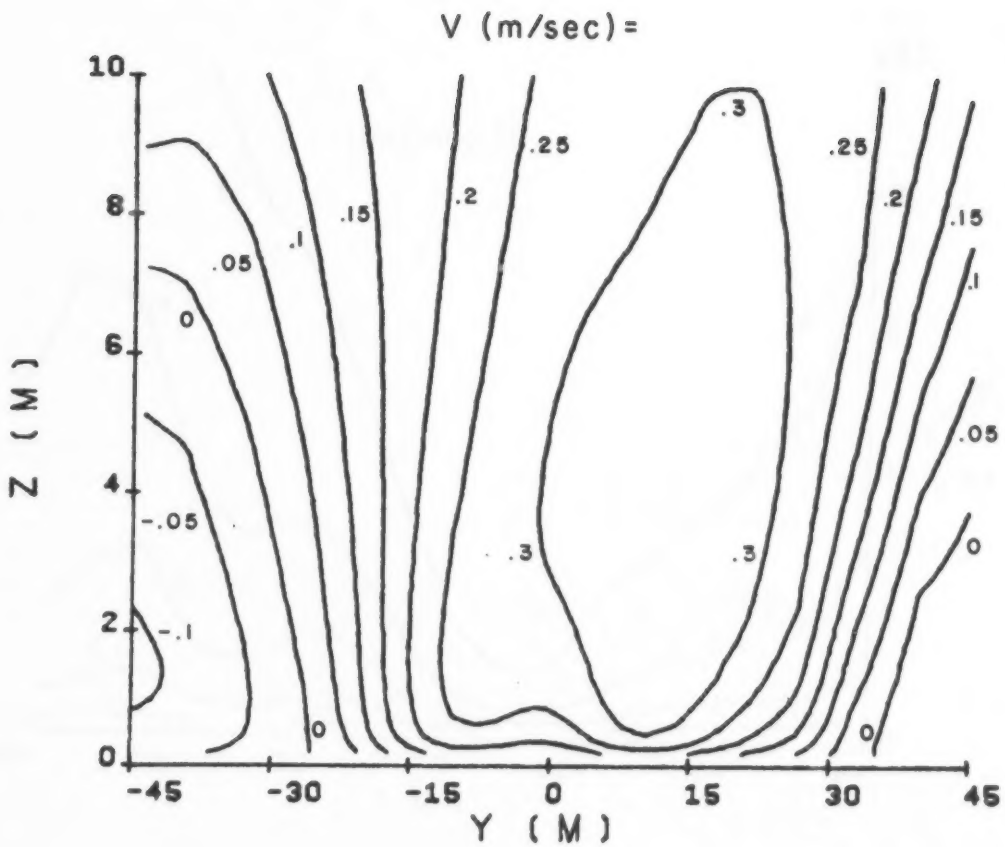

Figure C-12. The predicted contours of the V velocity for day 296.

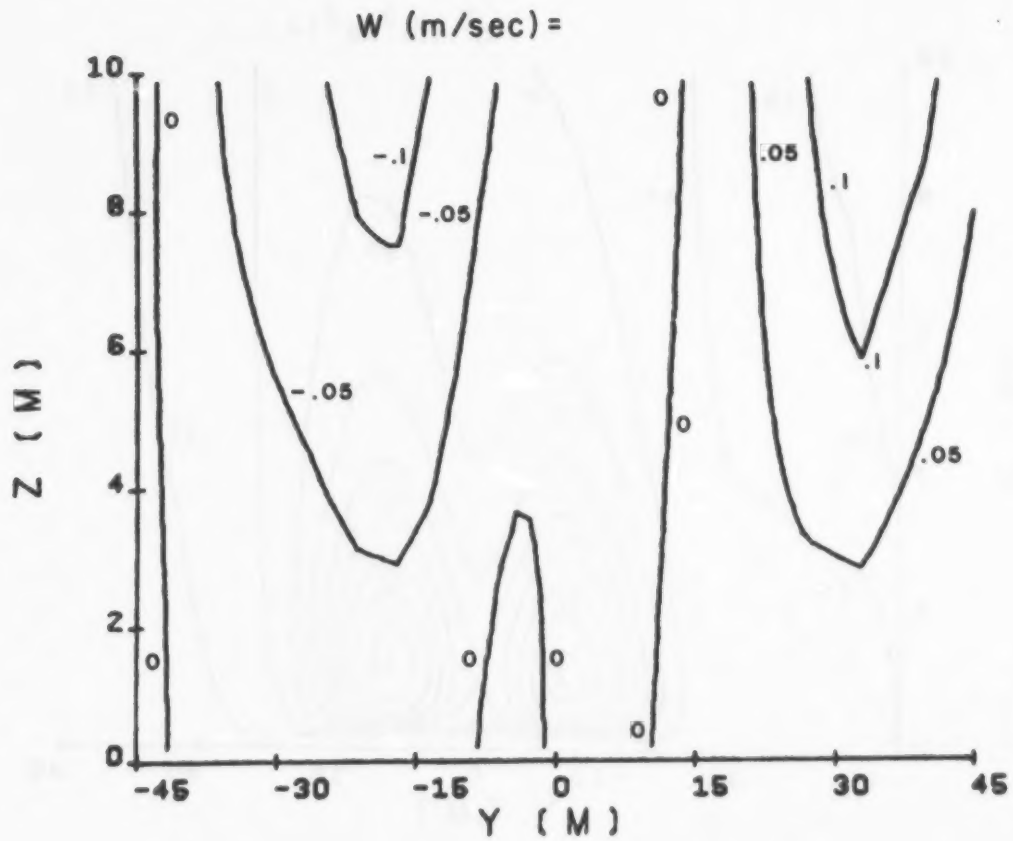

Figure C-13. The predicted contours of the W velocity for day 296.

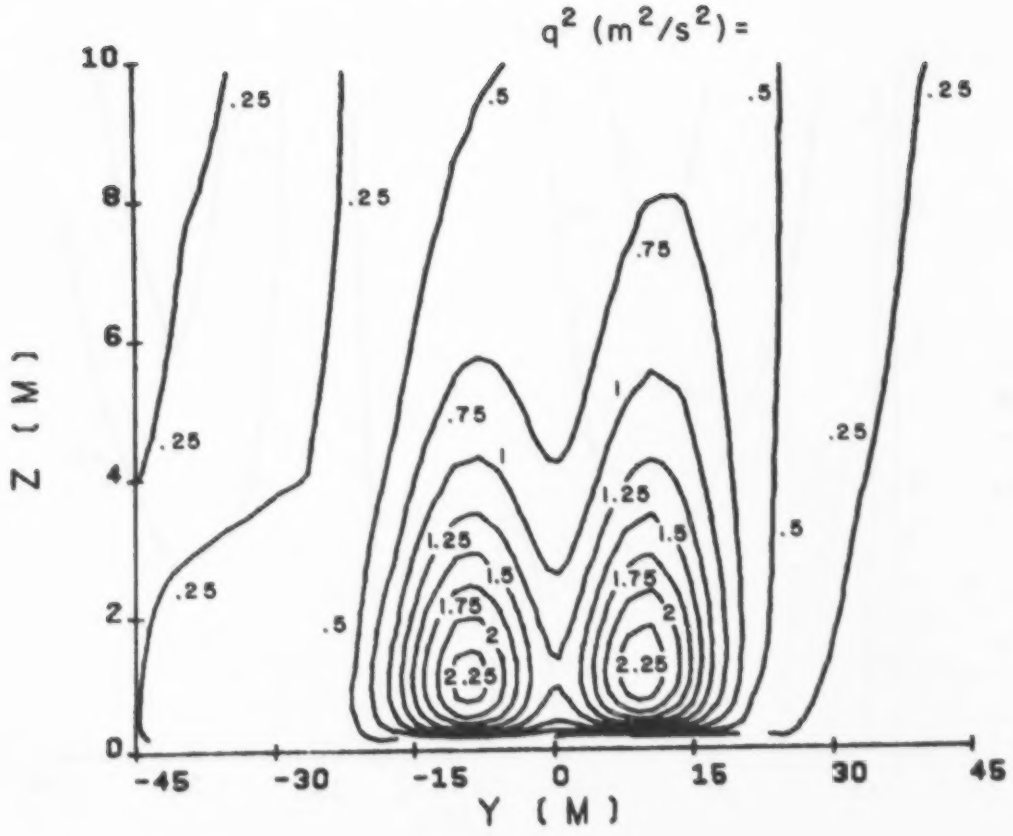

Figure C-14. The predicted contours of the q^2 correlation for day 296.

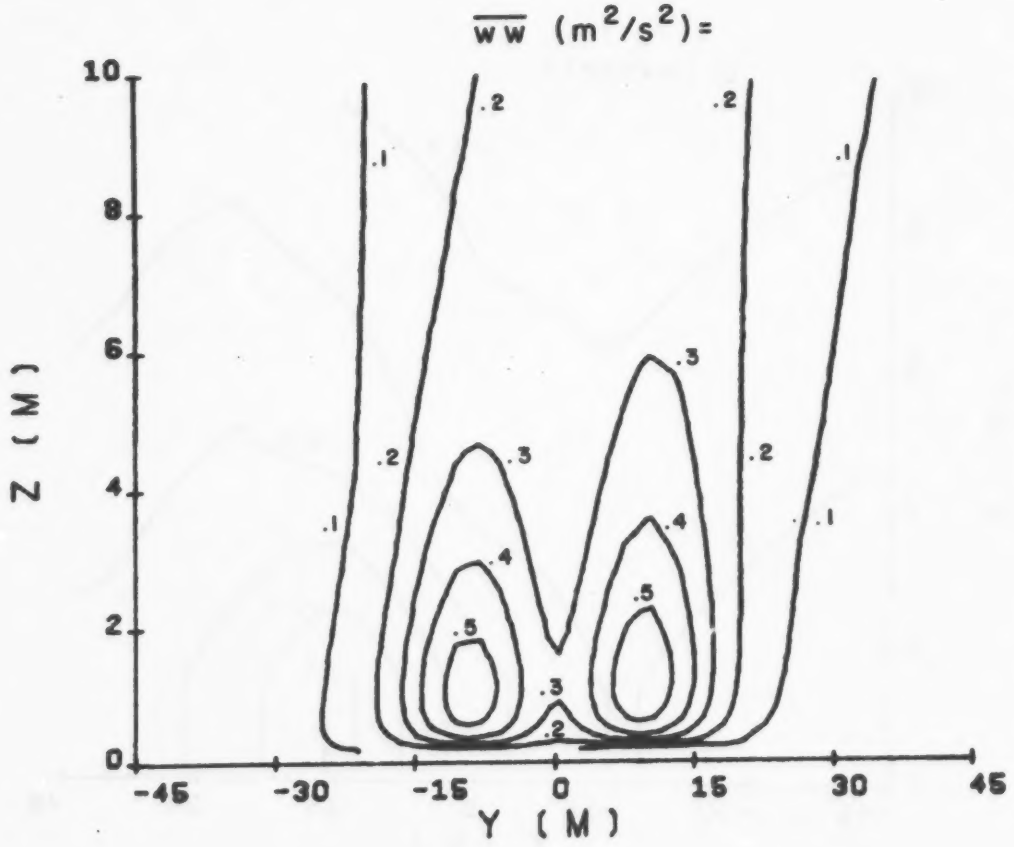

Figure C-15. The predicted contours of the $\overline{ww}$ correlation for day 296.

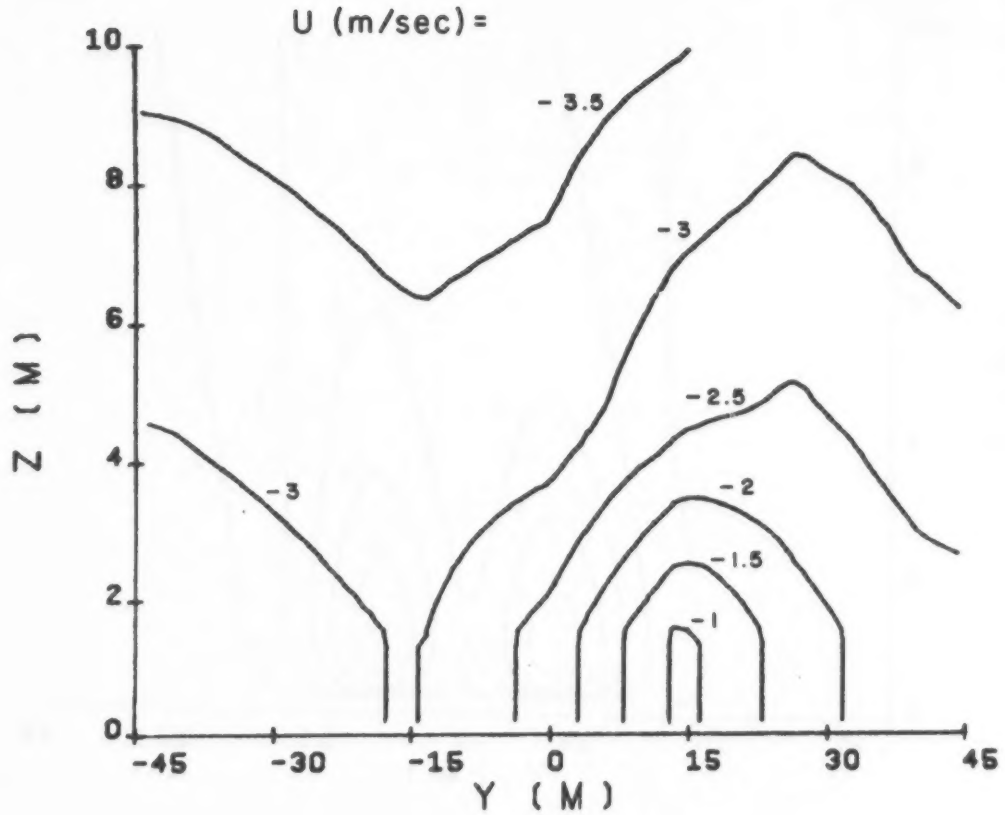

Figure C-16. The measured contours of the U velocity for day 296.

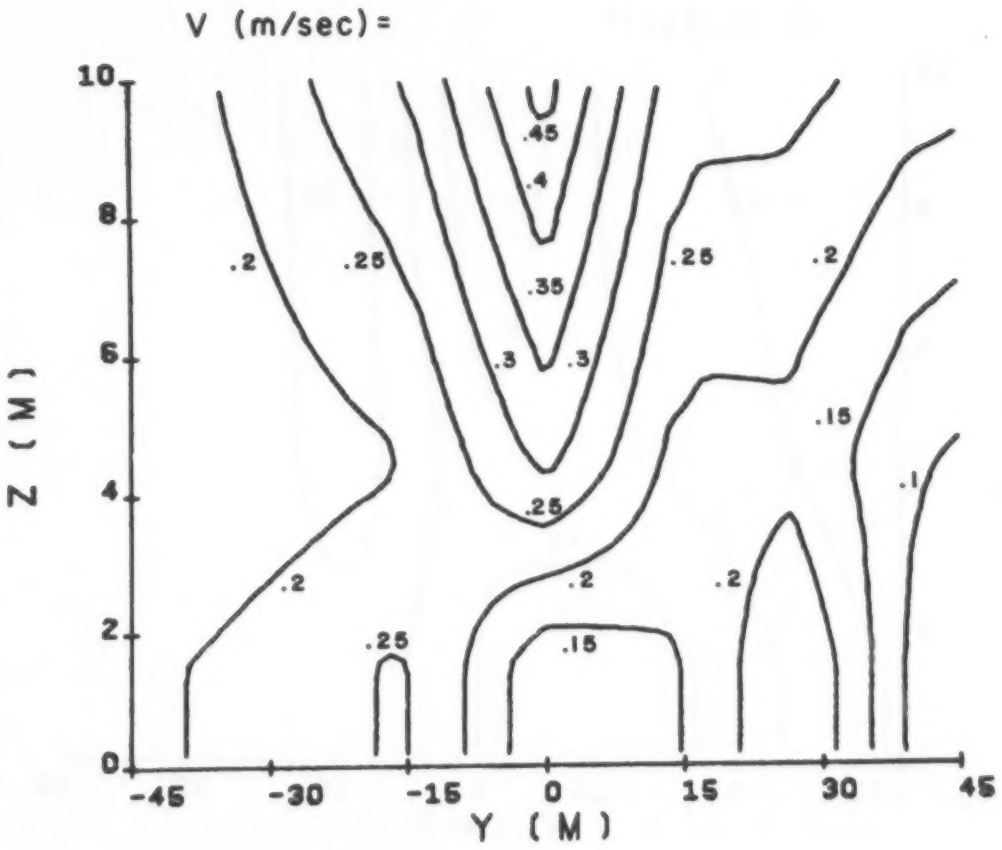

Figure C-17. The measured contours of the V velocity for day 296.

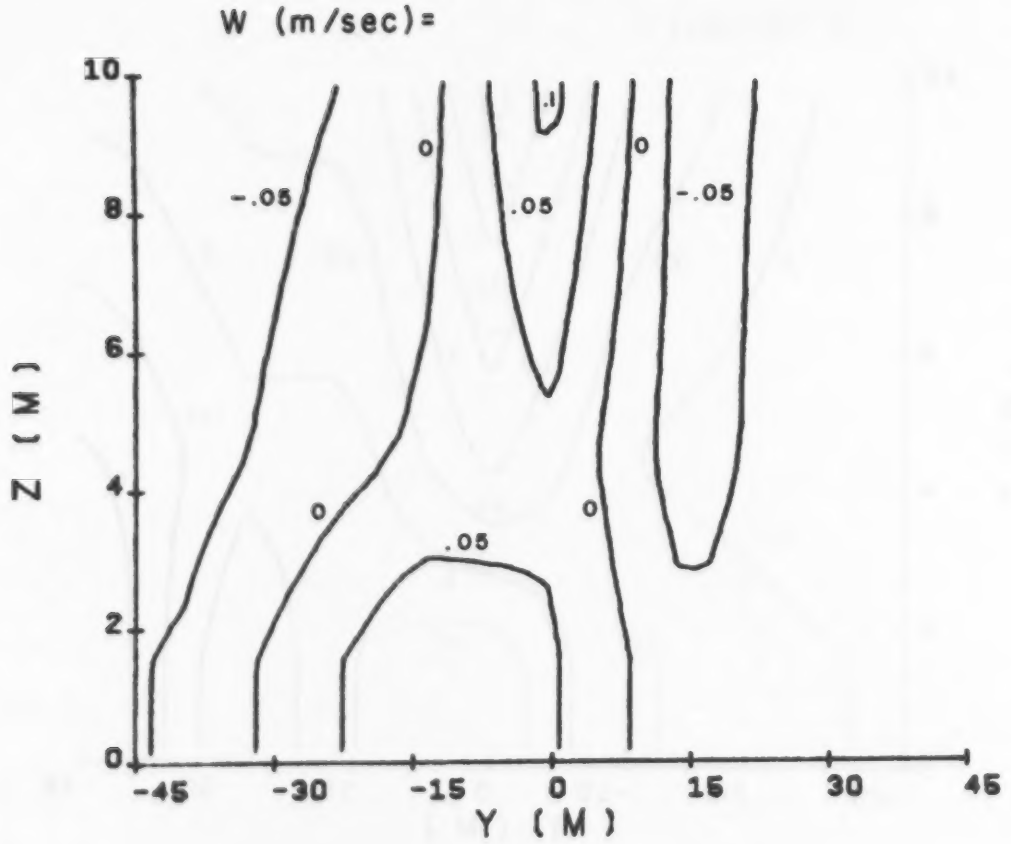

Figure C-18. The measured contours of the W velocity for day 296.

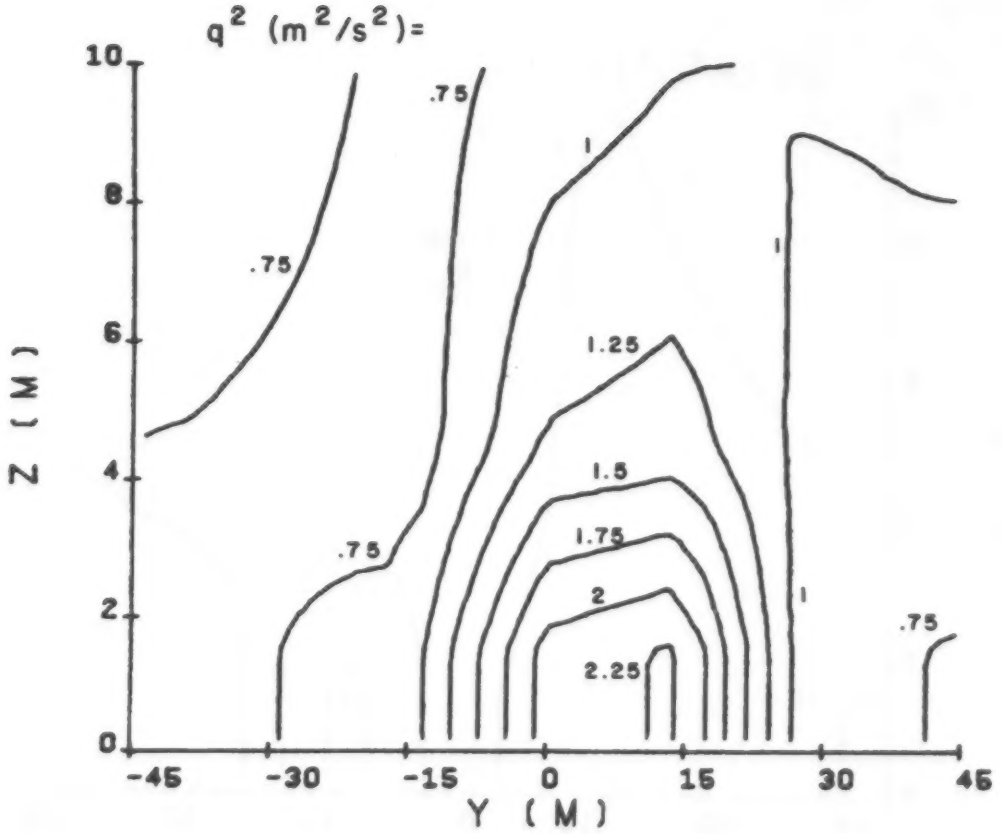

Figure C-19. The measured contours of the q^2 correlation for day 296.

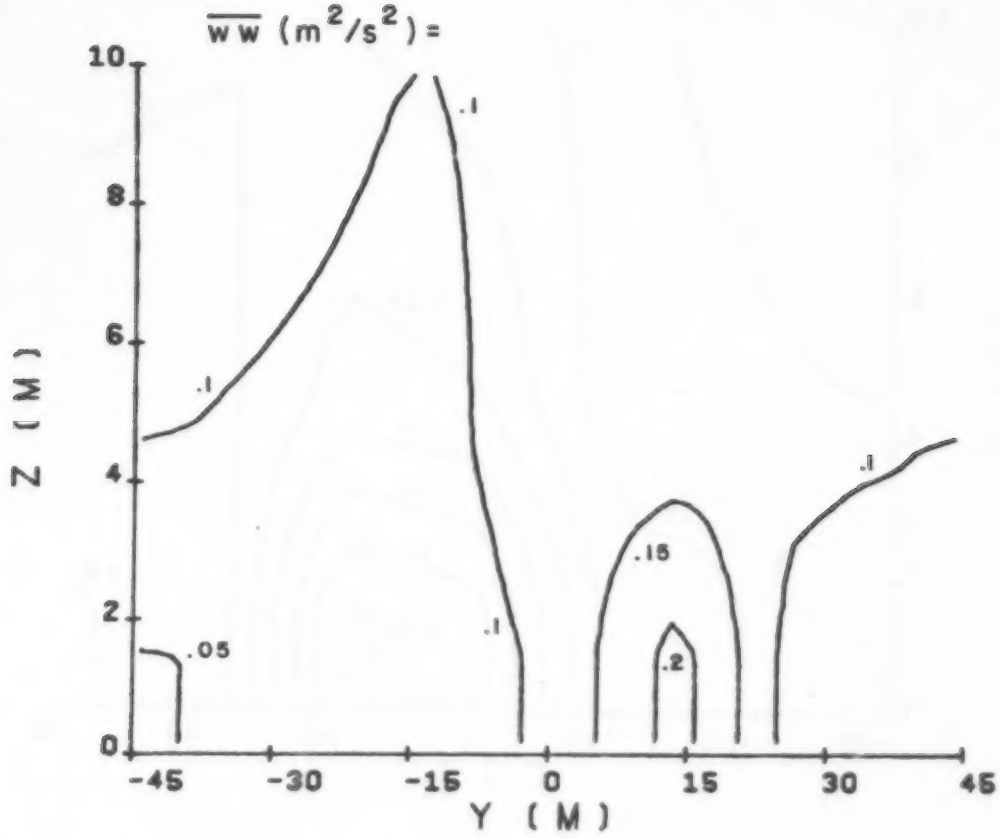

Figure C-20. The measured contours of the $\overline{ww}$ correlation for day 296.